

# Generalized Gaussian Structures: Models for Polymer Systems with Complex Topologies

Andrey A. Gurtovenko<sup>1,2</sup> (✉) · Alexander Blumen<sup>3</sup>

<sup>1</sup>Biophysics and Soft Matter Group,  
Laboratory of Physics and Helsinki Institute of Physics,  
Helsinki University of Technology, P.O.Box 1100, 02015 Helsinki, Finland  
*agu@fyslab.hut.fi*

<sup>2</sup>Institute of Macromolecular Compounds, Russian Academy of Sciences,  
Bolshoi Prospect 31, V.O., 199004 St. Petersburg, Russia  
*agu@fyslab.hut.fi*

<sup>3</sup>Theoretische Polymerphysik, Universität Freiburg, Hermann-Herder-Str. 3,  
79104 Freiburg, Germany  
*blumen@physik.uni-freiburg.de*

<b>1</b>	<b>Introduction</b> . . . . .	172
<b>2</b>	<b>Generalized Gaussian Structures: The Model</b> . . . . .	175
<b>3</b>	<b>Target Dynamical Quantities</b> . . . . .	177
3.1	Mechanical Viscoelastic Relaxation . . . . .	177
3.1.1	Dynamical Shear Modulus (Storage and Loss Moduli) and Viscosity . . . . .	177
3.1.2	Time-Dependent Relaxation Modulus and Relaxation Spectrum . . . . .	181
3.2	Dielectric Relaxation . . . . .	183
3.3	Displacement of Monomers under External Forces . . . . .	186
<b>4</b>	<b>Historical Retrospective: The Linear Rouse Chain</b> . . . . .	188
4.1	50 Years of the Rouse Model . . . . .	188
4.2	Successes and Limitations of the Rouse Approach: Comparison with the Zimm and the Reptation Pictures . . . . .	192
<b>5</b>	<b>Regular Mesh-Like Polymer Networks</b> . . . . .	195
5.1	Regular Network Models for Cooperative Interchain Relaxation . . . . .	196
5.1.1	3-D Model Networks . . . . .	196
5.1.2	2-D Model Networks . . . . .	200
5.2	Topologically-Regular Networks Built from Rouse Chains: Exactly Solvable Models . . . . .	202
5.2.1	Topologically-Cubic Networks . . . . .	202
5.2.2	Topologically-Square Networks . . . . .	209
5.3	Regular Networks Built from Complex Cells of Arbitrary Internal Topology	210
<b>6</b>	<b>Fractal Polymer Networks</b> . . . . .	213
6.1	General Approach: Generalized Viscoelastic Models . . . . .	213
6.2	A Simple Fractal Network: The Ladder Model . . . . .	217
6.3	Dual Sierpinski Gasket Structures . . . . .	219

<b>7</b>	<b>Heterogeneous Polymer Networks</b> . . . . .	222
7.1	Monodisperse Random Nets . . . . .	223
7.2	Small-World Rouse Networks . . . . .	225
7.3	Polymer Networks with Random (Nonfractal) Heterogeneities: Localization Effects . . . . .	228
7.4	Polydisperse Polymer Networks: Length Distribution of Network Strands .	230
7.5	Inhomogeneous Polymer Networks Consisting of Domains of Different Sizes . . . . .	231
7.5.1	General Approach for Describing Cross-Linked Polymers Consisting of Cross-Link Agglomerations . . . . .	231
7.5.2	Mesh-Like Inhomogeneous Polymer Networks . . . . .	234
7.5.3	Inhomogeneously Cross-Linked Polymeric Gels . . . . .	234
<b>8</b>	<b>Dendritic Polymers</b> . . . . .	236
8.1	Tree-Like Networks . . . . .	236
8.1.1	Tree-Like Gaussian Structures . . . . .	236
8.1.2	Tree-Like Networks Built from Rouse Chains . . . . .	239
8.2	Trifunctional Dendrimers . . . . .	242
8.3	Generalized Dendrimers . . . . .	246
8.4	Side-Chain Dendritic Polymers . . . . .	252
<b>9</b>	<b>Hyperbranched Polymers</b> . . . . .	255
9.1	Randomly-Branched Polymers . . . . .	256
9.2	Comblike Polymers . . . . .	262
9.3	Regular Hyperbranched Polymers . . . . .	264
<b>10</b>	<b>Hybrid Polymer Structures</b> . . . . .	268
10.1	Regular Structures Constructed From Small-World Rouse Networks . . . .	268
10.2	Polymer Networks Bearing Dendritic Wedges . . . . .	271
10.3	Dendrimer-Based Polymer Networks . . . . .	273
<b>11</b>	<b>Conclusions</b> . . . . .	276
	<b>References</b> . . . . .	277

**Abstract** A fundamental and long-standing problem in polymer physics is to deduce the relationship between the topology of a polymer and its dynamics. Generalized Gaussian structures (GGS), originating from the familiar Rouse model, represent a valuable tool for this purpose. This review summarizes theoretical efforts that have been undertaken in studying the dynamics of polymer systems with complex internal topologies by employing the GGS approach. The dynamic properties of a wide range of polymeric structures (ranging from polymer networks to dendritic and hybrid polymers) are discussed, while emphasizing systems that can be treated analytically (or semi-analytically). These studies provide considerable insight into the problem of relating the structure of a polymer to its dynamics. In many cases the GGS-treatment represents a first step in understanding the dynamics of polymers, and it may serve as a reference point for the development of more realistic models.

**Keywords** Polymers · Dynamics · Theory · Gaussian Structures · Networks · Dendrimers

## 1 Introduction

One of the basic challenges in polymer physics is to understand how the underlying geometries – and especially the topologies – of polymeric materials affect their dynamic behavior. This problem has a long-standing history and is becoming of increased importance as new polymeric materials with more and more complex architectures are synthesized. Polymers, being intricate systems, demonstrate a wide range of dynamic features that cannot be fully understood without elucidating the connections between structure and dynamics. Therefore, theoretical models that allow analytical insights into this problem are extremely valuable.

The pioneering ideas of Rouse, starting with the bead-and-spring model for linear flexible chains [1, 2] resulted in a basic approach that could be used to treat the dynamics of polymers. This (essentially coarse-grained) model was designed to study dynamic features of flexible macromolecules on scales larger than the distances covered by a few monomers: in the Rouse model a polymer chain is envisaged as being a sequence of beads connected by harmonic entropic springs. As such, the approach is very general (universal). Furthermore, the solvent (or, the surrounding medium consisting, say, of other polymer chains in the case of concentrated polymer systems) is substituted by a continuum, which is felt by the chain's beads through the viscous friction and the thermal noise. In a certain sense Rouse's approach leads to a "minimal" model which is very simplified, but which captures the most fundamental feature that distinguishes macromolecules from simple liquids, namely the polymer's *connectivity*. In spite of the fact that it disregards several important features, the Rouse model captures the dynamic properties of many systems, including concentrated polymer solutions and melts of rather short chains [2, 3].

The extension of Rouse's approach from linear chains to other polymer systems is quite straightforward and leads eventually to the concept of generalized Gaussian structures (GGS), which are the subject of this review. In the framework of the GGS approach, a polymer system is modeled as a collection of beads (subject to viscous friction), connected to each other by means of elastic springs in a system-specific way. Initially, the GGS concept was inspired by the study of cross-linked polymer networks; however, its applications have turned out to cover large classes of substances, such as dendritic polymers, hybrid polymers, and hierarchically-built structures.

A GGS, being a generalization of the Rouse model, has all the limitations of its predecessor: it does not account for excluded volume interactions and for entanglement effects. However, one may note that excluded volume effects are often screened. This occurs especially in rather dense media, such as dry polymer networks and polymer melts [2, 4]. The entanglement effects, in

turn, are not dominant as long as one stays below the entanglement limit. In the case of polymer networks this means high densities of cross-links, which then implies that the network strands between the cross-link points are rather short. The hydrodynamic, solvent-mediated interactions are also generally screened in dense systems [2]. We will not discuss their role in this review and we wish only to point out that they can be incorporated in the GGS as in the Zimm model, in a pre-averaged manner [5].

Bearing in mind all of the above restrictions (which may influence the global picture, depending on the situation at hand), the GGS approach represents an important step in the theoretical understanding and treatment of the dynamics of complex polymer systems. The basic simplicity of the GGS-approach often allows theoretical (analytical or semi-analytical) solutions to dynamical problems, even for very intricate polymer architectures. This great advantage is lost when the models become more and more involved, when they include interactions which the GGS disregards; such additions certainly make the models more realistic, but they also make them less tractable analytically. This eventually leads to a situation in which only computer simulations may help; these, on the other hand, are in general restricted to much shorter time domains than the temporal ranges accessible through GGS approaches.

In this article we review theoretical works which have employed the GGS model. We start – evidently – with the classical Rouse chain [1], but we will emphasize the developments that have occurred over the last decade. We want to stress from the beginning that our paper is essentially devoted to the *dynamics* of polymeric systems; a detailed analysis of the statistical equilibrium properties of Gaussian structures is beyond the scope of this paper. Also, we do not aim to provide an exhaustive exposition of the GGS literature. Our choice of topics reflects in large part our research interests and is, in this sense, biased. We would also like to point out that our choice covers only limited classes of complex polymeric systems, and that we focus on such particular systems in which one can attain, to a large degree, an (almost) analytical solution of the dynamical problem.

Our review starts with the general formulation of the GGS model in Sect. 2. In the framework of the GGS approach many dynamical quantities of experimental relevance can be expressed through analytical equations. Because of this, in Sect. 3 we outline the derivation of such expressions for the dynamical shear modulus and the viscosity, for the relaxation modulus, for the dielectric susceptibility, and for the displacement of monomers under external forces. Section 4 provides a historical retrospective of the classical Rouse model, while emphasizing its successes and limitations. The next three sections are devoted to the dynamical properties of several classes of polymer networks, ranging from regular and fractal networks to network models which take into account structural heterogeneities encountered in real systems. Sections 8 and 9 discuss dendrimers, dendritic polymers, and hyperbranched polymers.

Finally, we end the review with the so-called hybrid polymers, which display several levels of organization; examples for two-level organization are networks bearing dendritic wedges, dendrimer-based polymer networks, and regular lattices built from highly disordered subunits.

## 2 Generalized Gaussian Structures: The Model

In this section we formulate the theoretical framework of the so-called generalized Gaussian structures [6–9]. A generalized Gaussian structure (GGS) represents the extension of the classical Rouse model [1, 2], developed for linear polymer chains, to systems of arbitrary topology: it is modeled as a structure consisting of  $N_{\text{tot}}$  beads connected by harmonic springs, see Fig. 1. For simplicity, all of the beads of the GGS are subject to the same friction constant  $\zeta$  with respect to the surrounding viscous medium (the solvent). The GGS-approach is essentially a coarse-grained one: The friction constant of the GGS beads mirrors the overall friction of polymer fragments directly attached to a given point (bead). In turn, the chain fragments between the beads are assumed to be long enough, so that they obey Gaussian statistics. Normally, a chain fragment of about ten monomers fulfills this requirement. This allows each chain fragment to be satisfactorily modeled by an elastic (entropic) spring.

The potential energy of the GGS in the absence of external forces,  $U_{\text{elast}}$ , contains the elastic contributions of the harmonic springs (bonds) connected to each other:

$$U_{\text{elast}}(\{\mathbf{R}\}) = \frac{K}{2} \sum_{\text{bonds}} [\mathbf{R}_n - \mathbf{R}_m]^2 = \frac{K}{2} \sum_{n=1}^{N_{\text{tot}}} \sum_{m=1}^{N_{\text{tot}}} A_{nm} \mathbf{R}_n \mathbf{R}_m, \quad (1)$$

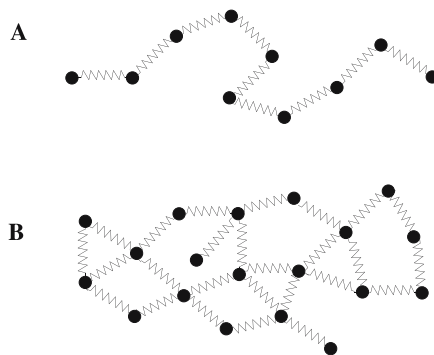


**Fig. 1** (A) Schematic representation of the bead-and-spring Rouse chain and (B) a particular example of a GGS

where  $\mathbf{R}_n(t) = (X_n(t), Y_n(t), Z_n(t))$  and  $\mathbf{R}_m(t) = (X_m(t), Y_m(t), Z_m(t))$  are the position vectors of the  $n$ th and  $m$ th GGS beads, respectively. The summation in the first sum of Eq. 1 goes over all pairs of beads  $n, m$  directly connected by elastic springs (bonds). The quantity  $K = 3k_B T/b^2$  is the elastic constant of a harmonic spring, where  $k_B$  is the Boltzmann constant,  $T$  is the temperature, and  $b^2$  is the mean square end-to-end distance for the unstretched spring. On the right-hand-side (rhs) of Eq. 1 we remark that the potential energy  $U_{\text{elast}}$  can be represented through the connectivity matrix  $A = (A_{nm})$  of the given GGS, which is also called the Kirchhoff matrix or the generalized Rouse matrix [6, 7, 10–12]. The connectivity matrix  $A$  contains all of the information about the topology of the GGS in question and is constructed as follows. Starting with all matrix elements equal to zero, we set the non-diagonal element  $A_{nm}$  equal to  $(-1)$  if the  $n$ th and  $m$ th beads are directly connected by a spring (otherwise,  $A_{nm}$  stays equal to zero). The diagonal element  $A_{nn}$  is set to equal the number of springs (bonds) emanating from the  $n$ th bead. Obviously,  $\det A = 0$  by construction and, therefore, at least one of its eigenvalues vanishes. If the structure does not separate into disjointed, unconnected substructures then the vanishing eigenvalue is non-degenerate. Note that for a linear polymer chain this procedure leads to the well-known Rouse matrix [1, 2].

The dynamics of the GGS are described by a set of linearized Langevin equations of motion. In addition to the friction and elastic forces, one has also stochastic forces due to the random collisions of the solvent with the solute (the GGS beads) and, in general, a superimposed field due to forces external to the polymer system. We note that at the time-scales usually treated in the study of polymers, the inertial term is rather unimportant; thus we neglect it. Taking all this into account, the Langevin equation of motion for the  $l$ th bead of the GGS reads:

$$\zeta \frac{d\mathbf{R}_l(t)}{dt} + K \sum_{m=1}^{N_{\text{tot}}} A_{lm} \mathbf{R}_m(t) = \mathbf{f}_l(t) + \mathbf{F}_l^{(\text{ext})}(t). \quad (2)$$

Here  $\mathbf{f}_l(t)$  are the stochastic forces and  $\mathbf{F}_l^{(\text{ext})}(t)$  is the external force acting on the  $l$ th GGS bead. Because of the fluctuation-dissipation theorem, the stochastic forces (thermal noise)  $\mathbf{f}_l(t)$  are connected with the dissipative force (friction). In Eq. 2 the thermal noise  $\mathbf{f}_l(t)$  is assumed to be Gaussian with zero mean value, so that one has  $\langle \mathbf{f}_l(t) \rangle = 0$  and  $\langle f_{l\alpha}(t) f_{m\beta}(t') \rangle = 2k_B T \zeta \delta_{lm} \delta_{\alpha\beta} \delta(t - t')$  (here  $\alpha$  and  $\beta$  denote the  $x$ ,  $y$ , and  $z$  directions).

It is important to keep in mind (see the ‘‘Introduction’’) that the GGS approach provides a rather simple description of polymer systems; it does not take into account interactions such as the excluded volume effects or entanglements. In some special cases (such as for polymer melts or dry polymer networks) the excluded volume interactions may be screened [2, 4]. The entanglement effects, in turn, are quite small for sufficiently short polymer chains [3]. Also, our GGS treatment here does not account for hydrodynamic

interactions which may be important in dilute polymer solutions. Note in this regard that the latter interactions may be included in the theory in a simplified, pre-averaged fashion [5, 13]. However, as will be demonstrated below, in spite of all these restrictions (crucial in some special cases), the GGS approach often leads to a reasonable description of polymer dynamics, allowing (due to its simplicity) analytical insights into the problem. Note that, despite the fact that we concentrate here mostly on homopolymers, the GGS approach allows extensions to heteropolymers, by allowing us to include several classes of beads and bonds into the picture (these beads and bonds may differ in their friction and elasticity constants, respectively) [14–21]. Thus, the GGS model can serve in many cases as a primary basis for understanding the fundamental problem of polymer physics, namely: how does the topology of a polymer affect its dynamical properties?

### 3

## Target Dynamical Quantities

### 3.1

#### Mechanical Viscoelastic Relaxation

#### 3.1.1

##### Dynamical Shear Modulus (Storage and Loss Moduli) and Viscosity

We start our exposition with basic dynamical features of polymers (often probed experimentally) and focus on mechanical relaxation. Here we encounter one of the most familiar properties of polymers, namely viscoelasticity. In general, polymers do not behave like solids or liquids; instead, they take an intermediate position, by which elastic or plastic behavior depends on the time-scale of the process under observation.

It is the aim of this subsection to present the derivation of analytic viscoelastic expressions in the GGS framework. As before, we take the GGS structure to be embedded in the viscous medium; for example, starting with a dilute polymer solution, the medium is given by the solvent. To measure the mechanical properties, one creates a macroscopic perturbation (strain) in the embedding medium. This external perturbation produces, in turn, a mesoscopic strain at the level of the polymer (GGS). A subsequent change of the polymer's configuration leads to the relaxation of the stress in the sample, which can be measured, allowing us to determine, for instance, the dynamic modulus.

Let us consider the influence of a flow (or velocity) field in the solvent. In terms of the Langevin equations of motion, Eq. 2, we then have [2, 22]:

$$F_l^{(\text{ext})}(t) = \zeta V_l(t), \quad (3)$$

where  $V_l(t)$  is the velocity of the solvent at the location of the  $l$ th GGS bead, given by the position vector  $R_l(t)$ . Focusing now on *shear* flow, the velocity field may be written as  $V_l(t) = (gY_l(t), 0, 0)$  where  $g$  is the velocity gradient. Such a two-dimensional flow can be generated in a polymer solution between two parallel plates, by letting one of them move. To obtain the frequency-dependent dynamic modulus and viscosity we consider the case of an oscillatory flow, where the velocity gradient  $g$  obeys  $g = g_0 \exp(i\omega t)$  [2, 3, 22]. Then the perturbation of the solvent becomes:

$$V_{xl}(t) = g_0 [\exp(i\omega t)] Y_l(t), \quad V_{yl}(t) = 0 \quad \text{and} \quad V_{zl}(t) = 0. \quad (4)$$

Furthermore, we assume that the applied velocity gradient  $g$  is small enough, so that the shear stress depends linearly on it; this is the domain of linear viscoelasticity.

Now the viscoelastic response of the polymer can be computed in two ways. The first consists of the direct evaluation of the stress arising in the polymer due to the strain induced by the perturbed viscous medium (solvent). The second way (which is in many ways equivalent to the first) is to calculate the additional virtual work which arises in the total system due to the presence of the polymer. Detailed descriptions of both methods can be found elsewhere [1, 2, 5, 9, 22–25]. Here we apply the second method, based on virtual work, in order to calculate the dynamic modulus and the viscosity.

The additional work  $W$  (the increase in energy loss) per unit volume and per unit time due to the presence of GGS in the solvent is given by [22]:

$$W = -\frac{1}{V} \sum_{l=1}^{N_{\text{tot}}} \langle F_l \cdot V_l^* \rangle = -\frac{1}{V} g_0 \exp(-i\omega t) \sum_{l=1}^{N_{\text{tot}}} \langle F_{xl} \cdot Y_l \rangle. \quad (5)$$

Here  $F_l$  is the force by which the perturbed viscous medium acts on the  $l$ th bead of the GGS and  $V_l$  is the velocity of the medium at the position of the  $l$ th GGS bead. Now  $V_l$  is given by Eq. 4 and the asterisk means complex conjugate; furthermore,  $V$  is the total volume of the system and  $\langle \dots \rangle$  denotes the average over the GGS configurations. Inserting the external forces imposed by the shear flow (see Eqs. 3 and 4) into Eq. 2 leads to the following set of equations of motion for the Cartesian coordinates of the position vectors of the GGS beads  $R_l(t) = (X_l(t), Y_l(t), Z_l(t))$ :

$$\zeta \left[ \frac{dX_l(t)}{dt} - g_0 \exp(i\omega t) Y_l(t) \right] + K \sum_{m=1}^{N_{\text{tot}}} A_{lm} X_m(t) = f_{xl}(t), \quad (6)$$

$$\zeta \frac{dY_l(t)}{dt} + K \sum_{m=1}^{N_{\text{tot}}} A_{lm} Y_m(t) = f_{yl}(t), \quad (7)$$

and a similar equation for  $Z_l(t)$ . Note that due to the shear character of the external forces (the  $X$  component of the perturbation velocity of the solvent depends on the  $Y$  component of the position vector of the bead on

which the perturbation acts), Eq. 6 and Eq. 7 for the  $X$  and  $Y$  coordinates get coupled. The force  $F_{xl}$  in Eq. 5 is due to the action of the perturbed viscous medium on the  $X$  coordinate of the  $l$ th GGS-bead. Thus, one has  $F_{xl} = \zeta[\dot{X}_l - g_0 \exp(i\omega t)Y_l]$ . Therefore, we can simplify Eq. 5 using Eq. 6. This leads to

$$W = \frac{1}{V} g_0 \exp(-i\omega t) K \sum_{m=1}^{N_{\text{tot}}} A_{lm} \langle X_m(t) \cdot Y_l(t) \rangle. \quad (8)$$

To proceed further it is necessary to transform the Cartesian coordinates  $\mathbf{R}$  to the normal coordinates  $\mathbf{Q}$ :

$$\mathbf{R}_l(t) = \sum_{k=1}^{N_{\text{tot}}} \mathbf{C}_{lk} \mathbf{Q}_k(t). \quad (9)$$

Since the perturbation of the viscous medium is assumed to be small ( $|g| \ll 1$ ), we can use the normal coordinates of the *unperturbed* GGS (in the absence of any external force  $F_l^{(\text{ext})}(t)$ , see Eq. 2) for our purposes. Then the transformation given by Eq. 9 simultaneously diagonalizes the potential energy  $U_{\text{elast}}$  of the unperturbed GGS, see Eq. 1, and preserves the diagonal form of the dissipative function  $R_{\text{diss}}$ :

$$U_{\text{elast}} = \frac{K}{2} \sum_{l=1}^{N_{\text{tot}}} \sum_{m=1}^{N_{\text{tot}}} A_{lm} \mathbf{R}_l \mathbf{R}_m = \frac{K}{2} \sum_{k=1}^{N_{\text{tot}}} \lambda_k \mathbf{Q}_k^2 \quad (10)$$

and

$$R_{\text{diss}} = \frac{\zeta}{2} \sum_{l=1}^{N_{\text{tot}}} \dot{\mathbf{R}}_l^2(t) = \frac{\zeta}{2} \sum_{k=1}^{N_{\text{tot}}} \dot{\mathbf{Q}}_k^2. \quad (11)$$

Here  $\lambda_k$  are eigenvalues of the connectivity matrix  $\mathbf{A}$  of the GGS. Each normal coordinate  $\mathbf{Q}_k = (Q_{1k}, Q_{2k}, Q_{3k})$  has a simple time behavior: it decays exponentially with time,  $\mathbf{Q}_k(t) \simeq \mathbf{Q}_k(0) \exp(-t/\tau_k)$ , where  $\tau_k$  is introduced through

$$\tau_k = \frac{\tau_0}{\lambda_k}, \quad (12)$$

and  $\tau_0 = \zeta/K$  is the characteristic relaxation time of the GGS. The normal mode transformation given by Eq. 9 reduces Eq. 8 to the following form:

$$W = \frac{1}{V} g_0 \exp(-i\omega t) K \sum_{k=2}^{N_{\text{tot}}} \lambda_k \langle Q_{1k}(t) \cdot Q_{2k}(t) \rangle. \quad (13)$$

Now the work  $W$  is fully determined by the correlation functions  $\langle Q_{1k}(t) \cdot Q_{2k}(t) \rangle$ . Note that in Eq. 13 the summation starts with  $k = 2$ , since we denote the vanishing eigenvalue (which is always present in a free-floating GGS) by  $\lambda_1$ , hence  $\lambda_1 = 0$ . The quantity  $\langle Q_{1k}(t) \cdot Q_{2k}(t) \rangle$  can be easily computed from the equations of motion, Eqs. 6 and 7. Here we just outline the way

to do it. After the normal mode transformation of Eqs. 6 and 7, both equations are multiplied by  $Q_{2k}(t)$  and averaged over the configurations. In this way one has from Eqs. 6 and 7:

$$\zeta \frac{d}{dt} \langle Q_{1k} \cdot Q_{2k} \rangle + 2K\lambda_k \langle Q_{1k} \cdot Q_{2k} \rangle - \zeta g_0 \exp(i\omega t) \langle Q_{2k}^2 \rangle = 0 \quad (14)$$

and

$$\frac{1}{2} \zeta \frac{d}{dt} \langle Q_{2k}^2 \rangle + K\lambda_k \langle Q_{2k}^2 \rangle = k_B T. \quad (15)$$

Equation 15 has the equilibrium solution  $\langle Q_{2k}^2 \rangle = k_B T / K\lambda_k$ . Inserting this solution into Eq. 14, one finally obtains for  $\langle Q_{1k}(t) \cdot Q_{2k}(t) \rangle$  (by taking it proportional to  $g_0 \exp[i\omega t]$ ):

$$\langle Q_{1k}(t) \cdot Q_{2k}(t) \rangle = k_B T g_0 \exp(i\omega t) \frac{\tau_k/2}{K\lambda_k [1 + i\omega\tau_k/2]}, \quad (16)$$

where we used Eq. 12. This leads immediately to the following closed form for  $W$ :

$$W = g_0^2 \frac{1}{V} k_B T \sum_{k=2}^{N_{\text{tot}}} \frac{\tau_k/2}{1 + i\omega\tau_k/2}. \quad (17)$$

The quantity  $W$  is directly related to the complex dynamic viscosity  $\eta^*$  through  $W(\omega) = g_0^2 \eta^*(\omega)$  [2, 22]. Therefore, one has for  $\eta^*$ :

$$\eta^*(\omega) = \nu k_B T \frac{1}{N_{\text{tot}}} \sum_{k=2}^{N_{\text{tot}}} \frac{\tau_k/2}{1 + i\omega\tau_k/2}, \quad (18)$$

where we introduced  $\nu = N_{\text{tot}}/V$ , the number of GGS beads per unit volume of polymer solution. Now, because of the relation  $G^* = i\omega\eta^*$  [1–3, 5, 22], the dynamic modulus  $G^*(\omega)$  is given by:

$$G^*(\omega) = \nu k_B T \frac{1}{N_{\text{tot}}} \sum_{k=2}^{N_{\text{tot}}} \frac{i\omega\tau_k/2}{1 + i\omega\tau_k/2}. \quad (19)$$

We recall that so far we considered dilute polymer solutions. It is noteworthy that even for concentrated solutions, as long as the entanglement effects are still negligible (this holds for polymers of low molecular weight), both the complex dynamic modulus and the viscosity continue to follow the structure of Eqs. 19 and 18, the only difference [3] being a change in the prefactor  $\nu k_B T$ . Given that we are mostly interested in the frequency dependences of the shear dynamic modulus and of the viscosity, we will present in the following the viscoelastic properties of the GGS mostly in terms of reduced quantities. As an example, in the case of the shear modulus  $G^*(\omega) = G'(\omega) + iG''(\omega)$ , the

reduced storage,  $[G'(\omega)]$  and loss,  $[G''(\omega)]$ , moduli read:

$$[G'(\omega)] = G'(\omega)/\nu k_B T = \frac{1}{N_{\text{tot}}} \sum_{k=2}^{N_{\text{tot}}} \frac{(\omega\tau_k/2)^2}{1 + (\omega\tau_k/2)^2} \quad (20)$$

and

$$[G''(\omega)] = G''(\omega)/\nu k_B T = \frac{1}{N_{\text{tot}}} \sum_{k=2}^{N_{\text{tot}}} \frac{\omega\tau_k/2}{1 + (\omega\tau_k/2)^2}. \quad (21)$$

In turn, for the reduced shear viscosity  $[\eta'(\omega)]$  (we recall that  $\eta^*(\omega) = \eta'(\omega) - i\eta''(\omega)$ ) we have:

$$[\eta'(\omega)] = \eta'(\omega)/\nu k_B T = \frac{1}{N_{\text{tot}}} \sum_{k=2}^{N_{\text{tot}}} \frac{\tau_k/2}{1 + (\omega\tau_k/2)^2}. \quad (22)$$

Here  $[\eta'(\omega)]$  is meant to be the viscosity due to the polymer (GGs) only, the contribution of the viscosity of the solvent being assumed to be already subtracted from Eq. 22. Note that the relaxation times involved in the mechanical relaxation,  $\tau_k/2$  in Eqs. 20, 21, and 22, are half those of the normal modes, Eq. 12. This is a direct consequence of the fact that only the second moments of the displacements (or, alternatively, only the  $\langle Q^2 \rangle$ ) contribute to the mechanical viscoelastic properties, as may be verified by reconsidering the derivation given above. As we will demonstrate in the following, this is not the case for the dielectric relaxation. It is instructive to emphasize that the derivation presented here does not use any assumptions about the topology of the GGS system. Therefore, the expressions for the shear dynamic modulus and the viscosity, Eqs. 20, 21, and 22, hold for arbitrary GGS topologies. Note also the fundamental fact that the eigenfunctions of the connectivity matrix  $\mathbf{A}$  of the GGS do not appear: in the GGS-scheme the shear modulus and the viscosity depend only on the eigenvalues of  $\mathbf{A}$ . Thus, in order to be able to evaluate  $G'(\omega)$  and  $G''(\omega)$  (as well as  $\eta'(\omega)$ ), it suffices to determine the eigenvalues  $\lambda_k$  (or the relaxation times  $\tau_k$ ) only. This simplifies our consideration of the dynamics of the particular GGS systems we are interested in.

### 3.1.2

#### Time-Dependent Relaxation Modulus and Relaxation Spectrum

We turn from the *frequency-dependent* shear modulus and viscosity considered above to the *time-dependent* relaxation modulus. As mentioned in the previous section, we focus on the *linear* viscoelastic domain, in which the shear stress  $\sigma(t)$  depends linearly on the velocity gradient  $g(t)$  [2]. The relaxation modulus  $G(t)$  is now implicitly introduced through a relation between

$g(t)$  and the ensuing stress  $\sigma(t)$ :

$$\sigma(t) = \int_{-\infty}^t G(t-t')g(t') dt' \quad (23)$$

and, using  $g(t) = g_0 \exp(i\omega t)$ ,

$$\sigma(t) = g_0 \exp(i\omega t) \int_0^{\infty} G(\tau) \exp(-i\omega\tau) d\tau. \quad (24)$$

On the other hand, the stress  $\sigma(t)$  imposed on the GGS by the perturbation of the viscous surrounding medium can be computed based on the additional work  $W$  due to the presence of the GGS; one finds that  $\sigma(t) = g_0 \exp(i\omega t)(1/i\omega)G^*(\omega)$  where  $G^*(\omega)$  is given by Eq. 19, see for example [2, 22, 24, 25]. Equating this expression to Eq. 24 leads to the connection between the complex shear modulus and the relaxation modulus:

$$G^*(\omega) = i\omega \int_0^{\infty} G(\tau) \exp(-i\omega\tau) d\tau. \quad (25)$$

Combining it with Eqs. 20 and 21 for the real and the imaginary components of  $G^*(\omega)$  results in a simple expression for  $G(t)$ . We write it in the reduced form

$$[G(t)] = G(t)/\nu k_B T = \frac{1}{N_{\text{tot}}} \sum_{k=2}^{N_{\text{tot}}} \exp\left(-\frac{2t}{\tau_k}\right), \quad (26)$$

where we divided the relaxation modulus  $G(t)$  by the factor  $\nu k_B T$ , with  $\nu$  being the number of GGS beads per unit volume. One should note that the equilibrium modulus  $G_e$  (which is zero for GGS in dilute solutions but may take a non-zero value in the case of, say, dry polymer networks) is not included in Eq. 26. Thus,  $[G(t)]$  describes only the transient time-dependent evolution of the system and vanishes at very long times.

A physically straightforward interpretation of the relaxation modulus  $[G(t)]$  is that it represents the response of the stress to a shear jump [2, 9]. Furthermore, the relaxation modulus  $[G(t)]$  (as well as the dynamic shear modulus  $[G^*(\omega)]$ ) can be rewritten in terms of the logarithmic density of relaxation times, the so-called relaxation spectrum  $H(\tau)$  [3, 26]:

$$[G(t)] = \int_0^{\infty} H(\tau) \exp(-t/\tau) d \ln \tau. \quad (27)$$

If one has a discrete set of relaxation times, the relaxation spectrum can be represented as a sum of delta functions (see Eqs. 27 and 26):

$$H(\tau) = \frac{2}{N_{\text{tot}}} \tau \sum_{k=2}^{N_{\text{tot}}} \delta\left(\tau - \frac{\tau_k}{2}\right). \quad (28)$$

In the case of a continuous spectrum of eigenvalues, in other words when the eigenvalues  $\lambda(\xi)$  are defined by some continuous variable  $\xi$ , the relaxation spectrum  $H(\tau)$  can be rewritten as (see [12] and also Sect. 7.5.1):

$$H(\tau) = -\frac{1}{N_{\text{tot}}} \frac{d\xi}{d \ln \tau}. \quad (29)$$

It is now important to note that the relaxation spectrum (the eigenvalue spectrum of the GGS) itself determines many important dynamical features. In particular, it fixes  $G(t)$  and  $G^*(\omega)$  through Eqs. 27 and 25. Also, global aspects such as scaling carry over. Thus, if the relaxation spectrum of the particular GGS decays as  $\tau^{-\alpha}$  where  $\alpha > 0$ , the viscoelastic dynamical properties of the GGS also scale, so that both the storage modulus  $G'(\omega)$  and the relaxation modulus  $G(t)$  exhibit power-law behavior; one finds, using Eqs. 27 and 25, that  $G'(\omega) \sim \omega^\alpha$  and  $G(t) \sim t^{-\alpha}$ .

### 3.2

#### Dielectric Relaxation

Besides mechanical viscoelastic experiments, one can also perform dielectric relaxation measurements, which constitute another well-established technique in polymer physics. Dielectric relaxation is related to the frequency-dependent complex dielectric susceptibility,  $\varepsilon^*(\omega)$ . One usually focuses on  $\Delta\varepsilon^*(\omega)$ , which is introduced as follows:

$$\Delta\varepsilon^*(\omega) = \frac{\varepsilon^*(\omega) - \varepsilon_\infty}{\varepsilon_0 - \varepsilon_\infty}. \quad (30)$$

In Eq. 30,  $\varepsilon_0$  and  $\varepsilon_\infty$  denote the limiting low- and high-frequency dielectric constants, respectively. In general, for the  $\Delta\varepsilon^*(\omega)$  of polar molecules embedded in non-polar solvents under an oscillatory electric field  $E = E_0 \exp(i\omega t)$  we have [27]:

$$\Delta\varepsilon^*(\omega) \simeq \int_0^\infty \left( -\frac{d}{dt} C_0(\mathbf{M}; t) \right) \exp(-i\omega t) dt, \quad (31)$$

when the local fields are not important. In Eq. 31  $C_0(\mathbf{M}; t)$  is the normalized autocorrelation function of the total dipole moment  $\mathbf{M}(t)$  of the polymer

system:

$$C_0(\mathbf{M}; t) = \frac{\langle \mathbf{M}(0)\mathbf{M}(t) \rangle}{\langle \mathbf{M}^2(0) \rangle}. \quad (32)$$

In general, the expression for  $\Delta\varepsilon^*(\omega)$ , Eq. 31, can not be reduced to a simple, compact form. However, we proceed to show that this becomes possible under certain conditions.

Here we focus on the dielectric response of a polar GGS whose bonds (springs) possess dipole moments directed along them (the material is then of type A following Stockmayer's classification) [22, 28, 29]. In other words, in the model one assigns a longitudinal dipole moment  $\mathbf{m}_j$  to each bond  $j$  of the GGS; the magnitude of every  $\mathbf{m}_j$  is directly proportional to the length of the  $j$ th bond, but its orientation is arbitrary. The total dipole moment  $\mathbf{M}(t)$  of the GGS is given then by:

$$\mathbf{M}(t) = \sum_{j=1}^{N_{\text{bond}}} \mu_j \mathbf{P}_j(t), \quad (33)$$

where  $N_{\text{bond}}$  is the total number of bonds of the GGS,  $\mu_j = d_j \mu$  is the dipole moment per unit length,  $d_j \in \{+1, -1\}$  gives the orientation, and  $\mathbf{P}_j = \mathbf{R}_l - \mathbf{R}_m$  is the end-to-end vector of the  $j$ th bond between the  $l$ th and the  $m$ th GGS beads.

To proceed, we assume that the orientations of the dipole moments  $\{\mathbf{m}_j\}$  along the GGS bonds (defined by  $d_j$ ) are random and uncorrelated [30–32]. This key feature simplifies the situation considerably. Then, for the autocorrelation function of  $\mathbf{M}(t)$ , after averaging over all possible distributions of bonds' orientations, with the average denoted below by  $\langle \cdots \rangle_{\text{orient}}$  (here we follow [31] closely), we have:

$$\begin{aligned} \langle \langle \mathbf{M}(0)\mathbf{M}(t) \rangle \rangle_{\text{orient}} &= \sum_{j=1}^{N_{\text{bond}}} \sum_{i=1}^{N_{\text{bond}}} \mu^2 \langle d_j d_i \rangle_{\text{orient}} \langle \mathbf{P}_j(0)\mathbf{P}_i(t) \rangle \\ &= \mu^2 \sum_{j=1}^{N_{\text{bond}}} \langle \mathbf{P}_j(0)\mathbf{P}_j(t) \rangle. \end{aligned} \quad (34)$$

In deriving Eq. 34 we made use of the condition of random orientation,  $\langle d_j d_i \rangle_{\text{orient}} = \delta_{ji}$ . Equation 34 can be simplified further with the help of the normal mode transformation, see Eq. 9:

$$\langle \langle \mathbf{M}(0)\mathbf{M}(t) \rangle \rangle_{\text{orient}} = \mu^2 \sum_{k=1}^{N_{\text{tot}}} \langle \mathbf{Q}_k^2 \rangle \exp(-t/\tau_k) \sum_{j=1}^{N_{\text{bond}}} \left( C_{lk}^{(j)} - C_{mk}^{(j)} \right)^2, \quad (35)$$

where we used the orthogonality of the normal modes  $\mathbf{Q}$  and also their simple exponential decay with time:  $\langle \mathbf{Q}_k(0)\mathbf{Q}_{k'}(t) \rangle = \delta_{kk'} \langle \mathbf{Q}_k^2 \rangle \exp(-t/\tau_k)$ . Here, as

before,  $\tau_k = \tau_0/\lambda_k$ . In Eq. 35 the superscript  $j$  of  $C_{lk}^{(j)}$  and of  $C_{mk}^{(j)}$  recalls that bond  $j$  is determined by  $\mathbf{R}_l$  and  $\mathbf{R}_m$ ; in other words  $\mathbf{P}_j = \mathbf{R}_l - \mathbf{R}_m$ . The quantity  $\langle \mathbf{Q}_k^2 \rangle$  can be easily determined from the Langevin equation of motion (see Eq. 2 with  $F_l^{\text{(ext)}}(t) = 0$ ). Performing the transformation of this equation to normal coordinates one finds, for each component  $\langle Q_{1k}^2 \rangle$ ,  $\langle Q_{2k}^2 \rangle$ , and  $\langle Q_{3k}^2 \rangle$ , an equation of the form of Eq. 15, from which the equilibrium solution for  $\langle \mathbf{Q}_k^2 \rangle = \langle Q_{1k}^2 \rangle + \langle Q_{2k}^2 \rangle + \langle Q_{3k}^2 \rangle$ , namely

$$\langle \mathbf{Q}_k^2 \rangle = \frac{3k_B T}{K\lambda_k} \quad (36)$$

follows [30, 31].

A further simplification of Eq. 35 for GGS follows by noting that the combination of Cartesian coordinates of the GGS beads involved in  $\langle \langle \mathbf{M}(0)\mathbf{M}(t) \rangle \rangle_{\text{orient}}$ , see Eq. 34, is directly related to the potential energy  $U_{\text{elast}}(\{\mathbf{R}\})$  of the GGS, see Eq. 1. Indeed, with the use of Eq. 10 one has [31]:

$$\begin{aligned} U_{\text{elast}}(\{\mathbf{R}\}) &= \frac{K}{2} \sum_{j=1}^{N_{\text{bond}}} \mathbf{P}_j^2 = \frac{K}{2} \sum_{k=1}^{N_{\text{tot}}} \langle \mathbf{Q}_k^2 \rangle \sum_{j=1}^{N_{\text{bond}}} \left( C_{lk}^{(j)} - C_{mk}^{(j)} \right)^2 \\ &= \frac{K}{2} \sum_{k=1}^{N_{\text{tot}}} \lambda_k \langle \mathbf{Q}_k^2 \rangle, \end{aligned} \quad (37)$$

and therefore [31]

$$\sum_{j=1}^{N_{\text{bond}}} (C_{lk}^{(j)} - C_{mk}^{(j)})^2 = \lambda_k. \quad (38)$$

Inserting Eq. 38 into Eq. 35 finally leads to the following compact form for  $\langle \langle \mathbf{M}(0)\mathbf{M}(t) \rangle \rangle_{\text{orient}}$  [30–32]:

$$\langle \langle \mathbf{M}(0)\mathbf{M}(t) \rangle \rangle_{\text{orient}} = \mu^2 \frac{3k_B T}{K} \sum_{i=1}^{N_{\text{tot}}} \exp(-t/\tau_k). \quad (39)$$

It is now a straightforward matter to compute the dielectric susceptibility  $\Delta\varepsilon^*(\omega)$ . From Eq. 39 the normalized autocorrelation function of the total dipole moment  $C_0(\mathbf{M}; t)$  reads:

$$C_0(\mathbf{M}; t) = \frac{1}{N_{\text{tot}}} \sum_{k=1}^{N_{\text{tot}}} \exp(-t/\tau_k), \quad (40)$$

where again  $\tau_k = \tau_0/\lambda_k$ . Inserting Eq. 40 in Eq. 31 now leads to the dielectric susceptibility  $\Delta\varepsilon^*$ ; expressing it in terms of its real and imaginary parts,

$\Delta\varepsilon^* = \Delta\varepsilon' - i\Delta\varepsilon''$ , we find [31, 32]:

$$\Delta\varepsilon'(\omega) = \frac{1}{N_{\text{tot}}} \sum_{k=2}^{N_{\text{tot}}} \frac{1}{1 + (\omega\tau_k)^2} \quad (41)$$

and

$$\Delta\varepsilon''(\omega) = \frac{1}{N_{\text{tot}}} \sum_{k=2}^{N_{\text{tot}}} \frac{\omega\tau_k}{1 + (\omega\tau_k)^2}. \quad (42)$$

Here again the sums are taken over all finite relaxation times; the infinite time  $\tau_1$  related to  $\lambda_1 = 0$  is not included, because the term corresponding to  $\lambda_1$  contributes a constant to  $C_0(M; t)$  in Eq. 40 and, therefore, vanishes in Eq. 31 after differentiation with respect to time.

The approach presented here was first developed for the dielectric relaxation of regular mesh-like polymer networks built from macromolecules with longitudinal dipole moments [30], and was later applied to disordered polymer networks [31, 32]. Its key assumption, namely the absence of any correlations in the orientations of the dipole moments of the different GGS bonds is obviously rather simplified. However, it leads, as shown above, to simple analytical expressions for the dielectric susceptibility, a very important dynamical quantity in experimental studies of polymers; we can now analyze it in great detail for particular GGS systems of interest. Another advantage of this model arises from the fact that one has a straightforward correspondence between the mechanical and the dielectric relaxation forms. From the expressions for the storage and loss modulus, Eqs. 20 and 21, and from those for the dielectric susceptibility  $\Delta\varepsilon^*$ , Eqs. 41 and Eq. 42, one sees readily that [31]

$$\Delta\varepsilon'(\omega) = 1 - [G'(2\omega)] \quad (43)$$

and that

$$\Delta\varepsilon''(\omega) = [G''(2\omega)]. \quad (44)$$

One may furthermore note that the dielectric susceptibility is determined by relaxation times which are twice larger than those appearing in the expressions for the mechanical relaxation. Again, we would like to emphasize that to calculate  $\Delta\varepsilon^*(\omega)$  (as well as  $G^*(\omega)$ ) we need only the eigenvalues  $\lambda_k$  (or the relaxation times  $\tau_k$ ) of the GGS, but not the corresponding eigenfunctions.

### 3.3

#### Displacement of Monomers under External Forces

One more dynamical characteristic to be considered here in detail is the displacement of GGS beads under external forces [7, 9, 33]. This dynamic quantity is also of special interest because of recent experimental developments that have demonstrated how to perform micromanipulations on polymers. In

particular, individual DNA molecules were dragged by optical or magnetic tweezers [34–36]; similar experiments were performed with magnetic beads in actin networks [37].

Let us consider a situation in which a time-dependent external force  $F_l^{(\text{ext})}(t)$  is applied to the GGS beads; see the Langevin equation of motion, Eq. 2. Now, averaging this equation over the thermal noise components  $f_l(t)$ , we have for  $\langle R_l(t) \rangle$ :

$$\frac{d\langle R_l(t) \rangle}{dt} + \frac{1}{\tau_0} \sum_{m=1}^{N_{\text{tot}}} A_{lm} \langle R_m(t) \rangle = \frac{1}{\zeta} F_l^{(\text{ext})}(t). \quad (45)$$

Equation 45 has the following formal solution [7, 9, 33]:

$$\langle R_l(t) \rangle = \frac{1}{\zeta} \int_{-\infty}^t d\tau \sum_{m=1}^{N_{\text{tot}}} \left( \exp \left[ -\frac{(t-\tau)}{\tau_0} A \right] \right)_{lm} F_m^{(\text{ext})}(\tau), \quad (46)$$

where  $A = (A_{lm})$  is the connectivity matrix of the GGS. As an example, we consider here the special case of a constant external force that is switched on at  $t = 0$  and acts only on one particular bead, say  $n$ , along the  $y$ -direction, so that

$$F_m^{(\text{ext})}(t) = \delta_{mn} F_0^{(\text{ext})} \theta(t) \cdot e_y. \quad (47)$$

For this kind of external force, Eq. 46 simplifies to

$$\langle Y_n(t) \rangle = \frac{1}{\zeta} F_0^{(\text{ext})} \int_0^t d\tau \left( \exp \left[ -\frac{(t-\tau)}{\tau_0} A \right] \right)_{nn}. \quad (48)$$

Note that  $\langle Y_n(t) \rangle$  still depends on the bead positions in the GGS; in other words on the index  $n$ . As a consequence, even for an external force of such a simple form we need both the eigenvalues and the eigenfunctions of the connectivity matrix  $A$  of the GGS in order to obtain the average displacement of the  $n$ th GGS bead. The need to determine the eigenfunctions may be overcome by further averaging over all beads in the GGS [7, 9, 33]:

$$\begin{aligned} \langle \langle Y(t) \rangle \rangle &= \frac{1}{N_{\text{tot}}} \sum_{n=1}^{N_{\text{tot}}} \langle Y_n(t) \rangle \\ &= \frac{F_0^{(\text{ext})}}{N_{\text{tot}} \zeta} \int_0^t d\tau \text{Tr} \left( \exp \left[ -\frac{(t-\tau)}{\tau_0} A \right] \right) \\ &= \frac{F_0^{(\text{ext})}}{N_{\text{tot}} \zeta} \int_0^t d\tau \sum_{k=1}^{N_{\text{tot}}} \exp \left[ -\frac{(t-\tau)}{\tau_0} \lambda_k \right], \end{aligned} \quad (49)$$

where  $\text{Tr}(X)$  denotes the trace of the matrix  $X$ . In Eq. 49 we used the fact that the trace is invariant under normal mode transformations, such as Eq. 9, which represents an orthogonal transformation which rotates the Cartesian axes.

To present Eq. 49 in a more meaningful form, we recall that for a GGS, which is a connected object, only one eigenvalue vanishes,  $\lambda_1 = 0$ . Separating this eigenvalue from the non-vanishing ones and performing the integration in Eq. 49, we finally obtain the following for  $\langle\langle Y(t) \rangle\rangle$  [7, 9, 33]:

$$\begin{aligned} \langle\langle Y(t) \rangle\rangle &= \frac{F_0^{(\text{ext})}}{N_{\text{tot}} \zeta} t + \frac{F_0^{(\text{ext})}}{N_{\text{tot}} \zeta} \tau_0 \sum_{k=2}^{N_{\text{tot}}} \frac{1 - \exp(-t \lambda_k / \tau_0)}{\lambda_k} \\ &= \frac{F_0^{(\text{ext})}}{N_{\text{tot}} \zeta} t + \frac{F_0^{(\text{ext})}}{N_{\text{tot}} \zeta} \sum_{k=2}^{N_{\text{tot}}} \tau_k [1 - \exp(-t / \tau_k)]. \end{aligned} \quad (50)$$

The first term in Eq. 50 mirrors the displacement (drift) of the GGS as a whole under the constant external force; it involves the friction which acts on the whole GGS,  $\zeta_{\text{GGS}} = N_{\text{tot}} \zeta$ . The second term displays the intra-GGS relaxation and is governed by the set of relaxation times (eigenvalues) of the GGS. As we will see in the following, the bead displacements given by Eq. 50 are a very useful tool in probing the dynamical features of polymer systems with complex topologies.

## 4

### Historical Retrospective: The Linear Rouse Chain

#### 4.1

##### 50 Years of the Rouse Model

In 1948, two Soviet physicists, Kargin and Slonimskii, published a paper in which they introduced a “bead and spring” model for linear polymers [38]. Their model did not include Brownian fluctuating forces and, in a certain sense, was a precursor to Bueche’s publication [39], which appeared six years later. Since the Kargin-Slonimskii model was only published in Russian, it did not make a strong impact internationally. In 1953 Rouse published his paper “A theory of linear viscoelastic properties of dilute solutions of coiling polymers” [1], in which he explicitly introduced stochastic Brownian forces into the bead and spring linear chain model. This fundamental model of polymer chain dynamics became known in the literature as the *Rouse model*; the paper by Rouse is one of the most cited publications in polymer physics (the search engine of the “Web of Science” finds over 2200 citations for the period from 1986 to 2003). In this section we succinctly recall its main features.

Let us consider a GGS that has a linear topology and that consists of  $N_{\text{tot}} \equiv N$  beads connected by elastic springs, see Fig. 1A. The Langevin equation of motion, Eq. 2, can be rewritten for the inner chain beads,  $1 < j < N$ , in the form [1, 2, 40, 41]:

$$\zeta \frac{d}{dt} \mathbf{R}_j(t) + K[2\mathbf{R}_j(t) - \mathbf{R}_{j+1}(t) - \mathbf{R}_{j-1}(t)] = \mathbf{f}_j(t), \quad (51)$$

where  $\mathbf{R}_j(t)$  is the position vector of the  $j$ th bead. The equations of motion for the end beads ( $j = 1$  and  $j = N$ ) are:

$$\zeta \frac{d}{dt} \mathbf{R}_1(t) + K[\mathbf{R}_1(t) - \mathbf{R}_2(t)] = \mathbf{f}_1(t) \quad (52)$$

and

$$\zeta \frac{d}{dt} \mathbf{R}_N(t) + K[\mathbf{R}_N(t) - \mathbf{R}_{N-1}(t)] = \mathbf{f}_N(t). \quad (53)$$

The determination of the eigenvalues of the  $A$  matrix corresponding to Eqs. 51, 52, and 53 is best performed by a transformation from Cartesian coordinates to normal coordinates, Eq. 9. Here the transformation can be formulated as:

$$\mathbf{R}_j(t) = \sum_{k=1}^N [A \sin(j\psi_k) + B \cos(j\psi_k)] \mathbf{Q}_k(t), \quad (54)$$

where  $\psi_k$  denotes the phase shift along the Rouse chain. Inserting Eq. 54 into Eq. 51 leads to the following expression for the non-vanishing eigenvalues in terms of the  $\psi_k$  [1, 2]:

$$\lambda_k = 2(1 - \cos \psi_k) = 4 \sin^2 \left( \frac{\psi_k}{2} \right). \quad (55)$$

The  $\psi_k$  are now fixed by Eqs. 52 and 53, which play the role of boundary conditions. It turns out that one finds, as before, a single vanishing eigenvalue,  $\lambda_1 = 0$ . The remaining  $(N - 1)$  non-vanishing eigenvalues  $\{\lambda_2, \dots, \lambda_N\}$  are fixed by having

$$\psi_k = \frac{\pi}{N}(k - 1), \quad k = 2, \dots, N \quad (56)$$

as solutions, to be inserted in Eq. 55. The corresponding relaxation times  $\tau_k$  are given by Eq. 12, while  $\tau_0 = \zeta/K$  is the characteristic relaxation time of the Rouse chain. It is a simple matter now to determine the maximal relaxation time  $\tau_{\text{chain}}$  of the Rouse chain of  $N$  beads ( $\tau_{\text{chain}}$  is often referred to as the Rouse time):

$$\tau_{\text{chain}} \equiv \frac{\tau_0}{\lambda_2} \simeq \frac{1}{\pi^2} N^2 \tau_0. \quad (57)$$

Hence  $\tau_{\text{chain}}$  grows as the square mass of the polymer chain,  $\tau_{\text{chain}} \sim M^2$ .

Remarkably, the boundary conditions, Eqs. 52 and 53, allow to establish the exact form of the normal mode transformation, Eq. 54, for the Rouse chain [40]:

$$\mathbf{R}_j(t) = \frac{1}{\sqrt{N}} \mathbf{Q}_1(t) + \sqrt{\frac{2}{N}} \sum_{k=2}^N \left[ \cos \left( j - \frac{1}{2} \right) \psi_k \right] \mathbf{Q}_k(t). \quad (58)$$

Here the numerical constants  $1/\sqrt{N}$  and  $\sqrt{2/N}$  were determined from the transformation of the potential energy and the dissipative function of the Rouse chain, see Eqs. 10 and 11. The normal coordinate  $\mathbf{Q}_1(t)$  corresponds to the vanishing eigenvalue  $\lambda_1 = 0$  and is related to the position vector of the center of mass  $\mathbf{R}_{\text{COM}}$ :

$$\mathbf{R}_{\text{COM}}(t) \equiv \frac{1}{N} \sum_{j=1}^N \mathbf{R}_j(t) = \frac{1}{\sqrt{N}} \mathbf{Q}_1(t). \quad (59)$$

Using Eq. 59 and the equation of motion for  $\mathbf{Q}_1(t)$ , it is a simple matter to compute the mean-square displacement of the center of mass of the Rouse chain at time  $t$ , averaged over the fluctuating forces:

$$\langle (\mathbf{R}_{\text{COM}}(t) - \mathbf{R}_{\text{COM}}(0))^2 \rangle = \frac{6k_B T}{N\zeta} t. \quad (60)$$

Therefore, the diffusion coefficient  $D_{\text{chain}}$  of the Rouse chain as a whole equals:

$$D_{\text{chain}} = \lim_{t \rightarrow \infty} \frac{1}{6t} \langle (\mathbf{R}_{\text{COM}}(t) - \mathbf{R}_{\text{COM}}(0))^2 \rangle = \frac{k_B T}{N\zeta}, \quad (61)$$

in other words, in the framework of the Rouse model,  $D_{\text{chain}}$  is inversely proportional to the mass of the chain ( $D_{\text{chain}} \sim M^{-1}$ ), a result which simply states that the chain feels all friction forces on its monomers additively. It is also instructive to study the relaxation of the end-to-end vector  $\mathbf{r}(t) = \mathbf{R}_N - \mathbf{R}_1$  of the Rouse chain. Its autocorrelation function can be reduced to the following compact form [2, 40, 41]:

$$\langle \mathbf{r}(t)\mathbf{r}(0) \rangle = \frac{6}{N} \frac{k_B T}{K} \sum_{k=2,4,6,\dots}^N \cot^2 \left( \frac{\psi_k}{2} \right) \exp(-t/\tau_k). \quad (62)$$

Based on this expression, one can estimate the decay of  $\langle \mathbf{r}(t)\mathbf{r}(0) \rangle$  in the intermediate time domain ( $\tau_0 \ll t \ll \tau_{\text{chain}}$ ):

$$\langle \mathbf{r}(t)\mathbf{r}(0) \rangle \simeq \frac{12}{\pi^2} \frac{k_B T}{K} N \exp \left( -\sqrt{\frac{t}{\tau_{\text{chain}}}} \right), \quad (63)$$

which obeys a square-root time dependence. For  $t > \tau_{\text{chain}}$  the autocorrelation function ends up with an exponential decay which is characterized by the Rouse time  $\tau_{\text{chain}}$ .

Now we turn to the dynamic viscoelastic properties of Rouse chains in dilute solutions. The storage and loss moduli of the Rouse chain are given by Eqs. 20 and 21, where the finite relaxation times are defined through Eqs. 55 and 56. Similar to all free-floating GGS, at very low frequencies,  $\omega \ll 1/\tau_{\text{chain}}$ , one has  $G'(\omega) \sim \omega^2$  and  $G''(\omega) \sim \omega$ . It is more interesting, however, to consider the behavior of the Rouse chain in the intermediate frequency domain,  $1/\tau_{\text{chain}} \ll \omega \ll \tau_0$ , where one has [1–3]:

$$[G'(\omega)] = [G''(\omega)] \simeq \frac{1}{2\sqrt{2}} \sqrt{\omega\tau_0}. \quad (64)$$

This square-root dependence on  $\omega$  is a fundamental feature of linear chains in the Rouse model. The shear modulus at intermediate frequencies is a signature of the internal, “intra-chain” dynamics, which is determined by the topology of the GGS. As stressed before, the viscoelastic relaxation forms can be expressed through the relaxation spectrum  $H(\tau)$ , see Eq. 27. Here one finds [3]:

$$H(\tau) \simeq \frac{1}{2\sqrt{2}} \frac{1}{\pi} \sqrt{\frac{\tau_0}{\tau}}, \quad \text{where } \tau_0 < \tau < \tau_{\text{chain}}. \quad (65)$$

One should note the appearance of a square-root behavior (now as a function of  $\tau$ ) in the  $H(\tau)$  of Rouse chains. Given the close relation between  $H(\tau)$  and  $G(t)$ , see Eq. 27, it can be shown that in the intermediate time domain,  $\tau_0 < t < \tau_{\text{chain}}$ , the relaxation modulus  $G(t)$  depends on time as:

$$[G(t)] \simeq \frac{1}{\pi\sqrt{2}} \sqrt{\frac{\tau_0}{t}}. \quad (66)$$

In other words, it also obeys a square-root dependence on time.

It has to be emphasized that the knowledge of the full form of the normal mode transformation, see Eq. 58, allows one to compute dynamic characteristics which are not averaged over the beads and which depend, therefore, on the position of the particular bead along the Rouse chain. To conclude this section, we will discuss two such examples.

First, let us focus on the mean-square displacement  $\langle \Delta R_j^2(t) \rangle = \langle (R_j(t) - R_j(0))^2 \rangle$  of the  $j$ th bead. Using Eq. 58, one obtains [41]:

$$\langle \Delta R_j^2(t) \rangle = \frac{6k_B T}{N\zeta} t + \frac{12k_B T}{NK} \sum_{k=2}^N \cos^2 \left[ \left( j - \frac{1}{2} \right) \psi_k \right] \frac{1 - \exp(-t/\tau_k)}{\lambda_k}. \quad (67)$$

At  $t \gg \tau_{\text{chain}}$ , the behavior of the  $\langle \Delta R_j^2(t) \rangle$  is governed by the first term in Eq. 67, which is simply the mean square displacement of the center of mass of the Rouse chain, see Eq. 60. Thus, we have the usual diffusive behavior of a free Brownian particle, whose root mean square behavior follows the ordinary law  $\sim t^{1/2}$ . At intermediate times,  $\tau_0 \ll t \ll \tau_{\text{chain}}$ , one has the following

behavior for  $\langle \Delta R_j^2(t) \rangle$ :

$$\langle \Delta R_j^2(t) \rangle \simeq \frac{12k_B T}{\pi K} \sqrt{\frac{t}{\tau_0}}. \quad (68)$$

Thus, in the intermediate time domain the root mean square displacement of a bead increases more slowly with time ( $\sim t^{1/4}$ ) than ordinary diffusion. The physical reason for this is clear: The fact that a given bead is connected to other beads in the chain effectively slows down its diffusive motion [41]. To complete the picture, we also consider the displacement of a bead under the influence of an external force, see Eq. 50; in the same domain of intermediate times ( $\tau_0 \ll t \ll \tau_{\text{chain}}$ ) one finds:

$$\langle \langle Y(t) \rangle \rangle \simeq \frac{2F_0^{(\text{ext})}}{\pi K} \sqrt{\frac{t}{\tau_0}}. \quad (69)$$

Not surprisingly, the temporal behavior in Eqs. 68 and 69 is the same (see also Eqs. 67 and 50), a consequence of the fluctuation-dissipation theorem, which relates the diffusion in the absence of an external field to the drift in such a field.

Finally, we consider the relaxation of the end-to-end subchain vector between neighboring beads,  $\mathbf{u}_j = (\mathbf{R}_{j+1} - \mathbf{R}_j)$ , where  $j = 1, \dots, (N - 1)$ . The autocorrelation function of the  $\mathbf{u}_j$  can also be computed using the normal mode transformation, Eq. 58. One finds [40]:

$$\langle \mathbf{u}_j(t) \mathbf{u}_j(0) \rangle = \frac{6k_B T}{NK} \sum_{k=2}^N \sin^2(j\psi_k) \exp(-t/\tau_k). \quad (70)$$

Interestingly, the expression for the autocorrelation function  $\langle \mathbf{u}_j(t) \mathbf{u}_j(0) \rangle$  is reminiscent of that of the relaxation modulus  $G(t)$ , Eq. 26. Their behaviors at  $\tau_0 \ll t \ll \tau_{\text{chain}}$  do indeed coincide (compare with Eq. 66):

$$\langle \mathbf{u}_j(t) \mathbf{u}_j(0) \rangle \simeq \frac{3k_B T}{\pi K} \sqrt{\frac{\tau_0}{t}}. \quad (71)$$

## 4.2

### Successes and Limitations of the Rouse Approach: Comparison with the Zimm and the Reptation Pictures

The Rouse model was initially designed to treat the dynamics of polymers in very dilute solutions [1]. Ironically, however, it turned out that dilute solutions are not appropriate systems for it. Indeed, in the Rouse model the maximal relaxation time,  $\tau_{\text{chain}}$ , and the diffusion coefficient,  $D_{\text{chain}}$ , scale with the molecular weight,  $M$ , as  $M^2$  and  $M^{-1}$ , respectively (see Eqs. 57 and 61). Furthermore, it is a straightforward matter to demonstrate that for the Rouse model at  $\omega = 0$  the zero shear viscosity  $[\eta'(0)]$  is proportional to  $M$ , see Eq. 22. All these theoretical findings disagree with the experimental data

on dilute polymer solutions, where in  $\theta$ -solvents one finds that  $\tau_{\text{chain}} \sim M^{3/2}$ ,  $D_{\text{chain}} \sim M^{-1/2}$ , and  $[\eta'(0)] \sim M^{1/2}$  [3]. The reason for this disagreement is that in dilute solutions the hydrodynamic interactions play a crucial role. These interactions are fully ignored in the Rouse model: the solvent is modeled as a continuous *immobile* medium, which is felt by the beads only through their viscous friction. However, in dilute polymer solutions the motion of a particular bead affects all the other beads through the perturbation of the solvent; in other words, the solvent mediates effective interactions between the beads. As was first demonstrated by Zimm [5], taking into account the hydrodynamic interactions significantly improves the agreement between experiment and model.

In the Zimm model (see Fig. 2A) the hydrodynamic interactions are included by employing the Oseen tensor  $H_{lm}$ ; the tensor describes how the  $m$ th bead affects the motion of the  $l$ th bead. This leads to equations of motion that are not linear anymore and that require numerical methods for their solution. In order to simplify the picture, the Oseen tensor is often used in its preaveraged form, in which one replaces the operator by its equilibrium average value [5]. For chains in  $\theta$ -solvents, this leads for the normal modes to equations similar to the Rouse ones, the only difference residing in the values of the relaxation times. An important change in behavior concerns the maximum relaxation time  $\tau_{\text{chain}}$ , which in the Zimm model depends on  $N$  as  $N^{3/2}$  and implies a speed-up in relaxation compared to the Rouse model. Accordingly, the zero shear viscosity decreases in the Zimm model and scales as  $N^{1/2}$ . Also, in the Zimm model the diffusion coefficient

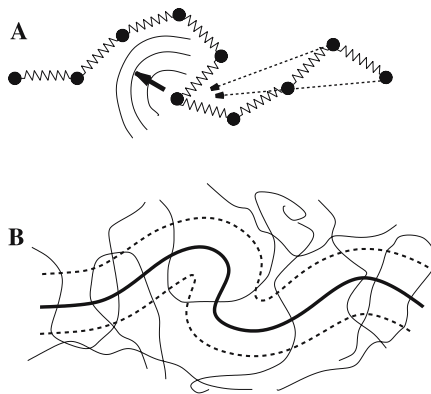


**Fig. 2** (A) Schematic representation of the Zimm model, which takes into account hydrodynamic interactions. The beads affect (through the solvent) the motion of a bead which is distant from them along the chain (not connected directly to them by means of springs). (B) Schematic representation of the reptation model. A given, long polymer chain moves in the tube formed by other chains

of chains,  $D_{\text{chain}} \sim N^{-1/2}$ , is larger than in the Rouse model. Moreover, the Zimm molecular mass dependencies of the maximal relaxation time, of the diffusion coefficient, and of the zero shear viscosity are all consistent with the experimental findings [3]. The Zimm model also agrees with the experiment with respect to the frequency dependence of the storage and loss moduli of dilute polymer solutions under  $\theta$ -conditions: both  $G'(\omega)$  and  $G''(\omega)$  show a  $\omega^{2/3}$ -behavior, in contrast to the Rouse situation, where the behavior turns out to be proportional to  $\omega^{1/2}$ , see Eq. 64 [2, 3].

As the concentration of the polymer solution increases, the experiments show a systematic change from Zimm-like to Rouse-like behavior (see for example the monograph of Ferry [3] and references therein). The reason for this finding is the screening of the hydrodynamic interactions: in the semidilute regime different polymer chains start to overlap and the hydrodynamic interactions between fragments of the same chain are screened from each other by the presence of other chains. The dynamic crossover from the Zimm to the Rouse behavior was the subject of a number of theoretical studies [42–44]. The dynamics of semidilute solutions is well-represented in terms of the so-called “blob” model. A blob is a group of monomers of a given chain, whose size is of the order of the hydrodynamic screening length  $\xi_H$ . At scales smaller than  $\xi_H$ , monomers of a particular chain do not feel the presence of the other chains and, therefore, the hydrodynamic interactions are not screened, leading to a Zimm-like behavior. At larger scales, the intra-blob (Zimm) relaxation ends, the blobs can be envisaged as being Stokes spheres, and the mutual interactions between them draw their mobility down, which gives rise to a Rouse-like behavior [44]. Furthermore, the results of recent computer simulations [45] show that the time scales matter as well as the length scales: at times shorter than the blob relaxation time there is no screening of the hydrodynamic interactions and the polymer motion is essentially Zimm-like on *all* length scales [45]. This also explains the experimental observation of an incomplete screening on length scales above the hydrodynamic screening length  $\xi_H$  [46].

With a further increase in concentration one reaches the regime of concentrated solutions and melts. Here it is crucial to distinguish two different situations, which involve either short (unentangled) or long (entangled) chains. The border line between these situations is given by the so-called entanglement length  $N_e$  [2, 3], which is different for different polymers (for instance, the molecular weight of a polystyrene macromolecule at entanglement length is about 20 000). For polymer melts of short chains ( $N < N_e$ ) the Rouse model provides an excellent description of the long-time dynamical behavior, a fact well-documented both experimentally [3, 47] and by computer simulations [48–53]; some deviations, however, have also been reported [54]. In melts of short chains the hydrodynamic interactions are absent (there is no solvent in the melt) and entanglement effects do not play a noticeable role. The dynamics of a particular chain in the melt can be viewed as being that

of a Rouse chain embedded in an effective viscous medium, created by the other chains of the melt [2, 3]. It should be noted that it is still an open question as to why such a complicated system as a short-chain polymer melt can be described well by means of the simple Rouse model.

In melts of long chains (longer than the entanglement length  $N_e$ ) the topological constraints lead to a considerable slowing down of the motion of the monomers. The individual chains do not follow the Rouse behavior anymore. The dynamics of such entangled melts can be described in terms of the reptation (tube) model, first proposed by de Gennes [4]. Here each chain moves in an effective tube formed by the other chains, see Fig. 2B. At short times the chain does not feel the tube and one finds an unconstrained Rouse-like behavior. This holds up to a time  $\tau_e$ , which is just the maximal relaxation time of a Rouse chain of length  $N_e$  ( $\tau_e \sim N_e^2$ ). At longer times the polymer chain can only move along the tube; evidently, in the course of time, the original tube is slowly destroyed by the forward and backward motions of the chain [2, 4, 55]. The longest relaxation time is the time of disengagement of the chain from the original tube (or, equivalently, the average lifetime of the tube); it is found to scale as  $N^3$  [2, 4, 41]. The diffusion of the chain in the entangled melt is also slowed down when compared to the Rouse behavior; in the tube model the diffusion coefficient turns out to be proportional to  $N^{-2}$  [2, 4]. An extension of the tube model to concentrated solutions and melts of *polydisperse* entangled polymers was also carried out [56]. We note that the crossover from the Rouse behavior to reptation has been confirmed through numerous computer simulations [48, 57–59]. Furthermore, reptation successfully explains the appearance of a plateau region in the relaxation modulus, as observed in uncrosslinked polymer melts of high molecular weight [3].

All in all, the Rouse model provides a reasonable description of polymer dynamics when the hydrodynamic interactions, excluded volume effects and entanglement effects can be neglected; a classical example of its applicability is short-chain polymer melts. Since the Rouse model is exactly solvable for polymer chains, it represents a basic reference frame for comparison with more involved models of polymer dynamics. In particular, the decoupling of the dynamics of the Rouse chain into a set of independently relaxing normal modes is fundamental and plays an important role in other cases, such as more complex objects of study, or in other models, such as the Zimm model.

## 5

### Regular Mesh-Like Polymer Networks

After the above historical retrospective devoted to linear Rouse chains, we follow the extension of this approach to polymer systems that have more complex topologies. We focus first on the dynamics of networks cross-linked from

Rouse chains. The fundamental feature here is the appearance of cooperative interchain motions due to cross-linking. First approaches to evaluating the dynamical properties of such networks started from the intrachain relaxation, and accounted for the connectivity between chains only in simplified, effective ways. For instance, the dynamics of Rouse chains that have fixed (constant) end-to-end distances were studied [60]. Alternatively, Mooney considered Rouse chains with fixed (immobile) ends as a model for a polymer network [3, 61]. In particular, he found that the relaxation modulus of such a chain coincides with that of a Rouse chain with free ends, except for a constant contribution, which can be considered as being the nonvanishing, equilibrium modulus of the network. However, the idea of the GGS formalism is to take the connectivity exactly into account, see Eqs. 1 and 2. In order to gradually increase the complexity of the networks, one can start by first considering chains cross-linked into regular spatial structures. This is the subject of the present section.

## 5.1

### Regular Network Models for Cooperative Interchain Relaxation

#### 5.1.1

##### 3-D Model Networks

The classical Rouse treatment was originally developed for linear chains. If one views the linear polymer chain as a one-dimensional regular string of beads connected by springs, then a straightforward and obvious extension is to build from beads and springs regular lattices of higher dimensions. Such an approach was suggested by Gotlib [62] for studying the low-frequency modes of polymer networks. Since real cross-linked polymers are normally 3-D structures, cubic networks were first to attract the attentions of researchers [24, 30, 62, 63]. Cubic networks were employed to study interchain friction effects [62, 63], dielectric relaxation [30], and various aspects of mechanical viscoelastic relaxation [24, 64, 65]. One should, of course, note at all stages of our discussion that only the *topological* structure of the networks is regular. In their *spatial appearance* in solution, the networks are quite disordered (stretched, folded, and twisted), as befits their very mobile beads. All of the GGS displayed in this review are drawn such as to render their *topologies* clear; hence the drawings are, in fact, very atypical of the general locations of the beads in *space*.

In the following we sketch some simple ways for determining the dynamics of simple cubic networks: here we prefer not to use the general approach, exemplified by Eqs. 2 and 9, which involves matrix diagonalizations [64, 65], because for cubic networks the analysis can be done in a simple way by means of normal mode (Fourier) transformations. We remark that simple cubic networks are also a coarse-grained model for more complex systems, like those

built from Rouse chains connected regularly into a cubic framework. We will study such systems in detail in Sect. 5.2.1. Coarse-graining implies replacing each Rouse chain by a spring; the price to be paid for this is that the intrachain eigenfrequencies are lost.

We hence start with a cubic network formed by beads which have an identical friction constant,  $\zeta$ , and which are connected to each other by means of elastic Hookean springs with elasticity constant  $K$ , see Fig. 3. The network is embedded into an effective viscous medium and is a regular structure in the sense of connectivity only. Every site of the cubic network is denoted by a three-dimensional index  $\Omega = (\alpha, \beta, \gamma)$ . The Langevin equation of motion, Eq. 2, can be rewritten here as:

$$\begin{aligned} \zeta \frac{d}{dt} \mathbf{R}(\alpha, \beta, \gamma; t) + K[6\mathbf{R}(\alpha, \beta, \gamma; t) - \mathbf{R}(\alpha + 1, \beta, \gamma; t) \\ - \mathbf{R}(\alpha - 1, \beta, \gamma; t) - \mathbf{R}(\alpha, \beta + 1, \gamma; t) - \mathbf{R}(\alpha, \beta - 1, \gamma; t) \\ - \mathbf{R}(\alpha, \beta, \gamma + 1; t) - \mathbf{R}(\alpha, \beta, \gamma - 1; t)] \\ = \mathbf{f}(\alpha, \beta, \gamma; t). \end{aligned} \quad (72)$$

Here  $\mathbf{R}(\alpha, \beta, \gamma; t)$  denotes the position vector of the network junction  $\Omega = (\alpha, \beta, \gamma)$  and  $\mathbf{f}(\alpha, \beta, \gamma; t)$  is the corresponding stochastic force (thermal noise), again assumed to be Gaussian with zero mean value.

In spite of the fact that it is easy to get a solution for the cubic polymer network with free boundaries (in a quite analogous way as for the linear Rouse chain with free ends), we will consider here a network with periodic boundary conditions (PBC). In doing so, we use the same formalism as later, when we consider more complex systems, for which analytical solutions are known only under PBC. In our case such PBC mean that  $\mathbf{R}(1, \beta, \gamma; t) = \mathbf{R}(N + 1, \beta, \gamma; t)$ ,  $\mathbf{R}(\alpha, 1, \gamma; t) = \mathbf{R}(\alpha, N + 1, \gamma; t)$ , and  $\mathbf{R}(\alpha, \beta, 1; t) = \mathbf{R}(\alpha, \beta, N + 1; t)$ , where  $N$  is a number of beads along a given di-

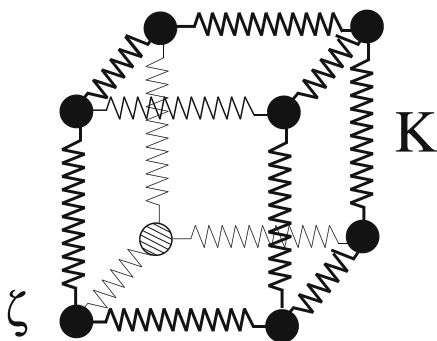


**Fig. 3** One elementary cell of a cubic network built from beads (each having friction constant  $\zeta$ ) which are connected by elastic springs each with elasticity constant  $K$

rection of the network (the total number of junctions in our cubic networks being equal to  $N^3$ ).

The Langevin equation of motion, Eq. 72, can be easily solved by means of a transformation from the Cartesian coordinates  $R$  to the normal coordinates  $Q$ , Eq. 9. The transformation reads:

$$R(\alpha, \beta, \gamma; t) = \frac{1}{N^{3/2}} \sum_{\mathbf{k}} \exp[i(\alpha k_1 + \beta k_2 + \gamma k_3)] Q(k_1, k_2, k_3; t). \quad (73)$$

Here the triple  $\mathbf{k} = (k_1, k_2, k_3)$  is not a reciprocal vector as in solid state physics, because the network does not possess translational symmetry. We will view  $\mathbf{k}$  rather as describing a phase shift between the different  $\Omega$ .

Inserting Eq. 73 into the Langevin equations of motions, Eq. 72, immediately leads to the eigenvalues of the simple cubic network [24, 30, 62, 63]:

$$\lambda(\mathbf{k}) = 2(3 - \cos k_1 - \cos k_2 - \cos k_3). \quad (74)$$

The periodic boundary conditions allow us, in turn, to restrict  $\mathbf{k}$  to the values:

$$k_1 = \frac{2\pi m_1}{N}, \quad k_2 = \frac{2\pi m_2}{N}, \quad \text{and} \quad k_3 = \frac{2\pi m_3}{N}, \quad (75)$$

where the integers  $m_1$ ,  $m_2$ , and  $m_3$  range from 0 to  $(N - 1)$ . Equations 74 and 75 fully determine the eigenvalues of the cubic network. Each normal mode  $Q(\mathbf{k}; t)$  then decays exponentially with the relaxation time (see also Eq. 12):

$$\tau(\mathbf{k}) = \frac{\tau_0}{\lambda(\mathbf{k})}, \quad (76)$$

where  $\lambda(\mathbf{k})$  are as in Eq. 74 and  $\tau_0$  is its characteristic relaxation time,  $\tau_0 = \zeta/K$ . Remarkably, since the normal modes (the eigenfunctions), Eq. 73, are also known, it is possible to obtain analytical expressions not only for the macroscopic dynamic characteristics (dynamic modulus and viscosity), but also for the local quantities (not averaged over the  $\Omega$ ), such as the autocorrelation function of the end-to-end chain vector between neighboring cross-links [66]. Note that Eq. 74 was also obtained in [64, 65], by means of rather complicated operations involving connectivity matrices.

Now we compare the viscoelastic mechanical properties of a topological cubic structure to those of a linear chain. Since for the former the relaxation times are known, see Eqs. 76, 74 and 75, it is now a straightforward matter to calculate the dynamic modulus and to estimate its behavior in different frequency domains analytically. It turns out that the storage modulus  $G'(\omega)$  of cubic networks obeys a  $\omega^{3/2}$  form in the region of intermediate frequencies; this is very different from the behavior of a Rouse chain, where in the intermediate range  $G'(\omega)$  has a  $\omega^{1/2}$  form, see Fig. 4.

The underlying reason for these findings is the fact that for a cubic network the relaxation spectrum  $H(\tau)$  decays as  $\tau^{-3/2}$ , and thus more quickly

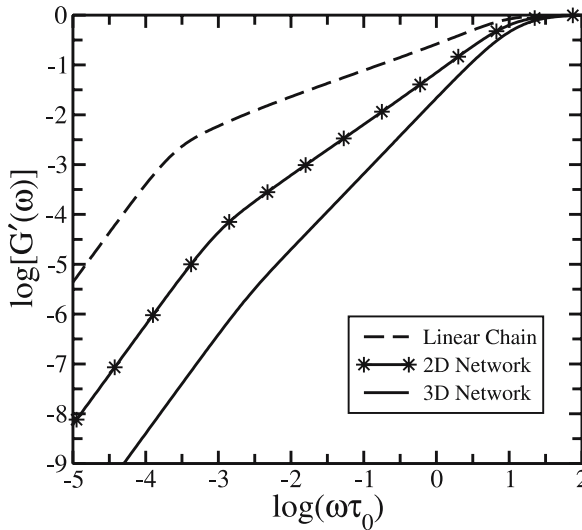


**Fig. 4** Reduced storage modulus  $[G'(\omega)]$  plotted on double logarithmic scales versus the reduced frequency  $\omega\tau_0$ . Shown are results for a linear Rouse chain of 250 beads (*dashed line*), for a topologically-square network ( $250 \times 250$ ), *solid line* with stars, and for a topologically cubic network ( $150 \times 150 \times 150$ ), *solid line*. For simplicity, the characteristic time  $\tau_0 = \zeta/K$  was chosen to be the same for all three systems

than for the Rouse chain, where  $H(\tau)$  obeys a  $\tau^{-1/2}$  form. This  $H(\tau)$ -behavior also leads to a faster decay of the relaxation modulus, which now follows  $G(t) \sim t^{-3/2}$  instead of  $G(t) \sim t^{-1/2}$  for the Rouse chain. Physically, the behavior of the cubic network can be understood based on the increased growth of the number of nearest neighbors, next-nearest neighbors, next-next-nearest neighbors, and so on. This picture is very akin to the definition of the fractal dimension; in fact, in Sect. 6 we will see that similar power-law forms for  $G'(\omega)$ ,  $G''(\omega)$ , and  $G(t)$  also hold for fractal networks, but that the exponents are related to the *spectral* dimension of the fractal.

It is perhaps also worth noting that the  $\tau^{-3/2}$  behavior of the relaxation spectrum  $H(\tau)$  of a cubic network is due to its three-dimensional connectivity character but *not* to the details of the particular network structure. In the fractal framework the spectral dimension of all these networks is 3, and the relaxation behavior is universal. In this regard the work of Denneman et al [64] is very instructive. The authors considered Hookean springs cross-linked into the three Bravais cubic lattices, namely simple cubic (sc) (this corresponds to the network considered above), body-centered cubic (bcc), and face-centered cubic (fcc). They succeeded in finding analytical expressions for the eigenvalues of the sc lattice (they coincide with Eq. 74) but not for the bcc and fcc lattices, which were treated numerically. It turns out (in agreement with the statement above), that the dynamic modulus for all

three cubic lattices has the same frequency behavior, the only difference being a slightly different value of the characteristic (minimal) relaxation time. In [64] it is found that  $\tau_{sc} > \tau_{bcc} > \tau_{fcc}$  and that this difference results in a shift of the corresponding modulus curves along the frequency axis.

### 5.1.2

#### 2-D Model Networks

In order to illustrate the fundamental role of the dimensionality in the dynamical behavior of networks, it is instructive to consider topologically two-dimensional networks, see Fig. 5 for an example. While as a rule many cross-linked polymers display a three-dimensional character, say, based on their  $H(\tau)$ -behavior, two-dimensional structures may be realized in polymer films, by deposition on surfaces, and so on. Furthermore, two-dimensional networks are intermediate between the two cases (1-D and 3-D) already discussed; two-dimensional systems have dynamical features which interpolate between the previous findings.

A comparative study of the equilibrium properties of coarse-grained topological cubic and square networks was performed by Ronca and Allegra, who employed electrical analogs for this purpose [67]. In particular, they found that the mean-square radius of gyration of a two-dimensional network increases logarithmically with the total number of network junctions, while it is of the same order of magnitude as that of a single bond in the case of a three-dimensional network. A more general result, based on fractal systems and ideas, and which also includes this finding, is provided in [6].

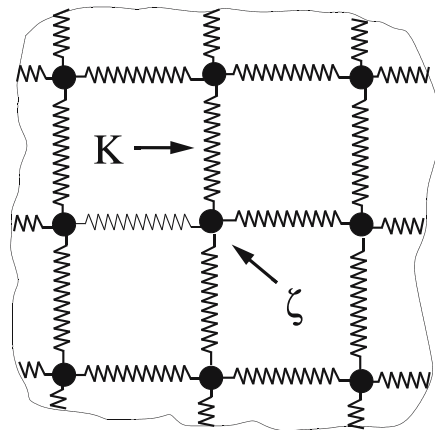


**Fig. 5** Sketch of a square network built from beads each with friction constant  $\zeta$ , which are connected by elastic springs each with elasticity constant  $K$

The dynamics of a topologically square network can be treated along the lines used for the cubic network above. The Langevin equations of motion for a square network are similar to those of the cubic network:

$$\begin{aligned} \zeta \frac{d}{dt} \mathbf{R}(\alpha, \beta; t) + K[4\mathbf{R}(\alpha, \beta; t) - \mathbf{R}(\alpha + 1, \beta; t) \\ - \mathbf{R}(\alpha - 1, \beta; t) - \mathbf{R}(\alpha, \beta + 1; t) \\ - \mathbf{R}(\alpha, \beta - 1; t)] \\ = f(\alpha, \beta; t), \end{aligned} \quad (77)$$

where  $\mathbf{R}(\alpha, \beta; t)$  denotes the position vector of a bead and where we set  $\boldsymbol{\Omega} = (\alpha, \beta)$ . Applying the two-dimensional analog ( $k_3 = 0$ ) of the normal mode transformation, Eq. 73, one obtains the following set of eigenvalues for the square network [68, 69]:

$$\lambda(\mathbf{k}) = 2(2 - \cos k_1 - \cos k_2), \quad (78)$$

where the phase shift  $\mathbf{k} = (k_1, k_2)$  between the  $\boldsymbol{\Omega}$  is given by Eq. 75 with  $k_3 = 0$ . The same analytical expression for the eigenvalues (relaxation times) was previously found by Denneman et al [65].

Analysis of the dynamical viscoelastic quantities shows that the relaxation spectrum  $H(\tau)$  of the two-dimensional network goes as  $H(\tau) \sim 1/\tau$  [65, 68–70]. Hence 2-D networks do indeed show dynamical behavior intermediate between that of linear chains and that of 3-D networks. Moreover, in a fractal picture, square networks may be viewed as being fractals and as having a spectral dimension of 2. Now  $H(\tau) \sim 1/\tau$  leads to an  $\omega^1$ -behavior for the storage modulus  $G'(\omega)$ , see Fig. 4, and to  $G(t) \sim 1/t$ .

At this stage one can already note the general scaling behavior of  $H(\tau)$  and its dependence on the dimensionality  $d$  of the networks. One can summarize our discussion by noting that for all  $d$  considered  $H(\tau) \sim \tau^{-d/2}$  and thus also  $G'(\omega) \sim \omega^{d/2}$  and  $G(t) \sim t^{-d/2}$ . In Sect. 6 we will see that these expressions stay unchanged when replacing  $d$  by  $\tilde{d}$ , the *spectral* dimension. Furthermore, the above-mentioned differences in the equilibrium properties of two- and three-dimensional networks are also manifest in the local dynamic properties, stressing the universal role of  $d$ . We mention that the mean-square displacement of a bead of a 2-D network under stochastic forces grows with the time  $t$  as  $\log(t/\tau)$ , while the same dynamical quantity in a 3-D network reaches a finite, limiting value at long times [68, 69]. This concurs with the findings of Ronca and Allegra [67], is in line with the previously mentioned findings on the mean-square radius of gyration (fluctuation-dissipation theorem), and is a special case of the fractal picture [6].

## 5.2

### Topologically-Regular Networks Built from Rouse Chains: Exactly Solvable Models

#### 5.2.1

#### Topologically-Cubic Networks

After the simple topological structures (cubic and square) just discussed, we turn now to the analysis of regular networks built from Rouse chains. This allows us to study an important problem in polymer network dynamics, namely the way in which the cross-linking of Rouse chains (or, as we will discuss in later sections, of more complex units) into larger structures is reflected in the dynamics of the resulting networks.

For simplicity we consider end-linked polymer networks and we disregard, as is usual with GGS, entanglement effects. A simple model of a three-dimensional structure, which explicitly takes into account the connectivity between polymer chains, is a regular cubic network cross-linked from Rouse chains. Remarkably, it turns out that under certain conditions the dynamical problem for such a network can be fully solved analytically [25, 66, 71]. This solution provides insight into the network's dynamics and is, therefore, worth detailed consideration.

We start with a regular cubic network which has cross-link points (network junctions) as vertices; these are connected by means of identical Rouse chains, see Fig. 6. All Rouse chains in the network consist of the same number  $n$  of beads (having a friction constant  $\zeta$ ); they are connected among

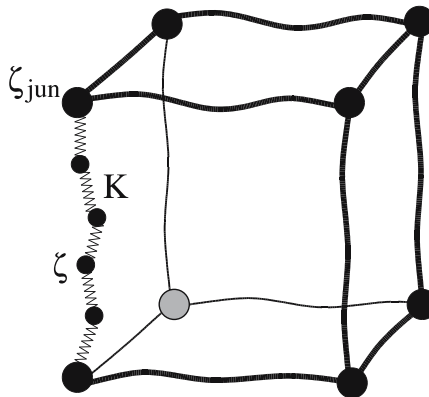


**Fig. 6** An elementary cell of a topologically-regular cubic network cross-linked from Rouse chains. One of the network chains between two cross-links (junctions) is shown in detail. Note that the dynamic problem of such a network can be exactly solved only under the condition that the friction constant of each network junction,  $\zeta_{\text{jun}}$ , is three times larger than that of a chain bead, see text for details

themselves and via the corresponding cross-links by  $(n + 1)$  identical elastic springs each with elasticity constant  $K$ . Each cell of the cubic network under study contains one junction (cross-link) and three Rouse chains attached to it; it is denoted by the three-dimensional index  $\boldsymbol{\Omega} = (\alpha, \beta, \gamma)$ . The network is assumed to consist of  $N^3$  junctions (cross-links), so there are  $N$  junctions along each of the three network directions and the  $\alpha$ ,  $\beta$ , and  $\gamma$  indices range from 1 to  $N$ . The whole network is embedded into a continuous viscous medium. Then one has the following Langevin equations of motion for the beads of the chains:

$$\zeta \frac{d}{dt} \mathbf{R}_p(\boldsymbol{\Omega}; j; t) + K[2\mathbf{R}_p(\boldsymbol{\Omega}; j; t) - \mathbf{R}_p(\boldsymbol{\Omega}; j + 1; t) - \mathbf{R}_p(\boldsymbol{\Omega}; j - 1; t)] = \mathbf{f}_p(\boldsymbol{\Omega}; j; t) \quad (79)$$

and for the network junctions (cross-linking points of the chains):

$$\begin{aligned} \zeta_{\text{jun}} \frac{d}{dt} \mathbf{R}_0(\alpha, \beta, \gamma; t) + K[6\mathbf{R}_0(\alpha, \beta, \gamma; t) - \mathbf{R}_1(\alpha, \beta, \gamma; 1; t) \\ - \mathbf{R}_1(\alpha - 1, \beta, \gamma; n; t) - \mathbf{R}_2(\alpha, \beta, \gamma; 1; t) \\ - \mathbf{R}_2(\alpha, \beta - 1, \gamma; n; t) - \mathbf{R}_3(\alpha, \beta, \gamma; 1; t) \\ - \mathbf{R}_3(\alpha, \beta, \gamma - 1; n; t)] \\ = \mathbf{f}_0(\alpha, \beta, \gamma; t). \end{aligned} \quad (80)$$

Here  $\mathbf{R}_p(\boldsymbol{\Omega}; j; t)$  denotes the position vector of the  $j$ th bead of the  $p$ th Rouse chain in the network cell  $\boldsymbol{\Omega} = (\alpha, \beta, \gamma)$  (we recall that  $j = 1, \dots, n$  and  $p = 1, \dots, 3$ ),  $\mathbf{R}_0(\boldsymbol{\Omega}; t)$  is the corresponding position vector of the network junction  $\boldsymbol{\Omega}$ , and  $\mathbf{f}_p(\boldsymbol{\Omega}; j; t)$  and  $\mathbf{f}_0(\boldsymbol{\Omega}; t)$  are stochastic forces acting on the chain beads and on the network junctions. Note that the chain beads and the network junctions (cross-links) may have different friction constants,  $\zeta$  and  $\zeta_{\text{jun}}$ , respectively. For simplicity, we apply periodic boundary conditions and choose, because of later convenience, to express them through the coordinates of the chain beads:

$$\mathbf{R}_1(0, \beta, \gamma; n; t) = \mathbf{R}_1(N, \beta, \gamma; n; t), \quad (81)$$

$$\mathbf{R}_2(\alpha, 0, \gamma; n; t) = \mathbf{R}_2(\alpha, N, \gamma; n; t), \quad (82)$$

and

$$\mathbf{R}_3(\alpha, \beta, 0; n; t) = \mathbf{R}_3(\alpha, \beta, N; n; t). \quad (83)$$

To solve the Langevin equations of motion, one can use the following transformations from Cartesian coordinates  $\mathbf{R}$  to normal coordinates  $\mathbf{Q}$ :

$$\mathbf{R}_p(\boldsymbol{\Omega}; j; t) = \sum_{\mathbf{k}, \psi} \exp(i\boldsymbol{\Omega} \cdot \mathbf{k})(A_p \sin j\psi + B_p \cos j\psi)\mathbf{Q}(\mathbf{k}; \psi; t) \quad (84)$$

and

$$\mathbf{R}_0(\boldsymbol{\Omega}; t) = \sum_{\mathbf{k}, \psi} \exp(i\boldsymbol{\Omega} \cdot \mathbf{k}) B_0 \mathbf{Q}(\mathbf{k}; \psi; t). \quad (85)$$

Here the triple  $\mathbf{k} = (k_1, k_2, k_3)$  is related to the “global” phase shift between different network cells and  $\boldsymbol{\Omega} \cdot \mathbf{k}$  is the scalar product. In contrast, the intrachain quantity  $\psi$  corresponds to “local” phase shifts between neighboring beads along the chains. As usual, an exponential decay of every normal mode is characterized by the relaxation time  $\tau(\psi)$  connected with the eigenvalues  $\lambda(\psi)$  of the corresponding connectivity matrix of the network through Eq. 12, with  $\tau_0 = \zeta/K$ . Inserting the normal mode transformation, Eq. 84, into the Langevin equations of motion for the beads of the chains, Eq. 79, leads to the following set of eigenvalues  $\lambda(\psi)$ :

$$\lambda(\psi) = 2(1 - \cos \psi). \quad (86)$$

Formally, the expression for the eigenvalues has the same form as that for the linear Rouse chain. Now, however, the intrachain phase shift  $\psi$  has to be coupled to the triple  $\mathbf{k} = (k_1, k_2, k_3)$ . The latter can be easily determined by inserting the equations of motion for non-junction chain beads, Eq. 79, into the periodic boundary conditions, Eqs. 81 to 83. It brings us again to Eq. 75 for  $k_1, k_2$ , and  $k_3$ .

In order to obtain the intrachain phase shift  $\psi$  as well as the transformation from the Cartesian coordinates to the normal coordinates, seven constants,  $A_1, A_2, A_3, B_0, B_1, B_2$ , and  $B_3$ , have to be determined, see Eqs. 84 and 85. For these purposes one can use the Langevin equations of motion for the network junctions (cross-links), Eq. 80. Formally we also add the following six conditions at the junction points:

$$\mathbf{R}_0(\alpha, \beta, \gamma; t) = \mathbf{R}_1(\alpha - 1, \beta, \gamma; n + 1; t), \quad (87)$$

$$\mathbf{R}_0(\alpha, \beta, \gamma; t) = \mathbf{R}_2(\alpha, \beta - 1, \gamma; n + 1; t), \quad (88)$$

$$\mathbf{R}_0(\alpha, \beta, \gamma; t) = \mathbf{R}_3(\alpha, \beta, \gamma - 1; n + 1; t), \quad (89)$$

$$\mathbf{R}_0(\alpha, \beta, \gamma; t) = \mathbf{R}_1(\alpha, \beta, \gamma; 0; t), \quad (90)$$

$$\mathbf{R}_0(\alpha, \beta, \gamma; t) = \mathbf{R}_2(\alpha, \beta, \gamma; 0; t), \quad (91)$$

$$\mathbf{R}_0(\alpha, \beta, \gamma; t) = \mathbf{R}_3(\alpha, \beta, \gamma; 0; t). \quad (92)$$

The physical meaning of Eqs. 87 to 92 is that we envisage the chains to be connected in such a way that three chain beads create a junction point. Equations 87 to 92 express the conditions that the coordinates of the beads 0 (or, equivalently,  $(n + 1)$ ) lie exactly at the positions of the junctions. Logically then, the friction constant of a network junction is three times larger than that of a network chain bead:

$$\zeta_{\text{jun}} = 3 \zeta. \quad (93)$$

It turns out that under these conditions the modes of the network system can be determined analytically. In this case the Langevin equations for the network junctions, Eq. 80, may be represented as a superposition of three equations of motion for chain beads, Eq. 79. Considering Eq. 80 and the boundary conditions for the cross-links points, Eqs. 87 to 92, jointly, leads to the following sets of allowed values for the intrachain phase shift  $\psi$  (which, in turn, fixes the eigenvalues through Eq. 86) [25, 66, 71]:

$$\cos [(n+1)\psi_1] = \frac{1}{3}(\cos k_1 + \cos k_2 + \cos k_3), \quad (94)$$

$$\sin [(n+1)\psi_2] = 0, \quad (95)$$

and

$$\sin [(n+1)\psi_3] = 0. \quad (96)$$

Or, alternatively, one has:

$$\psi_1 = \frac{2\pi}{n+1}l_1 \pm \frac{1}{n+1} \arccos \left[ \frac{1}{3} (\cos k_1 + \cos k_2 + \cos k_3) \right], \quad (97)$$

$$\psi_2 = \frac{\pi}{n+1}l_2, \quad (98)$$

and

$$\psi_3 = \frac{\pi}{n+1}l_3. \quad (99)$$

Here  $l_1 = 0, \dots, (n/2)$ ,  $l_2 = 1, \dots, n$ , and  $l_3 = 1, \dots, n$ , provided that  $n$  is an even integer. Note that in Eq. 97 the sign  $+$  should be taken for  $l_1 = 0$  and both signs  $\pm$  for  $l_1 \neq 0$ .

Equations 97 to 99 indicate that there are three branches in the relaxation spectrum of the polymer network under study. First, the main branch  $\psi_1$ , defined by Eq. 97, includes the phase shift along the Rouse chain (see the first term in Eq. 97) and also  $k = (k_1, k_2, k_3)$ . Therefore, this branch involves both intra- and interchain relaxation processes, which are coupled in a rather complicated way, see Eq. 97. Remarkably, when the intrachain phase shift does not contribute to  $\psi_1$  ( $l_1 = 0$  in Eq. 97) one has a purely interchain sub-branch,  $\psi_{\text{net}} \equiv \psi_1(l_1 = 0)$  [25, 66]:

$$\psi_{\text{net}} = \frac{1}{n+1} \arccos \left[ \frac{1}{3} (\cos k_1 + \cos k_2 + \cos k_3) \right], \quad (100)$$

which corresponds to the cooperative network relaxation only. In contrast, when  $l_1 \neq 0$ , intrachain relaxation also shows up. The corresponding sub-branch depends now on the phase shift  $k$  between the network sites. More specifically, each intrachain mode  $2\pi l_1/(n+1)$  in Eq. 97 is split into bands consisting of a large number of sublines. These sublines are related to the different values of  $k$ . Second, the sets  $\psi_2$  and  $\psi_3$ , defined by Eqs. 98 and 99, give the purely intrachain branches of the relaxation spectrum. In fact, this

is a single double-degenerated branch, which does not depend on the phase shift between the network cells and which coincides with the spectrum of the Rouse chain with fixed ends [25, 66].

At this point, it is worth pointing out the relation between the present network model built from Rouse chains and the coarse-grained interpretation of the cubic network considered in Sect. 5.1.1. The underlying idea is that, on sufficiently large scales ( $k \ll 1$ ), which correspond to the relaxation of the large network, both models must lead to the same set of relaxation times (eigenvalues). The comparison of Eq. 74 in the coarse-grained case with Eqs. 86 and 100 for a network cross-linked from Rouse chains leads to the following relationship between the characteristic relaxation times of both models [25, 66]:

$$\tau_{CG} = 3(n+1)^2 \tau_0, \quad (101)$$

where CG indicates coarse-graining. Equation 101 has a nice physical interpretation in terms of the elasticity and friction constants, namely  $K_{CG} = K/(n+1)$  and  $\zeta_{CG} = 3(n+1)\zeta$ . In other words, the elastic constant of a spring in a coarse-grained network is equal to the overall elasticity of the Rouse chain between the cross-links (one has  $(n+1)$  springs of elasticity  $K$  connected in series) and the friction of a junction in a coarse-grained network corresponds to the friction of a junction ( $\zeta_{\text{jun}} = 3\zeta$ ) in a network of Rouse chains plus half of the contributions of the six Rouse chains ( $6(n/2)\zeta$ ) directly attached to this junction. These relations provide a straightforward mapping of the cooperative interchain relaxation of a network built from Rouse chains to a less-detailed, coarse-grained model.

To summarize, the relaxation times (or eigenvalues) of a rather complex system such as a 3-D topologically-regular network end-linked from Rouse chains were determined analytically. In fact, one can do even better: it is possible to construct all of the *eigenfunctions* of the network analytically (which amounts to the transformation from Cartesian coordinates to normal coordinates). Briefly, to construct the normal mode transformation, see Eqs. 84 and 85, one has to combine the Langevin equations of motion of a network junction, Eq. 80, and the boundary conditions in the network junctions, Eqs. 87 to 92. After some algebra one finds [25, 66]:

$$\begin{aligned} R_p(\boldsymbol{\Omega}; j; t) \simeq & \sum_{k, \psi_1} \frac{\exp(ik_p) \sin(j\psi_1) + \sin[(n+1-j)\psi_1]}{\sin[(n+1)\psi_1]} \quad (102) \\ & \times \exp(i\boldsymbol{\Omega} \cdot \mathbf{k}) Q_1(\mathbf{k}; \psi_1; t) \\ & + \sum_{k, \psi_2} \exp(i\boldsymbol{\Omega} \cdot \mathbf{k}) f_p(\mathbf{k}, \psi_2) \sin(j\psi_2) Q_2(\mathbf{k}; \psi_2; t) \\ & + \sum_{k, \psi_3} \exp(i\boldsymbol{\Omega} \cdot \mathbf{k}) f_p(\mathbf{k}, \psi_3) \sin(j\psi_3) Q_3(\mathbf{k}; \psi_3; t). \end{aligned}$$

Here  $Q_1(\mathbf{k}; \psi_1; t)$ ,  $Q_2(\mathbf{k}; \psi_2; t)$ , and  $Q_3(\mathbf{k}; \psi_3; t)$  are three sets of normal coordinates (eigenfunctions), which are related to the corresponding branches of the relaxation spectrum ( $\psi_1$ ,  $\psi_2$ , and  $\psi_3$ ), the  $f_p(\mathbf{k}, \psi)$  are functions of  $\mathbf{k}$ ,  $\psi_2$ , and  $\psi_3$ ; furthermore, the index  $p$  represents a particular chain in a given network cell and can take the values 1, 2, or 3 for one of the three chains in the network cell, respectively, or the value 0 for a network junction.

Knowledge of the eigenfunctions, Eq. 102, allows us to get analytical expressions not only for the macroscopic dynamic characteristics (averaged over all monomers), but also for local quantities of interest, related to individual cross-links or individual chain monomers [25, 66]. In view of space restrictions we will not provide these details here, instead we turn to the discussion of the macroscopic viscoelastic properties of the system. The reader interested in the details is referred to the original papers [25, 66].

An analysis of the viscoelastic mechanical relaxation of polymer networks built from Rouse chains shows the appearance of a new characteristic time (in addition to  $\tau_0$ ), namely the (maximal) relaxation time of a chain between neighboring network junctions,  $\tau_{\text{chain}}$ . This time is of the order of magnitude of  $\tau_{\text{CG}}$ , see Eq. 101, in other words  $\tau_{\text{chain}} \simeq (n + 1)^2 \tau_0$ ; in general, it separates the intrachain from the interchain relaxation processes of the network. In particular, the storage modulus  $G'(\omega)$  at rather high frequencies,  $\omega > 1/\tau_{\text{chain}}$ , (in the domain of the intrachain relaxation) behaves as  $\omega^{1/2}$ , in other words

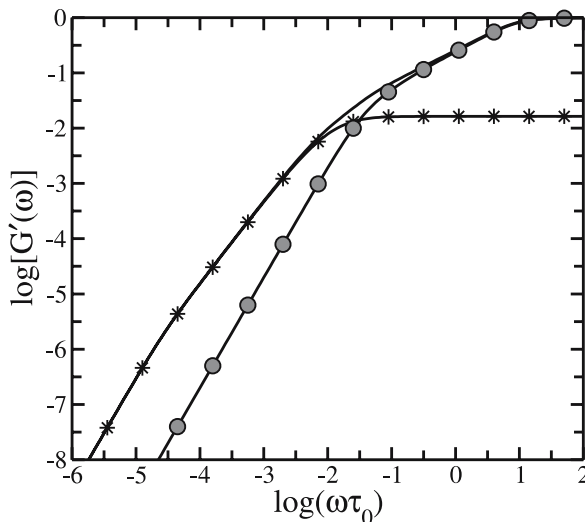


**Fig. 7** Reduced storage modulus  $[G'(\omega)]$  plotted on double logarithmic scales versus the reduced frequency  $\omega\tau_0$  for a 3-D topologically-regular cubic ( $40 \times 40 \times 40$ ) network cross-linked from Rouse chains of 20 beads each (solid line). Also shown are the contributions to the  $[G'(\omega)]$  that come from intrachain relaxation (solid line with circles) and interchain relaxation (solid line with stars)

in the same fashion as the linear Rouse chain, see Fig. 7. In contrast, in the domain of large-scale cooperative relaxation,  $\omega < 1/\tau_{\text{chain}}$ , one observes the  $\omega^{3/2}$ -behavior typical of topologically-regular cubic networks [25, 66, 71]. Furthermore, given that we have an analytical solution, one can directly compare the contributions of the intra- and of the interchain relaxation to the network's dynamics. For instance, under reasonable choices for the number of beads in the network's chains, the storage modulus  $G'(\omega)$  is determined mainly by interchain processes at low frequencies and by intrachain processes at high frequencies, see Fig. 7. The same holds with respect to the frequency behavior of the dynamic viscosity  $\eta'(\omega)$  of the system, plotted in Fig. 8. What is of particular interest here is that the intra- and interchain relaxation processes contribute in comparable ways to the viscosity at zero frequency [25], see Fig. 8. We recall that the analytical treatment of a topologically cubic network built from Rouse chains assumed that Eq. 93 holds, which relates the friction constants of the junctions to those of the chain beads. However, it turns out that this condition does not influence our general conclusions much. A special numerical analysis [21] found almost no changes in the dynamic modulus of the network when the ratio  $\zeta_{\text{jun}}/\zeta$  was varied between 0.1 to 10.

We close by noting that for rather long Rouse chains one can use a continuum description. The derivation of the relaxation times (eigenvalues) of the network then closely follows the procedure used above [71, 72]. The main results stay unchanged. For a three-dimensional polymer network one ob-

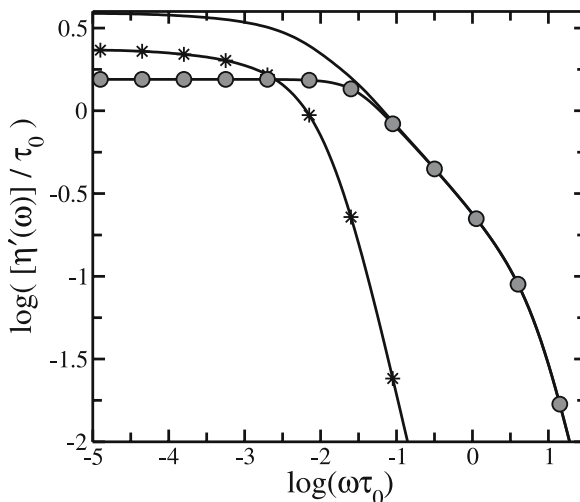


**Fig. 8** Reduced shear viscosity  $[\eta'(\omega)]$  plotted on double logarithmic scales versus the reduced frequency  $\omega\tau_0$  for the same network built from Rouse chains as in Fig. 7. Again, we show the contributions of intrachain relaxation (*solid line with circles*) and interchain relaxation (*solid line with stars*)

serves two major relaxation domains: a Rouse-like, rather small-scale intrachain relaxation region, where  $H(\tau) \sim \tau^{-1/2}$ , and a cooperative, large-scale network relaxation region, where  $H(\tau) \sim \tau^{-3/2}$  [71, 72]. Historically, networks built from continuous elastic chains were considered earlier than their discrete analogs. However, in the spirit of this review, we chose to focus our exposition on discrete networks, true GGS, built from Rouse chains.

### 5.2.2 Topologically-Square Networks

The considerations of the previous section carry over to topologically-regular networks of lower dimensionality; for example to a two-dimensional square network built from Rouse chains. We stress again that such a network is two-dimensional only in the sense of connectivity, and that we consider its motion in the three-dimensional Cartesian space (schematically the network behaves as a fishing net in water or, more accurately, honey). In the case of a square network built from Rouse chains an analytical solution is again possible if the friction constant of the network junctions is twice as large as that of the chain beads (see Eq. 93 for the three-dimensional case) [68, 69]. The derivation of the eigenvalues proceeds as in Sect. 5.2.1, again leading to Eq. 86, where the intrachain phase shift  $\psi$  is now given by (see Eqs. 97 to 99) [68, 69]:

$$\psi_1 = \frac{2\pi}{n+1} l_1 \pm \frac{1}{n+1} \arccos \left[ \frac{1}{2} (\cos k_1 + \cos k_2) \right] \quad (103)$$

and

$$\psi_2 = \frac{\pi}{n+1} l_2, \quad (104)$$

where  $l_1 = 0, \dots, (n/2)$  and  $l_2 = 1, \dots, n$  (here  $n$  is assumed to be even); furthermore,  $\mathbf{k} = (k_1, k_2)$  are restricted by Eq. 75. Of particular interest here is that the structure of the eigenmodes is simpler than in the three-dimensional case: the purely intrachain branch of the spectrum, which coincides with the spectrum of a single Rouse chain and which is doubly degenerate in a cubic network (see Eqs. 98 and 99 for  $\psi_2$  and  $\psi_3$ ) is not degenerate anymore (see Eq. 104 for  $\psi_2$ ).

The relaxation spectrum (as well as the viscoelastic quantities derived from it) obeys features typical of two dimensions: while one finds the standard Rouse chain behavior,  $H(\tau) \sim 1/\sqrt{\tau}$ , at rather short times (on small scales of motion), at longer times  $H(\tau)$  goes as  $1/\tau$ , a behavior intermediate between that of uncrosslinked Rouse chains and that of three-dimensional networks. Once again we note in the exponents of  $\tau$  the parallelism between regular and fractal networks, as discussed in Sect. 5.1.2.

It is noteworthy that the same results were found by Chompff and Duiser using a different approach [70]. They proposed a decoupling procedure which, upon being applied to polymer chains cross-linked into a network,

leads to an assembly of uncrosslinked chains of various lengths. The essence of the approach may be illustrated with a simple example: let us consider four chains of  $N$  monomers (beads), each of which is connected by one end to a certain cross-link point (single network junction), while the other end of each of these four chains is assumed to be fixed in space. It can be shown by means of simple operations involving the connectivity matrix that this system is equivalent to a single chain of  $2N$  monomers and to two chains of  $N$  monomers (all of the chains have fixed ends). The appearance of a chain of double length ( $2N$  monomers) reflects the interchain connections [70]. The relaxation spectrum, which is obtained by applying the above decoupling procedure to a square network consisting of Rouse chains, is found to follow a Rouse chain behavior at rather short times,  $H(\tau) \sim 1/\sqrt{\tau}$ , whereas at longer times  $H(\tau)$  goes as  $1/\tau$  [70], in other words it displays two-dimensional character.

### 5.3

#### Regular Networks Built from Complex Cells of Arbitrary Internal Topology

The analysis of the previous section centered on systems of Rouse chains end-linked into regular networks and demonstrated the influence of the GGS-structure on the dynamics; one observes Rouse chain behavior in determined (time or frequency) ranges, whereas in other ranges the relaxation is dominated by the large-scale network structure. In this section we extend this study to more complex systems and replace the Rouse chains by rather arbitrary building blocks (subunits). For such subunits, even when they are connected into regular networks, the possibility of a general analytical treatment gets lost. However, under certain conditions, the network's symmetry still provides opportunities to simplify the problem considerably.

For this we turn to a formalism which allows us to study the dynamics of regular networks built from topologically complex cells (substructures). We let the cells (consisting of beads connected by elastic springs) have an arbitrary internal architecture, and require only that they be topologically identical to each other, see Fig. 9. Obviously, the regular networks built from Rouse chains which were considered in Sect. 5.2 also fall into this category; in this case a cell of the network contains a junction and  $d$  Rouse chains directly attached to the junction (here  $d$  is the dimensionality of the network).

Below we consider a (topologically) cubic network (following [31, 74] closely). An elementary cubic cell of the network is denoted by  $\boldsymbol{\Omega} = (\alpha, \beta, \gamma)$  (here  $\alpha, \beta$ , and  $\gamma$  range from 1 to  $N$ ) and it contains  $s$  beads, which we number by the index  $j \in \{1, \dots, s\}$ . The whole network consists then of  $N_{\text{tot}} = sN^3$  beads, denoted by  $(j, \boldsymbol{\Omega}) \equiv (j, \alpha, \beta, \gamma)$ . All of the beads (which have identical friction constants  $\zeta$ ) are connected to their neighbors by means of elastic springs all of which have the same elasticity constant  $K$ . The Langevin equation of mo-

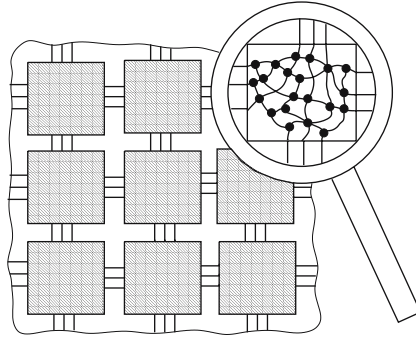


**Fig. 9** Schematic representation of a regular network built from complex cells. For clarity's sake a two-dimensional square network is shown. Each cell has some arbitrary internal GGS structure (see magnifying glass), which is identical in all cells

tion for the  $l$ th bead of the network is given by Eq. 2 with  $F_l^{(\text{ext})}(t) = 0$ . Because of the symmetry of the regular network, the determination of the eigenvalues of the connectivity matrix  $A$  simplifies considerably. The elastic term in Eq. 2 reads [31, 73, 74]:

$$\begin{aligned} \sum_{m=1}^{N_{\text{tot}}} A_{lm} \mathbf{R}_m(t) &= \sum_{i=1}^s \sum_{\Omega'} A_{j\Omega i\Omega'} \mathbf{R}_{i\Omega'}(t) \\ &= \sum_{i=1}^s A_{j\Omega i\Omega} \mathbf{R}_{i\Omega}(t) + \sum_{i=1}^s \sum_{\substack{\Omega' \\ \Omega' \neq \Omega}} A_{j\Omega i\Omega'} \mathbf{R}_{i\Omega'}(t). \end{aligned} \quad (105)$$

Here we let  $l \rightarrow (j, \Omega)$  and  $m \rightarrow (i, \Omega')$ . Because of symmetries, we can now set  $B_{ji}^{(\text{int})} \equiv A_{j\Omega i\Omega}$  and  $B_{ji}^{(\text{ext})}(\Delta) \equiv B_{ji}^{(\text{ext})}(\Omega - \Omega') \equiv A_{j\Omega i\Omega'}$  in Eq. 105. This brings us to [31, 74]:

$$\sum_{m=1}^{N_{\text{tot}}} A_{lm} \mathbf{R}_m(t) = \sum_{i=1}^s B_{ji}^{(\text{int})} \mathbf{R}_{i\Omega}(t) + \sum_{i=1}^s \sum_{\Delta} B_{ji}^{(\text{ext})}(\Delta) \mathbf{R}_{i\Omega-\Delta}(t), \quad (106)$$

where  $\Delta = \Omega - \Omega'$  denotes the difference between the network cells  $\Omega$  and  $\Omega'$ , given in the units of number of intervening cells in each direction. In Eq. 106 the matrix  $B^{(\text{int})} = (B_{ji}^{(\text{int})})$  specifies the connections inside a given cell consisting of  $s$  beads. In contrast, the matrices  $B^{(\text{ext})}(\Delta) = (B_{ji}^{(\text{ext})}(\Delta))$  define the intercell connections: their non-zero elements  $B_{ji}^{(\text{ext})}(\Delta)$  are equal to  $-1$ , indicating that bead  $j$  of cell  $\Omega$  and bead  $i$  of cell  $\Omega' = \Omega - \Delta$  are connected by a spring (bond). In a regular network built from cells, each elementary cell is directly connected to its nearest-neighbor cells only;

for a topologically-cubic network the  $\Delta$  are therefore given by the set  $\{(1, 0, 0), (-1, 0, 0), (0, 1, 0), (0, -1, 0), (0, 0, 1), (0, 0, -1)\}$ .

Due to the symmetry inherent in Eq. 106, the diagonalization of the connectivity matrix  $A$  of the network can be now simplified. From a formal point of view the situation is very close to that met in solid state physics (Bravais lattice with a basis) [75–77], where the basis of the lattice plays the role of our elementary network cell. Note, however, that in the arguments leading to Eq. 106 only the connectivity (a topological feature) enters. Hence, the networks considered here are not required to be translationally invariant. As an example, the positions of the beads  $(j, \Omega)$ ,  $(j, \Omega + \Delta)$ , and  $(j, \Omega + 2\Delta)$  are not necessarily related by a single translation operator, as would be (in first-order) the case in a crystal. Here we have a network consisting of flexible substructures (cells), whose conformations change widely under the underlying random stochastic forces, and hence differ much from cell to cell. Nevertheless, using Eq. 106, we can proceed quite formally: we apply periodic boundary conditions to the whole network and look for solutions to our Langevin equations of the form:

$$R_{j\Omega}(t) = \sum_{k_1, k_2, k_3} C_{jk} \exp(i[k_1\alpha + k_2\beta + k_3\gamma]) \exp(-\lambda(\mathbf{k})t/\tau_0). \quad (107)$$

Here  $\Omega=(\alpha, \beta, \gamma)$ , the  $C_{jk}$  are constants,  $\tau_0 = \zeta/K$  is the characteristic relaxation time, and  $\mathbf{k} = (k_1, k_2, k_3)$  is given by  $k_i = 2\pi m_i/N$ , where the  $m_i$  are integers with  $0 \leq m_i \leq (N - 1)$  for  $i = 1, 2$ , and  $3$  (see also Eq. 75). We recall that the triple  $\mathbf{k}$  is not a reciprocal vector, as in solid state physics; it is simply a means to count the eigenmodes. We now define the new matrices:

$$B_{ji}(\mathbf{k}) = B_{ji}^{(\text{int})} + \sum_{\Delta} B_{ji}^{(\text{ext})}(\Delta) \exp(-i\mathbf{k} \cdot \Delta). \quad (108)$$

The matrices  $B(\mathbf{k}) = \{B_{ji}(\mathbf{k})\}$  include all relevant information concerning the intra-cell topology and the way in which the cells of the network are connected to each other. All in all there are  $N^3$   $\mathbf{k}$ -values and therefore  $N^3$  different  $B(\mathbf{k})$  matrices. Using the  $B(\mathbf{k})$  matrices, the Langevin equations, Eq. 2, are reduced to [31, 73, 74]:

$$\lambda(\mathbf{k})C_{jk} = \sum_{i=1}^s B_{ji}(\mathbf{k})C_{ik}. \quad (109)$$

The symmetry, therefore, helped to simplify the problem: instead of having to diagonalize  $A$ , which is a  $(sN^3 \times sN^3)$ -matrix, we only need now to diagonalize  $N^3$  different  $(s \times s)$ -matrices [31, 74].

It is important to stress at this point that the derivation of Eq. 109 is general and that it holds for an arbitrary topological structure of the cells involved. Moreover, the cubic network considered here is only a particular example; the approach can be easily extended to other network types. For instance, all

of the results of this section are also valid for a square network built from complex substructures; to describe it one simply has to set  $k_3 = 0$  in all the  $k$ -dependent equations established so far. Also, the method discussed here can be extended to copolymer networks, whose building blocks (cells) may consist of different beads (say, with different mobilities) [21]. In the following sections we will use the general formalism developed in this section for various systems of complex topology, such as polymer networks bearing dendritic wedges [78], dendrimer-based polymer networks [74], and networks made up from disordered subunits [31, 73].

## 6

### Fractal Polymer Networks

After discussing the situation in topologically-regular, mesh-like polymer networks in the previous section, we turn now to the general situation. Here we will display the possibilities of describing complex networks using ideas of scale freedom. Typical of such approaches are models based on fractal structures and notions akin to them. In a first step we will consider a phenomenological, general approach that leads to classic viscoelastic models; this allows us to make connections both to the microscopic models discussed in the previous paragraphs and also to global descriptions, rooted in fractional differential equations. In the next steps we then turn our attention to simple fractal networks, such as ladder models, and to Sierpinski gasket structures.

#### 6.1

##### General Approach: Generalized Viscoelastic Models

Historically, the viscoelastic properties of polymers were initially modeled by combining springs and dashpots. A sequential combination of a spring and a dashpot is called the Maxwell model. Denoting the stress by  $\sigma$  and the strain by  $\varepsilon$ , we have for the spring

$$\sigma_1(t) = E \varepsilon_1(t) \quad (110)$$

and for the dashpot

$$\sigma_2(t) = \eta \frac{d\varepsilon_2(t)}{dt}, \quad (111)$$

where  $E$  is related to Young's modulus and  $\varepsilon$  to the viscosity. The equation for  $\sigma$  and  $\varepsilon$  then reads (constitutive equation):

$$\sigma(t) + \tau \frac{d\sigma(t)}{dt} = \tau E \frac{d\varepsilon(t)}{dt}, \quad (112)$$

with  $\tau = \eta/E$ . As already noted in Sect. 3.1.2, the response of  $\sigma(t)$  to a stepwise change in  $\varepsilon$  (to  $\varepsilon(t) = \varepsilon_0\theta(t)$ ) is the relaxation modulus  $G(t)$ . For the Maxwell model it follows:

$$G(t) = E \varepsilon_0 \exp(-t/\tau), \quad (113)$$

which is clearly the special case of Eq. 26 for one mode with  $\tau_k = 2\tau$ . Now, Eq. 25 can be rewritten in terms of the storage modulus

$$G'(\omega) \equiv \omega \int_0^{\infty} G(t) \sin(\omega t) dt \quad (114)$$

and of the loss modulus

$$G''(\omega) \equiv \omega \int_0^{\infty} G(t) \cos(\omega t) dt. \quad (115)$$

In the case of the Maxwell model these are simply

$$G'(\omega) = E \varepsilon_0 \frac{(\omega\tau)^2}{1 + (\omega\tau)^2} \quad (116)$$

and

$$G''(\omega) = E \varepsilon_0 \frac{\omega\tau}{1 + (\omega\tau)^2} \quad (117)$$

which are, again, special cases of Eqs. 20 and 21. Evidently, realistic polymer models are not well-represented by these simplistic forms, Eqs. 116 and 117; in general, Eqs. 20 and 21 have to be used. A notable exception occurs when  $G(t)$  is (at least, over a certain range of  $t$ ) self-similar; in other words when it is an algebraic function of time,

$$G(t) \sim t^{-\alpha}, \quad (118)$$

see Eq. 66 as an example. Then such a behavior can be captured by changing the derivatives in the constitutive equation, Eq. 112, to fractional derivatives [8, 9]. Furthermore, the scaling displayed by  $G(t)$  in Eq. 118 is typical of anomalous diffusion.

Regular diffusion, better known as Brownian motion, is characterized (in the absence of directed, external fields) by a linear increase of the mean-square displacement with time, see Eq. 60 for the motion of the center of mass. For anomalous diffusion this simple relation does not hold anymore. Then the temporal evolution of the mean-square displacement is non-linear, and at long times often obeys

$$\langle R^2(t) \rangle \sim t^\gamma, \quad (119)$$

with  $\gamma \neq 1$ . In the case that  $\gamma < 1$ , one denotes the behavior as subdiffusive. We remark that, in many instances, such as in the presence of a constant,

non-zero electric field (say, oriented along the  $y$ -axis), Eq. 119 turns out to be equivalent to the relation [2, 9, 13]

$$\langle Y(t) \rangle \sim t^\gamma, \quad (120)$$

where we have  $\mathbf{R} = (X, Y, Z)$ . For simply-structured particles (the ideal case being point-like objects) the pattern of motion of Eqs. 119 and 120 often results from disorder [79–84]; for polymer chains – as studied here, see Eq. 68 – the motion of the monomers also obeys Eq. 119 in the absence of disorder; the reason for this is the relaxation of the internal modes of the structure [85]. Furthermore, Eq. 119 is also obeyed during several motional stages in melts of polymer chains; then one has reptation [4] and the processes giving rise to disentanglement are characterized by different exponents  $\gamma$  in Eq. 119 [2, 4, 41].

Recently, besides the classical way of describing anomalous diffusion via continuous time random walks (CTRW) and Lévy-walk models [79–83, 86–92], descriptions based on fractional derivatives have also attracted much interest [8, 9, 93–95]. As a reminder, one has as the defining relation for fractional derivation the Riemann-Liouville expression:

$$\frac{d^\alpha f}{dt^\alpha} \equiv \frac{1}{\Gamma(-\alpha)} \int_0^t \frac{f(\tilde{t})}{(t-\tilde{t})^{\alpha+1}} d\tilde{t}. \quad (121)$$

In Eq. 121  $\Gamma(z)$  is the Gamma-function and the expression extends the (integer) recursive integration to the domain of real  $\alpha$ ; differentiation is obeyed for  $\alpha > 0$ , integration for  $\alpha < 0$ . In general, all differentiation rules such as

$$\frac{d^\alpha f}{dt^\alpha} = \frac{d^\beta}{dt^\beta} \left( \frac{d^{\alpha-\beta} f}{dt^{\alpha-\beta}} \right) \quad (122)$$

hold. Now it turns out that replacing the usual derivatives by fractional derivatives in the constitutive equation of the Maxwell-model, Eq. 112, leads to:

$$\sigma(t) + \tau^{\alpha-\beta} \frac{d^{\alpha-\beta} \sigma(t)}{dt^{\alpha-\beta}} = \tau^\alpha E \frac{d^\alpha \varepsilon(t)}{dt^\alpha} \quad (\text{with } 1 > \alpha > \beta), \quad (123)$$

an expression which offers an excellent description of many polymeric substances, see [8, 9] for details.

Following the developments outlined in [8, 9], we now stress the fact that anomalous diffusion in the scaling form of Eqs. 119 and 120 is closely connected to descriptions based on fractional derivatives, given that they allow us to invert, in a simple way, the integral expressions which follow from the theory of linear response, when the anomalous behavior has a power-law character going as Eq. 119, with  $\gamma < 1$ . For technical reasons and because of an intimate relation to linear response we prefer, as in [8, 9], to extend the lower integration limit in Eq. 121 to  $-\infty$ ; in this way we obtain the Weyl-form.

It is now a simple matter to show that the Weyl-form of fractional calculus is an exceedingly powerful mathematical method when treating materials whose internal processes obey algebraic decays. We follow here the description given in [9]. Denoting the response of the system to an external perturbation  $\Psi(t)$  by  $\Phi(t)$ , one can express the relation between these two functions in terms of  $\Phi_s(t)$ , the response of the system to a step perturbation  $\theta(t)$ . Namely, because of the superposition principle and of causality, in the framework of linear response one obtains:

$$\Phi(t) = \int_{-\infty}^t d\tilde{t} \Phi_s(t - \tilde{t}) \frac{d\Psi(\tilde{t})}{d\tilde{t}}. \quad (124)$$

In general, Eq. 124 is difficult to invert, being an integral relation. However, for algebraic  $\Phi_s$ , in other words  $\Phi_s \equiv \frac{C}{\Gamma(1-\gamma)} (\tau_0/t)^\gamma$ , where  $0 < \gamma < 1$ , it follows that

$$\Phi(t) = C\tau_0^\gamma \frac{1}{\Gamma(1-\gamma)} \int_{-\infty}^t \frac{d\tilde{t}}{(t-\tilde{t})^\gamma} \frac{d\Psi(\tilde{t})}{d\tilde{t}} = C\tau_0^\gamma \frac{d^\gamma \Psi(t)}{dt^\gamma}, \quad (125)$$

where we used the repeated differentiation given in Eq. 122. Clearly, now Eq. 125 can be readily inverted, since it is a simple fractional derivative. The inversion reads

$$\Psi(t) = \frac{1}{C\tau_0^\gamma} \frac{d^{-\gamma} \Phi(t)}{dt^{-\gamma}}. \quad (126)$$

Evidently, one can simply read-off from Eq. 126, by inverting the argument leading from Eq. 124 to Eq. 125, that the response  $\Psi_s(t)$  to a step perturbation  $\theta(t)$  of  $\Phi$  is:

$$\Psi_s(t) = \frac{C^{-1}}{\Gamma(1+\gamma)} \left( \frac{t}{\tau_0} \right)^\gamma. \quad (127)$$

This last relation makes it clear that the strain (extension) of the object under an external stress (force) now simply obeys, due to  $0 < \gamma < 1$ , the subdiffusive law expressed by Eq. 120. Given that many macromolecular systems display such a subdiffusive behavior, it now becomes evident why they can be described very well through expressions involving fractional derivatives; as long as the response is linear, scaling behavior and fractional derivatives reflect the same underlying physics. In the following subsections we will see that fractal GGS also show scaling, where  $\gamma$  is related to the spectral dimension  $\tilde{d}$  of the fractal.

## 6.2 A Simple Fractal Network: The Ladder Model

Here we start with the ladder model, which is a simple example of a hierarchical (scaling) network [26, 96–100]. The model has its electrical analog and turns out to be a basic element in the fractional differential picture [8, 9]. From a mathematical point of view, in a simple ladder model version the equations are identical to those of the Rouse model for a single chain. Ladder models are very useful for providing a microscopic (if somewhat idealized) picture of gels, as well as in modeling different gelation stages. If one focuses on end-linking reactions in a prepolymer which is far below the entanglement limit, one finds a power-law behavior,  $G^*(\omega) \sim (i\omega)^\alpha$ , near the gel point for the complex dynamic modulus [101–103]. This behavior appears in quite extended frequency ranges and is followed by a liquidlike behavior in the case of a pregel and by a solidlike behavior for a postgel structure. Moreover, for stoichiometrically-balanced gels, one often finds  $\alpha \cong 1/2$ . This value appears to be rather insensitive to the choice of the prepolymer, to the cross-linker functionality, and to the chain length [101, 102].

In order to describe pregel, postgel and gel situations, ladder models were used [100]. A ladder model is depicted schematically in Fig. 10; it consists of springs (with spring constants  $E_0, E_1, E_2, \dots$ ) along one of the struts of the ladder and dashpots (with viscosities  $\eta_0, \eta_1, \eta_2, \dots$ ) along the ladder rungs. Three different types of boundary conditions can now be envisaged: finite ladder arrangements are appropriate to model pregels and postgels; for a pregel the ladder finishes with a spring ( $E_n$ ) and a dashpot ( $\eta_n$ ) in series (a Maxwell element) and for a postgel with a spring ( $E_n$ ). On the other hand, an infinite ladder arrangement (Fig. 10) is necessary to model the gel point. The complex

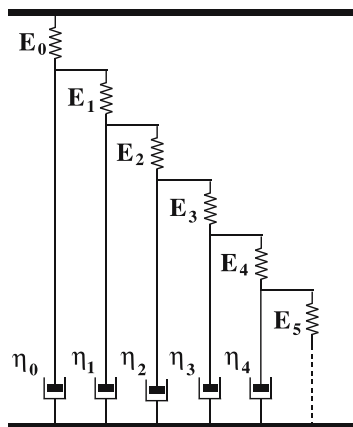


**Fig. 10** Infinite ladder model

dynamic modulus  $G^*(\omega)$  in the case of a pregel reads [100]:

$$G^*(\omega) = \frac{E_0}{1 + \frac{(i\omega)^{-1}(E_0/\eta_0)}{1 + \frac{(i\omega)^{-1}(E_1/\eta_1)}{1 + \frac{(i\omega)^{-1}(E_n/\eta_{n-1})}{1 + \frac{(i\omega)^{-1}(E_n/\eta_n)}{1}}}} \dots \quad (128)$$

and, correspondingly, one has for a postgel situation [100]:

$$G^*(\omega) = \frac{E_0}{1 + \frac{(i\omega)^{-1}(E_0/\eta_0)}{1 + \frac{(i\omega)^{-1}(E_1/\eta_1)}{1 + \frac{(i\omega)^{-1}(E_{n-1}/\eta_{n-1})}{1 + \frac{(i\omega)^{-1}(E_n/\eta_{n-1})}{1}}}} \dots \quad (129)$$

where the standard notation of continued fractions,  $a/(b + ) f = a/(b + f)$ , is used.

For  $G^*(\omega)$  at the gel point (an infinite ladder arrangement) the expression is akin to Eqs. 128 and 129, but it involves an infinite continued fraction. A simple special case may be obtained by making all of the springs and all of the dashpots equal ( $E_0 = E_1 = \dots = E$  and  $\eta_0 = \eta_1 = \dots = \eta$ ). Then at the gel point the complex dynamic modulus  $G^*(\omega)$  reduces to [100]:

$$G^*(\omega) = E(i\omega\tau_{\text{lad}})^{1/2} \left[ \left( 1 + \frac{i\omega\tau_{\text{lad}}}{4} \right)^{1/2} - \left( \frac{i\omega\tau_{\text{lad}}}{4} \right)^{1/2} \right], \quad (130)$$

where  $\tau_{\text{lad}} = \eta/E$  is the characteristic relaxation time of the ladder model under study. In the low-frequency domain,  $\omega\tau_{\text{lad}} \ll 1$ , Eq. 130 leads to a power-law behavior,  $G^*(\omega) \simeq E(i\omega\tau_{\text{lad}})^{1/2}$ . Thus, an infinite ladder arrangement built from identical springs and identical dashpots leads to a power-law behavior for the storage modulus,  $G'(\omega) \sim \omega^\alpha$ , with  $\alpha = 1/2$  [100].

That we recover the intermediate  $G'(\omega)$ -behavior of the Rouse model in this way is only surprising at first sight. In fact, a second look at Fig. 10 clarifies the equivalence between the ladder model and the Rouse chain. In both there is a sequential connection between neighboring elements through harmonic springs; furthermore, each element has a local, dissipating, energy sink. The behavior of finite ladder arrangements built from identical springs and dashpots may appear even more familiar now. Their storage modulus also demonstrates a  $\omega^{1/2}$ -behavior, but only in an intermediate frequency domain, which here extends up to a crossover frequency which was numerically found to be  $\omega\tau_{\text{lad}} \simeq 4/n^2$ , where  $n$  is related to the ladder length, see Eqs. 128 and 129. This corresponds exactly to the behavior of Rouse chains.

Moreover, for the pregel finite ladder ending with a Maxwell element (a spring and a dashpot in series) one finds at low frequencies a liquidlike behavior,  $G'(\omega) \sim \omega^2$ . For the postgel ladder, which consists of  $(n + 1)$  springs in series and whose ends are both springs, one finds a solidlike behavior,  $G'(\omega) \simeq E/(n + 1)$ ; this is also the low-frequency behavior of a Rouse chain whose ends are fixed.

Furthermore, recall that one often finds  $\alpha$  values which deviate from  $1/2$  [103]. It turns out that the above ladder model can be modified in several ways, so that  $\alpha$  can take arbitrary values between 0 and 1. One of these possibilities is to choose the spring constants  $E_k$  and the viscosities  $\eta_k$  so that they fulfill [97, 100]:

$$E_k = C_1 k^{(1-2\alpha)} \quad \text{and} \quad \eta_k = C_2 k^{(1-2\alpha)}, \quad (131)$$

where  $C_1$  and  $C_2$  are constants. It can be shown that the complex dynamic modulus  $G^*(\omega)$  of a ladder built from such springs and dashpots does indeed follow a  $\omega^\alpha$ -behavior [97]:

$$G^*(\omega) \sim \omega^\alpha. \quad (132)$$

Another possibility, which mimics the geometrical situation better, is to connect the dashpots through springs in a network structure, say a fractal one, while keeping the simple forms  $E_k = E = \text{const}$  and  $\eta_k = \eta = \text{const}$  [8, 9, 100]. Again, this model gives rise to a  $\omega^\alpha$ -behavior for  $G^*(\omega)$ . We close by noting that all these ladder models are mechanical realizations for fractal elements [8, 9], since they fulfill equations of the form

$$\sigma(t) = C \frac{d^\alpha \varepsilon(t)}{dt^\alpha}, \quad \text{with} \quad 0 \leq \alpha \leq 1. \quad (133)$$

### 6.3

#### Dual Sierpinski Gasket Structures

Let us turn now to GGS which show more complex structures. Foremost in our mind is to focus on GGS whose eigenvalue spectra can be readily determined. As previously discussed, the evaluation of the main relaxation forms, Eqs. 20, 21, and 50 is straightforward, under the condition that all eigenvalues are known. This also determines the way to proceed: what is needed is to diagonalize the  $A$  matrix in Eq. 10 in order to obtain the corresponding eigenvalues needed to compute the relaxation functions.

Given that the interesting intermediate temporal range is limited by the two (terminal) regions previously discussed, say, for  $G'(\omega)$  by the domains at quite small and at quite large frequencies, regions in which all finite GGS systems behave in the same way, one has to consider very large GGS. This is the case because one has to work out the behavior typical for the GGS-class under investigation, behavior which shows up only in the intermediate range; hence it is very important that the GGS considered be very large in order for the intermediate range to be sufficiently large.

Now, the problem that one faces when using numerical procedures is the limited options available when the size of the GGS gets large. In this case, the numerical procedures may fail, given that currently only matrices of up to  $5000 \times 5000$  elements can be readily diagonalized; one has to bear in mind

that we need *all* the eigenvalues of  $A$  in the subsequent calculations of the dynamical properties.

In the following we will focus on several regular fractal structures, for which, due to their particular features, it is possible to determine *all* of the eigenvalues semi-analytically. We stop first to note that in general the spectra of such objects are not smooth at all [104–106]. Nonetheless, as will become evident in the following, the fact that such spectra are discrete and highly discontinuous will (if at all) hardly show up in the relevant experimental quantities. Now, apart from very fine details, it turns out that the major factor that determines the scaling behavior of the relaxation forms considered by us in the intermediate frequency range is the spectral dimension [6–9, 94, 104–113]. Evidently, in order to be able to clearly show by numerical means that only the spectral dimension is decisive, we have to use very large GGS again.

The first class of deterministic fractals on which we focus are the so-called dual Sierpinski gaskets. As we proceed to discuss, they are very closely related to the general Sierpinski gaskets; the advantage of working with dual Sierpinski gaskets is that their spectra can be determined exactly through iterative procedures, without the need to diagonalize  $A$  numerically [105, 106, 110]. In this way we are in a position to study extremely large fractals. An example of a dual Sierpinski gasket is given in Fig. 11, with  $d = 2$  as embedding space.

As for all Sierpinski-type gaskets, the construction starts [106] from a simplex of  $\delta$ -sites ( $\delta = d + 1$  and in Fig. 11  $\delta = 3$ ); a triangle here. Such simplexes are then iteratively connected to each other. There are two commonly-used possibilities for continuing the construction. In the classical picture [114] all sites of the simplex also belong to other simplexes of the same kind; one hence superposes pairwise sites belonging to different simplexes, obtaining the usual Sierpinski gaskets [114]. A second possibility consists of connecting the given simplex via *additional bonds* to other simplexes; this is the situation displayed in Fig. 11. There, all basis sites of the smallest triangle are connected to the tips of further identical triangles. Hence the upper part of

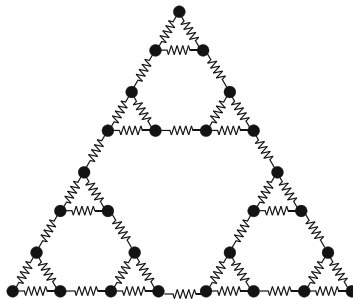


**Fig. 11** Dual Sierpinski gasket, embedded in  $d = 2$

Fig. 11 depicts one complete iteration, leading to the second generation of the fractal. The construction then gets iterated to higher generations, in Fig. 11 up to the third. In fact, the so-created object is identical to what would have been obtained by taking the usual Sierpinski gasket, inserting a vertex at the center of each of its triangles and connecting the vertices to each other [104]. We stop to note that both the Sierpinski gasket and also its dual are naturally embedded in the  $d = \delta - 1$  dimensional space, here in  $d = 2$ . Note that going from the usual Sierpinski gasket to its dual reduces the coordination number of the sites of the fractal from  $d + 2$  to  $d + 1$ . However, as can be easily seen (and as was also pointed out in [104–106, 110]), the usual gasket and its dual have exactly the same fractal  $\bar{d}$  and spectral  $\tilde{d}$  dimensions; these are, for a general  $d$ -dimensional embedding space, setting  $\delta = d + 1$ :

$$\bar{d} = \frac{\ln(d + 1)}{\ln 2} = \frac{\ln \delta}{\ln 2} \tag{134}$$

and

$$\tilde{d} = \frac{2 \ln(d + 1)}{\ln(d + 3)} = \frac{2 \ln \delta}{\ln(\delta + 2)}. \tag{135}$$

As a side-remark, we note that for special values of  $d$ , namely for  $d = 3, 7, 15$ , and so on,  $\bar{d}$  is an integer. Then, as shown in [106, 115], other possibilities for embedding the dual Sierpinski gaskets into Euclidean space exist.

The major advantage of focusing on dual Sierpinski gaskets is that their eigenvalues can be obtained iteratively [105, 106, 110]. One proceeds as follows: from the eigenvalue spectrum at stage  $n$ , one obtains the eigenvalues at stage  $n + 1$  by first assigning to each non-vanishing eigenvalue  $\lambda_{n-1}$  two new eigenvalues  $\lambda_n^\pm$  through the relation:

$$\lambda_n^\pm = \frac{(\delta + 2) \pm \sqrt{(\delta + 2)^2 - 4\lambda_{n-1}}}{2}, \tag{136}$$

with

$$\delta = d + 1. \tag{137}$$

In this way, we carry the degeneracies of  $\lambda_{n-1}$  over to  $\lambda_n^+$  and  $\lambda_n^-$ . Furthermore,  $\delta$ , with degeneracy  $[(\delta - 2)\delta^{n-1} + \delta]/2$ , and  $\delta + 2$ , with degeneracy  $[(\delta - 2)\delta^{n-1} - (\delta - 2)]/2$ , as well as the nondegenerate value  $\lambda_1 = 0$ , which corresponds to the translation of the whole GGS are added to this spectrum as eigenvalues. It is then a simple matter to verify that the number of eigenvalues at each stage is indeed equal to  $N = \delta^n$ . Moreover, in [106] these results were tested numerically by diagonalizing, for relatively small  $N$  values, the corresponding  $A$  matrices. These results support the correctness of the whole procedure in an additional, independent manner.

Using this procedure, it is now a simple matter to compute the eigenvalues iteratively by numerical means, even for very large values of  $N$ . Having

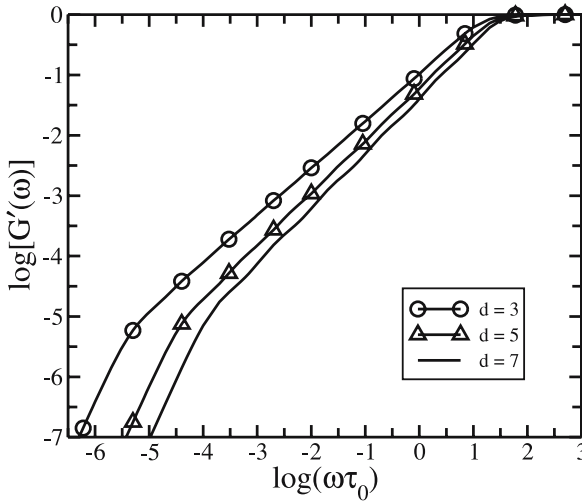


**Fig. 12** Reduced storage modulus  $[G'(\omega)]$  plotted on double logarithmic scales versus the reduced frequency  $\omega\tau_0$  for different dual Sierpinski gaskets with  $d = 3, 5$  and  $7$

found the eigenvalues, it is then straightforward to numerically determine the different relaxation quantities of interest.

Here we start by focusing on  $[G'(\omega)]$ , Eq. 20 together with Eq. 12, which is plotted in Fig. 12 in double logarithmic scales using the data of [106] for several dual Sierpinski gaskets, for  $d = 3$  ( $N = 4^3$ ),  $d = 5$  ( $N = 6^5$ ), and  $d = 7$  ( $N = 8^7$ ). Clearly evident is the limiting, connectivity-independent behavior at very small and very large  $\omega$ ,  $[G'(\omega)] \sim \omega^2$  and  $[G'(\omega)] \sim \text{const}$ , respectively. In the intermediate regime, in which  $[G'(\omega)] \sim \omega^\alpha$  holds (where  $\alpha$  is  $d$ -dependent), a careful analysis [106] demonstrates that to a very good approximation  $\alpha = \tilde{d}/2$ , where  $\tilde{d}$  is the spectral dimension. For larger  $d$  one also sees some oscillations in the intermediate regions; these are due to the hierarchical structure of the underlying dual Sierpinski gasket [106]. Similar behavior is also found for  $[G''(\omega)]$ , where  $[G''(\omega)] \sim \omega^\alpha$ , with  $\alpha = \tilde{d}/2$  in the intermediate domain. It remains to consider  $\langle\langle Y(t) \rangle\rangle$ , which for small and for large  $t$  is a linear function of  $t$ . In its intermediate domain one finds  $\langle\langle Y(t) \rangle\rangle \sim t^\gamma$ , but now  $\gamma = 1 - \tilde{d}/2$  [106].

We close this section by noting that the relations between the scaling exponent and the spectral dimension are very general. We will meet them again in Sect. 9.3, in the study of regular hyperbranched fractals. It is also noticeable that the inclusion of hydrodynamic interactions into the dynamic picture leads to the loss of scaling for Sierpinski-type polymers in the intermediate regime [116, 117].

## 7 Heterogeneous Polymer Networks

Up to now we have focused on the dynamics of regular networks. However, most polymer networks and gels are random, so regular models do not reflect the experimental situation accurately [118–126]. The wealth of possible inhomogeneities in real cross-linked polymers is, in fact, huge and it precludes any possibility of achieving a complete, unified theoretical treatment for all types of heterogeneous networks. A plethora of factors affect the way in which polymers form, and they lead to networks with large structural and dynamical differences. Structural factors that may differ widely include the lengths of the strands, the appearance of dangling chains, different local cross-link densities, and cross-link agglomerations. In this section we will outline several theoretical approaches developed to treat inhomogeneous polymer networks, although we do not aim to present a complete coverage of the subject.

### 7.1 Monodisperse Random Nets

We start with the approach of Martin and Eichinger [10, 127, 128], who considered regular network structures and introduced randomness into them through cross-linking. They started from a regular network consisting of  $N$  vertices (cross-links), an example might be a simple ring. Now every vertex is assigned the same functionality  $f$ , where  $f$  is larger than the number,  $2d$ , of nearest neighbors in the regular network. We then add to the network  $(f - 2d)N/2$  bonds. The procedure then consists of increasing the functionality of all of the vertices in steps of one. This was achieved in [10, 127, 128] by inserting additional bonds sequentially and stochastically into the network. In Fig. 13 we show a possible realization of a random network with trifunctional junctions,  $f = 3$ . By repeating this procedure, we can generate random

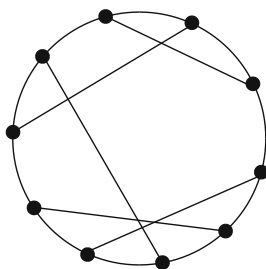


**Fig. 13** Example of a random net (reduced net) consisting of  $N = 10$  trifunctional beads. All beads have the same functionality,  $f = 3$ , and there are no double bonds

nets with junctions of higher functionality. Such random networks are called “reduced nets” [10, 127, 128]. Note that the above procedure automatically leads to connected networks.

Following the creation of reduced nets, one diagonalizes their connectivity matrices. This is done for different realizations, with  $f$  and  $N$  fixed ( $10 \leq N \leq 100$ ) [127]. In all cases, in the limit of large  $N$ , the eigenvalues  $\lambda_k$  of the reduced nets appear to be linear functions of  $k$ ; in other words one finds that [127]:

$$\lambda_k \simeq \frac{a}{N}k + b, \quad (138)$$

where  $a$  and  $b$  are constants. In fact, in [127] the constants  $a$  and  $b$  in Eq. 138 were found to obey (for  $f > 2$ ):

$$a \simeq 2\sqrt{3f} \left( 1 - \frac{f-3}{2N} \right) \quad (139)$$

and

$$b \simeq f - \sqrt{3f} + \frac{f + (f-3)\sqrt{3f/4}}{N}. \quad (140)$$

Remarkably, the spectrum of eigenvalues of a trifunctional reduced net ( $f = 3$ ) differs from that of reduced nets with higher cross-link functionality,  $f \geq 4$ : Eqs. 139 and 140 give  $a = 6$  and  $b = 3/N$  for  $f = 3$ , so that the minimal eigenvalues of a trifunctional net decrease as  $1/N$  when the size  $N$  of the net goes up (see Eq. 138 with  $k = 1$ ). In contrast, for  $f \geq 4$  the minimal eigenvalue of reduced nets is of the order of unity, so it does not depend on the net size in the limit of large  $N$  [127].

The above reduced net model is then modified to account for local intrachain degrees of freedom in randomly cross-linked networks. For this purpose each Gaussian bond of the reduced net is replaced by a Rouse chain consisting of  $n$  beads, in other words  $(n + 1)$  springs [128]. The whole network then contains  $N(1 + nf/2)$  beads; this makes a direct numerical diagonalization of the corresponding connectivity  $(N(1 + nf/2)) \times (N(1 + nf/2))$  matrix hardly feasible, even for only moderately large networks. It turns out that such large matrices can be handled by first reducing them algebraically to smaller ones; for details see [10, 128]. This procedure, when applied to a reduced net built from Rouse chains, yields [128]:

(i)  $n$  eigenvalues of the form:

$$\lambda_k = 2 \left( 1 - \cos \frac{\pi k}{n+1} \right) = 4 \sin^2 \frac{\pi k}{2(n+1)}, \quad k = 1, 2, \dots, n; \quad (141)$$

which are  $N(f - 2)/2$  times degenerate and coincide with those of Rouse chains with fixed ends [61].

(ii)  $Nn$  non-degenerate eigenvalues, given by:

$$\lambda_k = 2(1 - \cos \theta_{\sigma,k}) = 4 \sin^2 \theta_{\sigma,k}/2. \quad (142)$$

Here  $\theta_{\sigma,k}$  is one of the  $n$  real solutions of the following trigonometric polynomial of order  $(n + 1)$  [128]:

$$\cos [(n + 3/2)\theta] + (f - 1) \cos [(n + 1/2)\theta] - (f - \Lambda_\sigma) \cos [\theta/2] = 0, \quad (143)$$

where  $\Lambda_\sigma$  is one of the  $N$  eigenvalues of the connectivity matrix of the underlying reduced net.

(iii)  $N$  eigenvalues obtained from the complex solutions to Eq. 143, namely one for each  $\Lambda_\sigma$ . These solutions may be estimated as being  $\theta \simeq \pi - i \ln(f - 1)$ , leading to eigenvalues approximately equal to  $f^2/(f - 1)$  [10, 128].

The relaxation spectrum  $H(\tau)$  for such systems was found to obey  $\tau^{-0.54}$  and  $\tau^{-0.53}$  for tetrafunctional and trifunctional networks, respectively [128]. Remarkably, the authors found that the ratio of the maximal relaxation time of the random network,  $\tau_{\text{net}}$ , to that of the Rouse chain,  $\tau_{\text{chain}}$  (see also Eq. 57), is approximately [128]:

$$\frac{\tau_{\text{net}}}{\tau_{\text{chain}}} \simeq \frac{\pi^2(f + (f + 2)/n)}{2(f - 2\sqrt{f - 1})}, \quad (144)$$

which is around 87 for  $f = 3$  and around 37 for  $f = 4$  in the case of long Rouse chains between the vertices,  $n \gg 1$ . Thus, the random network considered here has a substantial domain of cooperative interchain relaxation ( $\tau_{\text{net}}/\tau_{\text{chain}} \gg 1$ ). On the other hand, the relaxation spectrum of the random network is still very narrow; it does not depend on the network size (on the number of vertices in the underlying reduced net,  $N$ ).

We conclude by noting that [128] finds in the intermediate domain  $1/\tau_{\text{net}} < \omega < 1/\tau_{\text{min}}$  that  $G'(\omega) \sim \omega^{0.57}$  and  $G''(\omega) \sim \omega^{0.50}$ ; this means that this result here should be considered with care, since in the domain  $1/\tau_{\text{chain}} < \omega < 1/\tau_{\text{min}}$  the storage modulus  $G'(\omega)$  is expected to mirror the behavior of a Rouse chain. Some deviations are possible only in the domain of cooperative relaxation,  $1/\tau_{\text{net}} < \omega < 1/\tau_{\text{chain}}$ . However, the width of this domain is finite and rather small, see Eq. 144; for  $f = 3$  it amounts to about two orders of magnitude. Therefore, it does not seem possible to extract reliable information about scaling from the  $G'(\omega)$ -plot. Finally, we remark that the above model of random networks is, in a certain sense, too regular, since all vertices have the same functionality  $f$ . As we will see in the next section, removing this requirement renders a cross-linked system much more disordered and, consequently, less tractable.

## 7.2

### Small-World Rouse Networks

In very dilute solutions, long flexible macromolecules hardly see each other. It is then reasonable, at least as a first step, to consider each chain separately. Now, given the flexibility of the chain and the stochastic features involved, monomers that are distant from one another along the chain's backbone may get to be close to each other in space. Such monomer pairs can be then chemically cross-linked by means of, say, irradiation. The polymer structure obtained by cross-linking in this fashion represents a realization of a so-called "small-world network" (SWN) [129–135].

In general, SWN are built starting from an underlying, fully-ordered lattice (say one-dimensional), in which one inserts (with probability  $q$ ) additional bonds between randomly-chosen points. In this way the SWN are intermediate between regular lattices and random graphs: on the one hand, a SWN has well-defined local connections, provided by the underlying regular lattice. On the other hand, the small amount of additional bonds strongly reduces the minimal distances between lattice points [129, 130]. One intriguing property of SWN built from a linear chain (ring) consists of the appearance of a so-called "pseudo-gap" in the density of states,  $\varrho(\lambda)$ , which goes for small  $\lambda$  as [133]:

$$\varrho(\lambda) \sim \sqrt{\frac{1}{\lambda}} \exp\left(-\frac{C}{\sqrt{\lambda}}\right), \quad (145)$$

where  $C$  is a constant. Equation 145 implies that the probability of finding SWN eigenvalues very close to  $\lambda = 0$  is extremely small.

Now, the cross-linked chain discussed above may be viewed as being a SWN. Here the original chain plays the role of the underlying regular lattice, while the random cross-linking of the monomers by irradiation creates the extra bonds. Or, one starts from a SWN and views its sites as being beads and its bonds as being elastic springs, see Fig. 14 as an example. Such GGS are called small-world Rouse networks (SWRN), as introduced by Jespersen et al [136].

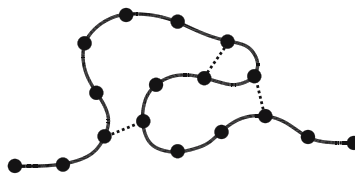


**Fig. 14** Example of a SWRN constructed from a Rouse chain by inserting into it additional bonds (shown here as *dashed lines*) between randomly chosen beads

To study how the disorder (additional bonds) introduced into a regular lattice affects its dynamics, several features were investigated [32]. For this a specific realization of a SWRN is constructed starting from a Rouse chain consisting of  $N = 1000$  beads connected by elastic springs. Then additional links (AL) – springs with the same elastic constant – are inserted; these connect each bead of the initial Rouse chain to another bead, picked randomly, with probability  $q/N$ , see Fig. 14. The eigenvalues of the corresponding connectivity matrix are then computed using direct numerical diagonalization techniques; after accumulating the eigenvalues from a sufficient number of realizations (in [32], 100 are used), one uses them to calculate, among others, the dynamic functions  $[G'(\omega)]$  and  $[G''(\omega)]$ .

In Fig. 15 we display the storage modulus  $[G'(\omega)]$  of such a SWRN for different values of  $q$ . The case  $q = 0$  is the standard Rouse chain, whose  $[G'(\omega)]$  (and  $[G''(\omega)]$ ) were amply discussed in Sect. 4. In particular, for  $q = 0$  one can distinguish in Fig. 15 three characteristic scaling domains; in them  $[G'(\omega)]$  scales (from the low frequency side) as  $\omega^2$ ,  $\omega^{1/2}$ , and  $\omega^0$ , respectively. The non-trivial behavior is the intermediate one; for the Rouse chain one finds a  $\omega^{1/2}$ -law [1–3]. This behavior changes drastically when  $q \neq 0$ : even a small number of additional bonds inserted into the Rouse chain destroys the scaling in the intermediate range. In Fig. 15 this already takes place for  $q = 0.02$ . Moreover, with increasing  $q$  the intermediate range itself gets smaller; this is due to the fact that the additional bonds increase the stiffness of the system

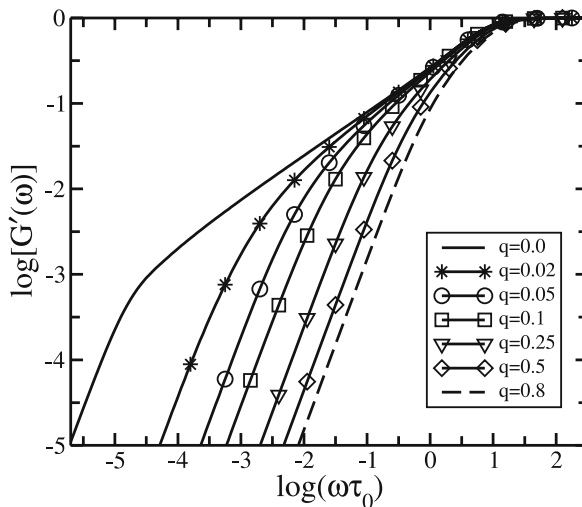


**Fig. 15** Reduced storage modulus  $[G'(\omega)]$  plotted on double logarithmic scales versus the reduced frequency  $\omega\tau_0$  for a SWRN consisting of  $N = 1000$  beads. The probability  $q$  of having additional links present varies from  $q = 0$  (Rouse chain) to  $q = 0.8$ . All  $[G'(\omega)]$ -curves were averaged over 100 SWRN realizations

and lead to the disappearance of low-lying modes, the so-called “pseudo-gap” SWRN situation [32]. Hence, by starting from  $q = 0$  and increasing  $q$ , the  $[G'(\omega)]$ -curves in the domain of the terminal,  $\omega^2$ -relaxation shift strongly to the right. This fact can be used, in particular, to experimentally determine changes in the spectrum due to disorder.

As for the loss modulus  $[G''(\omega)]$ , the effects of disorder on it are similar to those on  $[G'(\omega)]$ .  $[G''(\omega)]$  displays a maximum, whose position is mainly determined by rather high frequency modes, which correspond to the motion of just a few SWRN beads; hence the position of the maximum depends only weakly on  $q$ . At intermediate frequencies, as discussed in Sect. 4, the loss modulus of the Rouse chain ( $q = 0$ ) also obeys the scaling behavior  $[G''(\omega)] \sim \omega^{1/2}$  on the left side of the maximum, see Eq. 64 [1–3]. Even a slight increase of  $q$  quickly destroys the intermediate scaling behavior: scaling is extremely sensitive to the presence of even a few additional bonds, which transform the Rouse chain into a SWRN [32]. Also, the largest deviations of  $[G''(\omega)]$  from the Rouse chain case happen on the low-energy side, again reflecting the fact that it is here that most changes of the spectrum occur. Another interesting feature of  $[G''(\omega)]$  is the fact that for fixed  $N$  its maximum increases with increasing  $q$ . The explanation is straightforward: the increase in disorder (number of additional bonds) in SWRN does not lead to an increase in the energy loss, which is related to the area under the  $[G''(\omega)]$ -curves in linear scales. However, since with increasing  $q$  the shape of the  $[G''(\omega)]$ -curves is strongly squeezed in the low-frequency domain, the maximal value of the loss modulus  $[G''(\omega)]$  has to increase with  $q$  in order to keep the aforementioned area constant [32]. In summary, the dynamical properties of SWRN show a strong sensitivity to disorder.

Similar conclusions can be drawn from considering the motion of SWRN beads under external forces [136], as given by  $\langle\langle Y(t) \rangle\rangle$ , see Eq. 50, when the parameter  $q$  is varied. For  $q = 0$  one finds the usual Rouse behavior at intermediate times  $\langle\langle Y(t) \rangle\rangle \sim \sqrt{t/\tau_0}$ , see Eq. 69. Again, introducing additional bonds into the Rouse chain changes the situation drastically: increasing  $q$  increases the stiffness of the polymer system, and therefore decreases the maximum relaxation time of the SWRN. This shortens the domain of intermediate times and for large  $q$  even leads to the appearance of a plateau-type behavior [136].

### 7.3

#### **Polymer Networks with Random (Nonfractal) Heterogeneities: Localization Effects**

Vilgis and Heinrich [137, 138] studied the segmental dynamics of polymer networks with random (nonfractal) heterogeneities based on an earlier treatment by Deam and Edwards [139]. The starting point was a long flexible chain of  $N$  segments which is randomly cross-linked instantaneously at  $M$  sites,

which creates inhomogeneities (clustering) in the local cross-link density. In this approach the cross-links act as constraints on the motion of the chain; the constraints are taken into account by applying additional (localization) harmonic potentials to the chain [137–139].

Essentially, the model under study is a GGS with additional harmonic potentials; the corresponding Langevin equations of motion are given by Eq. 2, with an external “localizing” force  $F_l^{(\text{ext})}$  [137, 138, 140]:

$$F_l^{(\text{ext})}(t) = \frac{b^2 k_B T}{3} q_0^2(\mathbf{R}) \mathbf{R}_l(t), \quad (146)$$

where  $b$  is the length of the Kuhn segment and  $q_0(\mathbf{R})$  is the so-called localization parameter given by [137, 138, 140]:

$$q_0(\mathbf{R}) \equiv q_0 + \delta q_0(\mathbf{R}) = \frac{6M(\mathbf{R})}{Nb^2}. \quad (147)$$

The quantity  $M(\mathbf{R}) = M_0 + \delta M(\mathbf{R})$  is a cross-link distribution. In heterogeneous networks the cross-links are distributed nonuniformly; in other words the cross-link distribution  $M(\mathbf{R})$  (as well as the localization parameter  $q_0(\mathbf{R})$ ) is spatially dependent. It is assumed that its spatially dependent term  $\delta M(\mathbf{R})$  obeys a simple Gaussian distribution [137, 138]:

$$P(\{\delta M(\mathbf{R})\}) = N \exp \left[ -\frac{1}{2\Delta} \int d^3R \delta M^2(\mathbf{R}) \right], \quad (148)$$

so that

$$\langle \delta M(\mathbf{R}) \rangle = 0 \quad \text{and} \quad \langle \delta M(\mathbf{R}) \delta M(\mathbf{R}') \rangle = \Delta \delta(\mathbf{R} - \mathbf{R}'), \quad (149)$$

where  $\Delta$  is a measure of the heterogeneity of the network.

It should be emphasized that the Langevin equations in the form given by Eqs. 2 and 146 are not simple to solve because one needs to average over both the stochastic Brownian forces  $f_i(t)$  and the random part of the localization parameter  $\delta q_0(\mathbf{R})$  (the crosslink density  $\delta M(\mathbf{R})$ ). Such calculations were performed in [137, 138] with the use of perturbation theory, taking  $\delta q_0(\mathbf{R})$  as being a small parameter. As an illustration, here we present the final expression for the mean square displacement of a network bead [137, 138]:

$$\langle (\mathbf{R}_l(t) - \mathbf{R}_l(0))^2 \rangle \simeq \left[ \frac{t/\tau_0}{1 + \sqrt{1 + 4\Delta t^2/\zeta} + q_0^2(t/\tau_0)} \right]^{1/2} \quad (150)$$

where, as before,  $\tau_0 = \zeta/K$ . Using Eq. 150, one obtains different limiting behaviors. First of all, the usual Rouse  $\sqrt{t/\tau_0}$ -behavior of the mean-square displacement of the chain segment in the absence of cross-links follows readily from Eq. 150 for  $\Delta = 0$  and  $q_0 = 0$  (compare with Eq. 68). Next, if there is no disorder in the cross-link distribution (if  $\Delta = 0$ ), a network segment still follows the Rouse behavior at relatively short times  $t \ll \tau_0 q_0^{-2}$  and becomes localized at longer times,  $\langle (\mathbf{R}_l(t) - \mathbf{R}_l(0))^2 \rangle \sim q_0^{-1}$ . This is a known result [141],

also confirmed experimentally [47]. Finally, in a random network the heterogeneities enhance (on average) the localization. The disorder introduces a new characteristic time scale  $\tau_\Delta \sim \sqrt{\zeta/\Delta}$ ; for  $t > \tau_\Delta$  a new (larger) localization parameter is effective, namely  $q_{\text{eff}}^2 = q_0^2 + (\Delta/K)$ . Again, localization takes place for  $t \rightarrow \infty$  [137, 138].

## 7.4

### Polydisperse Polymer Networks: Length Distribution of Network Strands

In this section we focus on an approach originated by Sommer [142] for treating polydisperse polymer networks. Sommer considered moderately cross-linked networks, in which the chains between cross-links are long enough to obey Gaussian statistics but are still shorter than the average entanglement distance. In this case the standard Rouse model can be used for treating the dynamics of the chains. The key assumption is now the separation of time-scales between the motions of the network chains and the motions of the cross-link points [142]. The chains' subsystem turns then into a set of independently moving chains of various lengths.

Taking the cross-linking process to be stochastic and uncorrelated, one expects the distribution of cross-links to obey a Poisson form. This, in turn, implies an exponential distribution in the length  $N$  of the chains [142]. Explicitly, the distribution is

$$P(N) \simeq \frac{1}{N_c} \exp \left[ -\frac{N}{N_c} \right], \quad (151)$$

where  $N_c$  is the average number of chain beads. Such a length distribution was also obtained in [143] and verified through computer simulations [144].

The relaxation modulus  $G(N; t)$  of a single Rouse chain consisting of  $N$  beads is given by Eq. 26, and its relaxation times  $\tau_k(N) = \tau_0/\lambda_k(N)$  obey Eqs. 55 and 56. In the domain of long times,  $G(N; t)$  depends mainly on the longest relaxation time,  $\tau_{\text{chain}}(N)$ , see Eq. 57, and may be approximated by  $G(N; t) \sim (t/\tau_0)^{-1/2} \exp(-t/\tau_{\text{chain}})$  [142]. The total relaxation modulus  $G(t)$  of a polydisperse polymer network is the sum over the relaxation moduli  $G(t; N)$  of different network chains, taken with their corresponding weights  $P(N)$  according to Eq. 151:

$$G(t) \simeq \int P(N)G(N; t) dt. \quad (152)$$

In the domain of long times this integral can be evaluated with the use of the saddle-point method. Finally, one has [142]:

$$G(t) \sim \left( \frac{\tau_{\text{chain}}(N_c)}{t} \right)^{1/3} \exp \left[ -C \left( \frac{t}{\tau_{\text{chain}}(N_c)} \right)^{1/3} \right], \quad (153)$$

where  $C$  is a constant and  $\tau_{\text{chain}}(N_c)$  is the longest relaxation time of a Rouse chain of length  $N_c$ . As a result, one expects from Eq. 153 the relaxation modulus to display a stretched exponential pattern with a Kohlrausch exponent of  $1/3$ . A rather good agreement between this theoretical expression and the experimental data for natural rubber [145, 146] seems to hold [142]. Evidently, at very long times the modes of the network will also make themselves felt, which may change the overall picture.

## 7.5

### Inhomogeneous Polymer Networks Consisting of Domains of Different Sizes

In this section we consider polymer networks in which the heterogeneities may be visualized as cross-link agglomerations; such agglomerations may appear because of the random arrangements of cross-links. This kind of heterogeneity is well-documented experimentally [125, 126, 147–150]. For instance, dynamic and static light scattering experiments on polyacrylamide hydrogels [150] reveal densely cross-linked regions embedded in surroundings with smaller cross-link densities. Below we discuss a GGS framework for treating polymer networks that have such heterogeneities.

#### 7.5.1

##### General Approach for Describing Cross-Linked Polymers Consisting of Cross-Link Agglomerations

To address the existence of cross-link agglomerations in polymer networks and gels, the following simple model was proposed [151]. An inhomogeneous cross-linked polymer is treated as an ensemble of regions (domains) with finite sizes, see Fig. 16. Two assumptions here are that (i) the domains are independent (they do not interact with each other), and (ii) the internal topological structures of all the domains are identical. Each domain is taken now to be a GGS, consisting of beads connected by elastic springs in an arbitrary

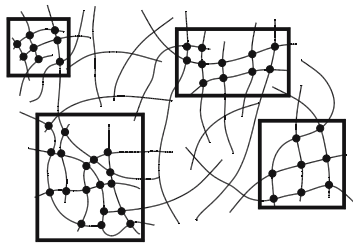


**Fig. 16** Sketch of a heterogeneous polymer network consisting of domains (cross-link agglomerations) of different sizes

way (but the same for all of the domains). The detailed structure inside the domains may be a mesh-like network, a fractal network, a dendritic structure, and so on. The only difference between the domains is the numbers  $N_u$  of relaxing units inside each domain, the number density of the relaxing units  $\nu_u$  being the same for all of the domains. Note that  $N_u$  is not necessarily the number of beads in the GGS; relaxing units, in general, can contain several GGS-beads like, say, elementary cells of mesh-like networks. Thus, in the present model the disorder associated with the randomness of cross-linking is reduced to a broad size distribution of the domains in the network.

First, we focus on the relaxation inside a single domain of finite size; to get the dynamical behavior of the whole heterogeneous network one needs then to average over all of the domains in the system. The shear dynamic modulus  $G^*(\omega)$  (and, correspondingly, the relaxation modulus  $G(t)$ ) of polymer networks and gels often shows a power law behavior (especially at the sol-gel transition), see [101, 102, 152–154] and also Sect. 6. Therefore, we consider here a class of GGS-domains for which the relaxation modulus  $G(N_u; t)$  obeys this power law behavior in the region of internal, “intra-domain” relaxation:

$$[G(N_u; t)] \simeq \left( \frac{t}{\tau_u} \right)^{-\gamma}. \quad (154)$$

Here  $[G(N_u; t)]$  is the reduced relaxation modulus of a domain (divided by  $\nu_u k_B T$ , where  $\nu_u$  is the number density of relaxing units),  $\gamma$  is a positive constant,  $\gamma > 0$ , and  $\tau_u$  is the characteristic relaxation time of a relaxing unit, which is assumed to be the same for all of the domains.

As was pointed out in Sect. 3.1, the mechanical relaxation is characterized by the relaxation spectrum  $H(\tau)$  which is connected to  $[G(N_u; t)]$  through Eq. 27. If  $[G(N_u; t)]$  scales as given by Eq. 154, the corresponding relaxation spectrum  $H(N_u; \tau)$  also follows a scaling behavior [3, 151, 155]:

$$H(N_u; \tau) \simeq \gamma \left( \frac{\tau}{\tau_{\text{char}}} \right)^{-\gamma}. \quad (155)$$

Since the domains are finite, they can be characterized by their maximal relaxation times  $\tau_{\text{max}}(N_u)$ , which depend on the number of relaxing units  $N_u$  inside them. It is a straightforward matter to demonstrate, using Eqs. 155 and 29, that as long as the power law behavior of  $[G(N_u; t)]$  holds inside the domain ( $t < \tau_{\text{max}}(N_u)$ ), the relaxation times can be represented as  $\tau(\xi) \simeq \tau_u(N_u/\xi)^{1/\gamma}$ , where  $\xi$  is a continuous variable  $\xi$ , see Sect. 3.1.2 and [151]. Therefore, for  $\tau_{\text{max}}(N_u)$  one immediately has ( $\xi = 1$ ):

$$\tau_{\text{max}}(N_u) \simeq \tau_u N_u^\alpha \quad (156)$$

with  $\alpha = 1/\gamma$ . Note that  $\alpha > 0$ , since  $\tau_{\text{max}}(N_u)$  increases as the size of the domains increases. At times exceeding  $\tau_{\text{max}}(N_u)$  one has an exponential decay of

the relaxation modulus  $[G(N_u; t)]$  of a domain of finite size [151]:

$$[G(N_u; t)] \simeq \frac{1}{N_u} \left( \frac{\tau_{\max}(N_u)}{t} \right) \exp \left( - \frac{t}{\tau_{\max}(N_u)} \right). \quad (157)$$

In other words, at  $t > \tau_{\max}(N_u)$  the relaxation modulus of the domain is mainly governed by the maximal relaxation time  $\tau_{\max}(N_u)$  which, in turn, is defined by the number of relaxing units inside the domain, see Eq. 156.

Now, to obtain the relaxation modulus of the whole heterogeneous network one has to average over all of the domains, in a similar way to the previous section, see Eq. 152. To proceed, one has to assume a distribution for the domain sizes; we let this distribution  $P(N_u)$  have the rather general form [151]:

$$P(N_u) \simeq N_u^\sigma \exp \left[ - C \left( \frac{N_u}{N_d} \right)^\delta \right], \quad (158)$$

where  $\delta$  and  $\sigma$  are parameters ( $\delta > 0$ ),  $N_d$  is the number of relaxing units in a domain of *average* size, and  $C$  is a constant. Performing now the averaging with respect to the distribution function  $P(N_u)$  and focusing on long times (therefore, assuming that the main contribution comes from the terminal relaxation of each domain, see Eq. 157), we finally end up with the following asymptotic expression for the relaxation modulus  $[G(t)]$  of the heterogeneous network [151]:

$$[G(t)] \simeq \frac{1}{N_d} \left( \frac{t}{\tau_d} \right)^{(\sigma-3\delta/2)/(\alpha+\delta)} \exp \left[ - C' \left( \frac{t}{\tau_d} \right)^{\delta/(\alpha+\delta)} \right], \quad (159)$$

where  $C'$  is a constant and

$$\tau_d \simeq \tau_{\max}(N_d) = \tau_u N_d^\alpha, \quad (160)$$

see Eq. 156 for  $N_u = N_d$ . Thus, Eq. 159 indicates that the  $[G(t)]$  of inhomogeneous polymer networks formed by non-interacting domains of different sizes decays at long times,  $t \gg \tau_d$ , following a stretched exponential pattern whose exponent is  $\delta/(\alpha + \delta)$ . This exponent ranges between 0 and 1 for all positive values of  $\delta$  and  $\alpha$ . Note that mathematically this nonexponential behavior arises from the averaging with respect to the distribution, Eq. 158; it has the same mathematical origin as Eq. 153 discussed in the previous section for polydisperse polymer networks [142]. Stretched exponential forms were also reported in several studies which dealt with the free-volume theory of glassy relaxation [156], with the electric birefringence in dilute solutions of polyelectrolytes [157], with trapping processes [158, 159], and so on.

A concrete form of the distribution  $P(N_u)$ , Eq. 158 – in other words values for the parameters  $\delta$  and  $\sigma$  – may be determined based on physical arguments. For instance, the distribution of chain lengths in polydisperse polymer networks was shown to have a Poisson form [142], see Eq. 151 of the previous section. Therefore, one has in this case  $\delta = 1$  in Eq. 158 and also  $\alpha = 2$ ,

since now each domain is just a single Rouse chain, see Eq. 156. This leads immediately to a stretched exponential behavior with index  $\delta/(\alpha + \delta) = 1/3$ , so that we reproduce Sommer's result [142], Eq. 153. We note that a power-law prefactor  $N_u^\sigma$  in the distribution function  $P(N_u)$ , Eq. 158, influences only the power-law preexponential term in Eq. 159. Given that the asymptotic behavior of  $[G(t)]$  is governed mainly by the stretched exponential term, we skip the power-law terms of Eqs. 158 and 159 in the examples that we provide below.

### 7.5.2

#### Mesh-Like Inhomogeneous Polymer Networks

We start by choosing for the domains of Fig. 16 topologically-cubic networks built from Gaussian springs [151, 160], see Sect. 5.1.1. The relaxation spectrum  $H(\tau)$  of such domains obeys a  $\tau^{3/2}$  behavior, see [24, 30, 62–65] and also Sect. 5.1.1. According to Eq. 156, each such domain containing  $N_u$  cross-links has a maximal relaxation time  $\tau_{\max} \simeq \tau_0 N_u^{2/3}$ ; in other words, here we have  $\alpha = 2/3$ . For  $P(N_u)$ , see Eq. 158, an analog of the Poisson distribution of Eq. 151, namely  $P(N_u) \sim \exp[-(N_u/N_d)]$  is used [151, 160]. We recall that this distribution corresponds to random and uncorrelated cross-linking. Thus, in this case  $\delta = 1$ , and from Eq. 159 one has for the relaxation modulus  $G(t)$  of the 3-D heterogeneous mesh-like network as a whole [151, 160]:

$$[G(t)] \sim \exp \left[ -C' \left( \frac{t}{\tau_d} \right)^{3/5} \right]. \quad (161)$$

Besides 3-D heterogeneous networks, it is also interesting to consider their two-dimensional analogs. For this we take as domains the topologically-square networks studied in Sect. 5.1.2. It is then straightforward to demonstrate that the parameter  $\alpha$  in Eq. 156 is equal to 1, since  $H(\tau)$  follows a  $1/\tau$  behavior [65, 68–70, 151]. Furthermore, in order to average over the domains one can use here the same form for  $P(N_u)$  as that employed above for the 3-D networks, with  $\delta = 1$ . As a result, the relaxation modulus  $[G(t)]$  of the heterogeneous 2-D network has the following long-time behavior [151]:

$$[G(t)] \sim \exp \left[ -C' \left( \frac{t}{\tau_d} \right)^{1/2} \right]. \quad (162)$$

This is another example of a stretched exponential behavior at long times. In principle, one can apply the same calculations to any network built from domains of arbitrary internal architecture, as long as the relaxation spectrum inside the domains obeys a power-law form, see Eq. 155. For instance, the networks may belong to any type of regular lattice topology (bcc, fcc, tetrahedral, triangular, hexagonal) or even be fractal structures.

### 7.5.3

#### Inhomogeneously Cross-Linked Polymeric Gels

In this section we apply the above approach to inhomogeneous polymeric gels which display random cross-link agglomerations. In Sect. 6.2 we pointed out that the shear modulus of gels often displays a power law decay and that this behavior can be well reproduced by the ladder model [100]. Therefore, here we employ the ladder model, see Fig. 10, for the internal structure of the domains. We are interested in units of finite size, so that the ladder ends either with a spring or with a Maxwell element (a spring and a dashpot in series) [100]. We use here ladders with Maxwell elements as final elements (pre-gel regime), since in this case the condition that different domains relax independently is easier to justify: this corresponds to cross-link agglomerations (domains) inserted into a more dilute environment.

As was discussed in Sect. 6.2, the complex shear modulus  $G^*(\omega)$  of the simplest ladder model follows a  $\omega^{1/2}$  behavior [100], so Eq. 156 gives us  $\tau_{\max} \simeq \tau_{\text{lad}} N_u^2$  (so  $\alpha = 2$ ). Note that the same dependence of  $\tau_{\max}$  on the size of a ladder network was also proved numerically [100]. Therefore, using a Poisson-type distribution,  $P(N_u) \sim \exp[-(N_u/N_d)]$  and setting  $\delta = 1$ , one has from Eq. 159 [151]:

$$[G(t)] \sim \exp \left[ -C' \left( \frac{t}{\tau_d} \right)^{1/3} \right]. \quad (163)$$

Thus, we again find for inhomogeneously cross-linked gels a stretched exponential decay of the relaxation modulus  $G(t)$  on scales larger than the average size of the structural inhomogeneities (cross-link agglomerations). Remarkably, the stretched exponential index here,  $1/3$ , coincides with that found by Sommer for polydisperse polymer networks [142], see Sect. 7.4. This is an expected result, since a ladder model is equivalent to a linear Rouse chain, see Sect. 6.2.

Furthermore, the above treatment can be easily extended to a more general situation when the internal structure of the domains is given by ladder models for which the shear modulus  $G^*(\omega)$  follows a  $\omega^\beta$ -behavior with  $0 < \beta < 1$  inside the domains, see Eq. 132 of Sect. 6.2. In this case  $\tau_{\max} \simeq \tau_{\text{lad}} N_u^{1/\beta}$  (so  $\alpha = 1/\beta$ ), and using a Poisson distribution with  $\delta = 1$  leads to (see Eq. 159):

$$[G(t)] \sim \exp \left[ -C' \left( \frac{t}{\tau_d} \right)^{\beta/(1+\beta)} \right]. \quad (164)$$

Thus, the microscopic (intra-domain) power-law behavior of the relaxation modulus of inhomogeneous gels,  $[G(t)] \sim t^{-\beta}$  with  $0 < \beta < 1$ , is replaced on much larger scales by a stretched exponential decay, Eq. 164. Note that Eq. 163 follows from Eq. 164 for  $\beta = 1/2$ .

As regards applications, a recent study [161, 162] of the stress relaxation in near-critical gels (where the same long-time relaxation behavior of gels was derived on the basis of quite different considerations) is of particular interest. As a model for polymeric gels, the authors considered a system consisting of  $N$  vertices (monomers in the context of gelation) which were randomly connected by means of  $cN$  edges (cross-links), where  $c$  is the concentration of cross-links. A pre-gel situation was considered ( $c < c_{\text{crit}}$  where  $c_{\text{crit}}$  is the critical concentration at the percolation transition). Then a given realization of the system can be decomposed into finite connected components (clusters). The density of eigenvalues for such a system was calculated analytically in the mean-field approximation. It was found [161, 162] that the eigenvalue density shows a Lifshits tail for small eigenvalues, giving rise to a stretched exponential decay for the relaxation modulus at very long times,  $\exp[-(t/\tau^*)^{1/3}]$ .

## 8

### Dendritic Polymers

#### 8.1

##### Tree-Like Networks

##### 8.1.1

##### Tree-Like Gaussian Structures

In this section we focus on the dynamics of tree-like polymer networks [11, 163, 164]; these have no closed loops, which makes them simpler than usual networks with mesh-like topologies, see Sect. 5. There were several early studies of the dynamics of tree-like structures built from elastic Gaussian springs. For instance, Chompff treated small tree-like structures [163] (“branched stars” according to his terminology) using the decoupling procedure, see also [165] and Sect. 5.2.2. Ronca determined the dynamical structure factor for tree-like networks [166]. A comprehensive treatment of tree-like Gaussian networks was performed by Graessley [11], whose work we outline below.

Graessley analyzed the equilibrium and the dynamical properties of polymers based on small, tree-like micronetworks [11, 167, 168]. These Gaussian micronetworks represent perfectly branched, symmetrical GGS, which grow from a central bead, see a particular example in Fig. 17; the micronetworks are finite Cayley trees (dendrimers). The peripheral beads of these micronetworks are assumed to be fixed in space. When calculating the quasi-equilibrium elastic properties, the peripheral beads are taken to move affinely with the macroscopic deformations [167, 168]. The evaluation of the relaxation spectrum  $H(\tau)$  and of the relaxation modulus  $G(t)$  is done in two steps. First, the spectrum of an ensemble of isolated tree-like micronetworks with

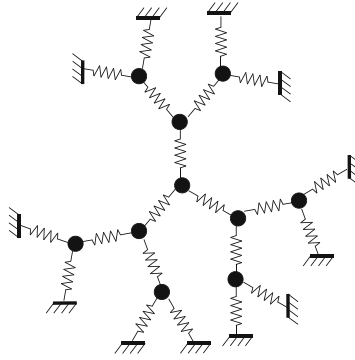


**Fig. 17** A tree-like Gaussian micronetwork of third order,  $J = 3$ , which is built from trifunctional beads,  $f = 3$

fixed peripheral beads is computed; then the contribution associated with the relaxation of the beads which are remote from the periphery is determined [11].

A single tree-like Gaussian micronetwork is built, following the GGS procedure, from beads with friction constant  $\zeta$  which are connected by springs with elasticity constant  $K$ , see Fig. 17. All beads have the same functionality  $f$  and  $J$  denotes the order of the tree; the peripheral beads are attached to immobile points, fixed in space. Graessley determines the relaxation spectrum of these micronetworks by analytical steps, aiming at diagonalizing the corresponding connectivity matrices  $A$ , see Eq. 2. The diagonalization is based on the successive partitioning of the determinant of  $(A - \lambda I)$  and leads to the following characteristic equation [11]:

$$C_1^{f[(f-1)^{J-2}]}. C_2^{f[(f-1)^{J-3}]} \dots C_{J-1}^f \cdot \left[ C_J - \frac{1}{(f-1)C_{J-2}} \right] = 0. \quad (165)$$

Here the  $C_m(f, \lambda)$  are defined iteratively as follows:

$$C_1(f, \lambda) = f - \lambda$$

and

$$C_m(f, \lambda) = f - \lambda - \frac{f-1}{C_{m-1}(f, \lambda)}. \quad (166)$$

Hence the  $C_m(f, \lambda)$  have the structure of continued fractions. Then, in the limit of large  $J$ , the relaxation modulus  $G(t)$  of the micronetwork ensemble is given by (we omit here the constant equilibrium modulus  $G_e$ ) [11]:

$$G(t) = M k_B T \frac{f(f-2)}{f-1} \sum_{m=1}^{J-2} (f-1)^{J-1-m} \sum_{r=1}^m \exp \left[ -\frac{2t}{\tau_m(r)} \right], \quad (167)$$

where  $M$  is the number of micronetworks per unit volume. In Eq. 167 the relaxation times  $\tau_m(r)$  are, as before, related to the eigenvalues through  $\tau_m(r) = \tau_0/\lambda_m(r)$ , see also Eq. 76, and, as usual,  $\tau_0 = \zeta/K$ . The eigenvalues  $\lambda_m(r)$  of the connectivity matrix  $A$  of the tree-like micronetwork are the roots of Eq. 165 and are found to fulfill [11]:

$$\lambda_m(r) = f - 2\sqrt{f-1} \cos \frac{\pi r}{m+1}, \quad \text{with } r = 1, \dots, m. \quad (168)$$

Following Graessley, the relaxation modulus of a macroscopic network is associated with contributions to the modulus from beads which are remote from the periphery [11]. Now, the sum over  $m$  in  $G(t)$ , Eq. 167, is related to the beads which are at a distance of  $m$  strands from the fixed peripheral beads [11]. Therefore, the contributions from beads remote from the periphery are related to terms in Eq. 168 with  $m$  large. Thus, to determine the relaxation times of the macroscopic network, it is enough to consider the limiting contribution,  $m \rightarrow \infty$ ; this implies a continuous set of relaxation times [11]:

$$\tau(\xi) \simeq \frac{\tau_0}{f - 2\sqrt{f-1} \cos \pi \xi}, \quad (169)$$

where  $0 < \xi < 1$ , see also Sect. 3.1.2. Now, the relaxation spectrum  $H(\tau)$  of the macroscopic network can be calculated with the use of Eq. 29; finally, one finds [11]:

$$H(\tau) \simeq \nu k_B T \frac{1}{2\pi\sqrt{f-1}} \frac{\tau_0/\tau}{\sqrt{1 - \frac{1}{4(f-1)}(f - \tau_0/\tau)^2}}, \quad (170)$$

where  $\nu$  is the number of beads per unit volume. In turn, the relaxation modulus  $G(t)$  reads [11]:

$$G(t) \simeq \nu k_B T \exp[-2ft/\tau_0] I_0[4\sqrt{f-1} t/\tau_0], \quad (171)$$

where  $I_0[x]$  stands for the modified Bessel function of order zero [11].

Equation 169 implies that the relaxation spectrum ranges from  $\tau_{\min} = \tau_0/(f + 2\sqrt{f-1})$  to the maximal relaxation time

$$\tau_{\max} = \frac{\tau_0}{f - 2\sqrt{f-1}}. \quad (172)$$

Note that Eq. 168 correctly reproduces the limiting case  $f = 2$  corresponding to the standard Rouse chain, see Eq. 55. On the other hand, Eq. 172 has to be viewed with care for  $f = 2$ . Furthermore, due to the limit  $m \rightarrow \infty$ ,  $\tau_{\max}$  does not depend on the network's size (on  $J$ ). Moreover, the width of the relaxation spectrum is characterized by the ratio  $\langle \tau^2 \rangle / \langle \tau \rangle^2$ , which is found to be equal to  $f/(f-2)$  [11]. This means that the spectrum gets narrower with increasing  $f$ . Thus, the relaxation spectrum of the tree-like network built from Gaussian

springs is rather narrow and is limited by the longest relaxation time  $\tau_{\max}$ , Eq. 172, which does not depend on the network's size.

**8.1.2  
Tree-Like Networks Built from Rouse Chains**

A decade later, Graessley's model of tree-like networks was extended by Kloczkowski et al [12, 169], mainly by replacing the bonds between the beads by Rouse chains. In [12, 169] the tree grows from a central chain, see Fig. 18 (not from a central bead, as in Graessley's case). Here, the branching points (junctions) are connected by means of Rouse chains; each chain consists of  $(n - 1)$  beads each with friction constant  $\zeta$  and  $n$  elastic springs each with elasticity constant  $K$ . Again, the two-step approach of Graessley [11] is used to compute the relaxation spectrum of the network. First, one calculates the spectrum of a tree-like micronetwork with fixed periphery, which is characterized by the functionality  $f$  of junctions (branching points) and by the number of tiers  $J$ . Then, one determines the part of the spectrum related to the motion of beads far away from the fixed points.

In solving the eigenvalue problem, use is made of the symmetry of the tree-like structure [12, 169, 170]. The system's symmetry reduces the characteristic equation for the eigenvalues of the connectivity matrix  $A$ ,  $\det(A - \lambda I) = 0$ , to the product of determinants of submatrices corresponding to subsequent generations (tiers). The characteristic equation which defines the eigenvalues  $\lambda$  is then [12]:

$$A_1^{m_J} \cdot A_2^{m_{J-1}} \cdots A_{J-1}^{m_2} (A_J^2 - 1) = 0. \tag{173}$$

Here  $m_l = 2(f - 1)^{l-1}$  with  $2 \leq l \leq J$  and

$$A_k = a_k U_{n-1}(1 - \lambda/2) - U_{n-2}(1 - \lambda/2), \quad 1 \leq k \leq J, \tag{174}$$

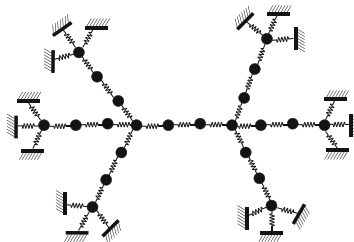


**Fig. 18** Sketch of a tetrafunctional ( $f = 4$ ) tree-like micronetwork built from Rouse chains. The network consists of two tiers of chains; each Rouse chain between tetrafunctional branching points has three springs ( $n = 3$ )

where  $U_n(x) = \sin[(n+1)x]/\sin(\arccos x)$  are the Chebyshev polynomials of the second kind [171] and the coefficients  $a_k$  satisfy the recurrence relation

$$a_k = f - \lambda - \frac{(f-1)[a_{k-1}U_{n-2}(1-\lambda/2) - U_{n-3}(1-\lambda/2)]}{a_{k-1}U_{n-1}(1-\lambda/2) - U_{n-2}(1-\lambda/2)}, \quad (175)$$

for  $2 \leq k \leq J$ , with  $a_1 = (f - \lambda)$ .

From the characteristic equation, Eq. 173, one obtains the following (rather involved) equations for the eigenvalues  $\lambda$  [12]:

$$U_k(F(1-\lambda/2)) + \sqrt{f-1} U_{n-2}(1-\lambda/2)U_{k-1}(F(1-\lambda/2)) = 0 \quad (176)$$

for  $1 \leq k \leq (J-1)$  and

$$\left[ \frac{U_k(F(1-\lambda/2)) + \sqrt{f-1} U_{n-1}(1-\lambda/2)U_{k-1}(F(1-\lambda/2))}{U_{k-1}(F(1-\lambda/2)) + \sqrt{f-1} U_{n-1}(1-\lambda/2)U_{k-2}(F(1-\lambda/2))} \right]^2 = \frac{1}{f-1} \quad (177)$$

for  $k = J$ , where the function  $F(x)$  is given by:

$$F(x) = \frac{U_n(x) + (f-2)U_{n-1}(x) - (f-1)U_{n-2}(x)}{2\sqrt{f-1}}. \quad (178)$$

By then applying Graessley's procedure, the authors [12] extract the contribution to the spectrum from beads far away from the periphery in the limit when the number of tiers  $J$  goes to infinity. They show that a solution of the eigenvalue problem, see Eqs. 176 and 177, can be obtained in the limit  $k \rightarrow \infty$  from [12]

$$F\left(1 - \frac{\lambda}{2}\right) = \cos \frac{\pi r}{k+1}, \quad \text{with } r = 1, \dots, k, \quad (179)$$

where  $F(x)$  is given by Eq. 178. This simplified equation is then solved analytically in the cases that  $n = 1$  or that  $n = 2$ . When  $n = 1$  (a single spring between the branching points, see the previous section) one recovers Graessley's solution [11], see Eq. 168. For  $n > 2$  the eigenvalues  $\lambda$  can be found numerically from Eqs. 179 and Eq. 178. It turns out, however, that the relaxation spectrum  $H(\tau)$  (the distribution function of relaxation times  $\tau$ ) can be obtained without the numerical solution of Eq. 179. As discussed above, one can introduce a continuous variable  $\xi = r/(k+1)$  ( $0 < \xi < 1$ ), see Eq. 179;  $H(\tau)$  is calculated then using Eq. 29 [12], obtaining:

$$H(\tau) = \frac{\nu k_B T \tau_0}{2\pi\tau} \frac{F'(x)}{\sqrt{1-F^2(x)}}, \quad (180)$$

where  $\tau_0 = \zeta/K$ ,  $\nu$  is the number of beads per unit volume,  $F(x)$  is given by Eq. 178,  $F'(x)$  denotes the derivative  $(d/dx)F(x)$ , and

$$x = 1 - \frac{\lambda}{2} = 1 - \frac{\tau_0}{2\tau}. \quad (181)$$

Now, making use of Eqs. 27 and 180, one has for the relaxation modulus  $G(t)$  [12]:

$$G(t) = \nu k_B T \exp[-4t/\tau_0] \frac{1}{\pi} \int_{-\infty}^1 dx \frac{F'(x)}{\sqrt{1-F^2(x)}} \exp[4tx/\tau_0]. \quad (182)$$

Analysis of Eq. 180 shows that  $H(\tau)$  consists of continuous bands of relaxation times; the number of bands increases with  $n$ , in other words with the length of the Rouse chains between the branching points [12]. To be noted is that in logarithmic scales in an intermediate regime the bands of  $H(\tau)$  show an almost linear behavior with slope 1/2 as a function of  $\tau$ ; the Rouse chains between branching points seem to be responsible for this behavior. Also, it is shown in [12] that the maximal relaxation time  $\tau_{\max}$  of the whole relaxation spectrum is approximately given by

$$\tau_{\max} \simeq \tau_0 \frac{n(nf - f + 2)}{2(f - 2\sqrt{f-1})}. \quad (183)$$

For the special case  $n = 1$ , Eq. 183 recovers Graessley's result, Eq. 172. For quite long chains,  $n \gg 1$ , the maximal relaxation time  $\tau_{\max}$  goes as  $n^2\tau_0$ , which leads to a considerable broadening of the relaxation spectrum in the domain of short times, a fact due to the inclusion of the chains between the branching points. Thus, for tree-like networks the relaxation spectrum turns out to be broader than in Graessley's model of the previous section.

However, this change does not affect the long-time regime, determined by the relaxation of the whole network. Indeed, one can easily connect  $\tau_{\max}$  with the maximal relaxation time  $\tau_{\max}^{\text{CG}}$ , Eq. 172, of Graessley's structure, viewed as being a coarse-grained model. Here "CG" stands for "coarse-grained", by which we imply, as in Sect. 5, that the Rouse chains between branching points are replaced by single elastic springs each with elasticity constant  $K_{\text{CG}} \simeq K/n$ , and that a coarse-grained bead (junction) accumulates the overall friction of half of each chain directly attached to it; in other words that  $\zeta_{\text{CG}} \simeq f(n/2)\zeta$ ; then the characteristic times of both models,  $\tau_0$  and  $\tau_{\text{CG}}$ , are related as follows:

$$\tau_{\text{CG}} \simeq \frac{fn^2}{2} \tau_0. \quad (184)$$

Taking Eq. 183 for large  $n$ , inserting Eq. 184 into it and recalling Eq. 172 leads to:

$$\tau_{\max} \simeq \tau_0 \frac{n^2 f}{2(f - 2\sqrt{f-1})} \simeq \tau_{\text{CG}} \frac{1}{f - 2\sqrt{f-1}} = \tau_{\max}^{\text{CG}}. \quad (185)$$

In other words, the maximal relaxation times of both models coincide. As already observed, these times do not depend on the size of the network (on  $J$ ).

Moreover, in both models the relaxation spectrum is quite narrow. The reason for this behavior is that in both models the peripheral beads are kept fixed; this prevents big network portions from moving with respect to each other and, therefore, eliminates the very low-frequency modes. Furthermore, letting the number of tiers  $J$  go to the limit  $J \rightarrow \infty$  is also questionable; a perfect tree with  $f > 2$  cannot grow indefinitely in 3-D because the number of monomers increases exponentially with  $J$ .

## 8.2

### Trifunctional Dendrimers

Recently, interest in polymers with perfect tree-like topologies was enhanced by developments in the synthesis of regular branched structures (dendrimers). Dendrimers are macromolecules that have regularly branched architectures [172–175]. They display a series of unique properties, which are well characterized by their generation number  $g$ ; their applications are broad and range from serving as building blocks for constructing complex polymer materials with new architectures to their use as novel non-viral vectors for drug and gene delivery.

Several works have been devoted to the theoretical studies of the equilibrium and dynamic properties of dendrimers [13, 33, 176–184]. These studies were complemented by computer simulations [185–191]. In most studies trifunctional dendrimers were considered (the functionality of the branching points was taken to be three,  $f = 3$ ). The reason for this is two-fold. First,  $f = 3$  holds for polyamidoamine [172] and polyether [173] dendrimers, which were extensively studied experimentally. Second, the number of monomers in a dendrimer increases exponentially with the generation number  $g$ , and, for a given  $g$  the increase depends on  $f$ . Therefore, larger  $f$  mean much larger dendritic systems at the same  $g$ . This leads to larger connectivity matrices within the GGS (Rouse-Zimm) formalism and to more densely packed structures when Monte Carlo or molecular dynamics simulations are used.

Now, in a GGS approach one has to determine the eigenvalues of the connectivity matrix  $A$  of the dendrimer. Most work centered then on the direct diagonalization of  $A$  with the use of analytical [179] or numerical methods [13, 33, 180]. In this respect, the theoretical study of Cai and Chen [179] is of particular interest. They considered the GGS dynamics of trifunctional dendrimers built from beads (each having a friction constant  $\zeta$ ) and springs (each having an elasticity constant  $K$ ). The model is certainly appropriate when viewing it as arising from a dendrimer structure consisting of flexible, long spacers. We note that many dendrimers with several spacers between the branching points were synthesized. On the other hand, the GGS approach is an approximation when the inter-bead bonds are stiff or when, due to density, other interactions may enter the picture.

In general, it has to be emphasized that many interactions may become important for the dynamics of dendrimers, depending on their geometrical features and on the dendrimers' concentration in solution. For instance, excluded volume interactions play a fundamental role when the dendritic structure is densely packed, as is the case for covalently-bound dendritic (Cayley) trees without spacers. For such molecules one cannot even define a  $\theta$ -temperature at which the dendrimer would behave in a quasi-ideal (Gaussian) fashion. The reason is that to compensate the three-body repulsions which increase with increasing density (with increasing  $g$ ), one has to decrease the supposed  $\theta$ -temperature in order to render the two-body attractions stronger [182, 191–193]. This compensation, however, cannot be achieved fully. On the other hand, the hydrodynamic interactions turn out to be important for dilute solutions of dendrimers; in contrast to linear chains, however, the pre-averaging techniques have to be used with care [194]. For instance, important features of dendrimer solutions such as the non-monotonic dependence of the zero-shear rate viscosity of dendrimers on the generation number can be only observed when the hydrodynamic interactions are explicitly taken into account [190]. With increasing concentration the hydrodynamic interactions are getting screened and the GGS approximation seems to be acceptable as long as the dendrimer density (the number of generations) does not get quite high. We note that since the strands between the branching points of dendrimers are as a rule rather short, entanglement effects in dendrimers can in general be neglected [195].

Cai and Chen attacked the problem through a direct analytical diagonalization of the connectivity matrix of trifunctional dendrimers and gave a very clear physical interpretation for the normal modes and relaxation times encountered [179]. In particular, they found that the normal modes can be categorized into two general groups: (i) normal modes involving bead motions with a mobile central monomer (which is also called core) and (ii) normal modes involving motions with an immobile core [179]. In the linear viscoelasticity framework of our review, any displacement of the dendrimer beads can be formulated as a linear combination of these normal modes. A trifunctional dendrimer of generation  $g$  consists of

$$N_{\text{tot}} = 3(2^g - 1) + 1 \quad (186)$$

beads. Note that  $g$  differs here from  $J$ , the order of a tree in Graessley's model, see Sect. 8.1.1; one has  $g = (J - 1)$ . As before, the displacement of the dendrimer as a whole is determined by the vanishing eigenvalue  $\lambda = 0$ . For the other  $(N_{\text{tot}} - 1)$  non-vanishing eigenvalues Cai and Chen find implicit analytical expressions, based on the underlying dendrimer symmetry [179]. Compared to the work reported in the last two sections, these equations are more transparent, since they involve trigonometric and hyperbolic functions only.

It turns out that exactly  $g$  nonvanishing eigenvalues of the first group (modes involving a mobile core) exist, which can be found by solving the following equation [179]:

$$2 \left[ \sin(g+2)\chi - \sqrt{2} \sin(g+1)\chi \right] = \sin g\chi - \sqrt{2} \sin(g-1)\chi, \quad (187)$$

where  $\chi$  is given by

$$\chi = \arccos \left[ (3 - \lambda) / 2\sqrt{2} \right], \quad (188)$$

with  $0 < \chi < \pi$ . All  $g$  eigenvalues of this group lie in the range  $(3 - 2\sqrt{2}, 3 + 2\sqrt{2})$ . Since significant contributions to several various dynamical quantities come from the smallest eigenvalues, these eigenvalues are of particular interest and importance. For large dendrimers,  $g \gg 1$ , the smallest eigenvalue  $\lambda_{\min}^{(1)}$  involving the motion of the core is approximately [179]:

$$\lambda_{\min}^{(1)} \simeq 3 - 2\sqrt{2} \cos(\pi/g), \quad (189)$$

very close to  $(3 - 2\sqrt{2})$  for large  $g$ .

The second group of normal modes (for an immobile core) involves beads belonging to two subbranches which stem from a common root (branching point). The motions may involve displacements of rather large parts of the molecule with respect to each other; such parts may be either the main branches themselves or smaller subbranches. All in all, there are  $g$  subgroups within this group, in which the central bead (core) stays immobile. A specific feature of this group of normal modes is their degeneracy. In the case when the main branches move as a whole with respect to each other, the degeneracy equals 2; it increases when larger and larger parts of the dendrimer stay immobile. The smallest eigenvalue  $\lambda_{\min}^{(2)}$  of this group of normal modes fulfills the relation [179]:

$$\sinh(g+1)\chi = \sqrt{2} \sinh g\chi, \quad (190)$$

with

$$\chi = \ln \left[ \frac{1}{2\sqrt{2}} \left( 3 - \lambda + \sqrt{1 - 6\lambda + \lambda^2} \right) \right], \quad \chi > 0. \quad (191)$$

For large  $g$  one has approximately [179]:

$$\lambda_{\min}^{(2)} \simeq 2^{-(g+1)}. \quad (192)$$

One may note this important result; for a freely floating dendrimer the smallest eigenvalue depends exponentially on the generation number (on the dendrimer's size).

Using Eqs. 189 and 192, one can now compare the corresponding maximal relaxation times  $\tau_{\max} = \tau_0 / \lambda_{\min}$ , where  $\tau_0 = \zeta / K$ , stemming from the two

different groups of eigenmodes. One has:

$$\tau_{\max}^{(1)} \simeq \frac{\tau_0}{3 - 2\sqrt{2}} \quad (193)$$

and

$$\tau_{\max}^{(2)} \simeq \tau_0 2^{(g+1)}. \quad (194)$$

Note that the maximal relaxation time  $\tau_{\max}^{(1)}$  of the first group, Eq. 193, does not depend on the dendrimer's size and coincides with the maximal relaxation time of Graessley's coarse-grained tree-like network with a fixed periphery, see Eq. 172. In contrast, the maximal relaxation time of the second group,  $\tau_{\max}^{(2)}$ , increases exponentially with the number of generations. It often represents the longest relaxation time of the dendrimer as a whole, because, for large  $g$ , it significantly exceeds  $\tau_{\max}^{(1)}$ . As a side remark, we note that the underlying physical reason for the extremely narrow relaxation spectrum of a tree-like network with fixed peripheral beads is due to the fact that its immobile periphery prevents the motion of whole (sub)branches relative to each other and the related appearance of the corresponding size-dependent eigenmodes. From Eq. 186 it is evident that the longest relaxation time is proportional to the total number of beads,  $N_{\text{tot}}$ , of the dendrimer, so  $\tau_{\max}^{(2)} \simeq \tau_0 N_{\text{tot}}$ . Therefore, the longest relaxation time of a dendrimer is smaller than that of a linear chain ( $\tau_{\text{chain}}$ ) of the same molecular weight (see Eq. 57), but much larger than that of a chain consisting of  $g$  beads [179].

The dynamic properties of trifunctional dendrimers were studied in [13, 33] by numerically diagonalizing the connectivity matrices of dendrimers with  $g$  ranging from  $g = 3$  to  $g = 9$ . Excellent agreement was found between the eigenvalues determined in this way and those obtained using the analytical procedure of Cai and Chen [179]. The eigenvalues were then used to calculate the displacements of monomers under external forces and also the dynamic shear modulus, see Sect. 3. Remarkably, no power-law behavior (no scaling) was found in the domain of intermediate frequencies (times) [13, 33]. This is in contrast to the behavior of linear polymer chains, of topologically-regular and of mesh-like and fractal networks. Instead, for dendrimers one sees a nearly logarithmic behavior in the double logarithmic plots of  $G'(\omega)$ ,  $G''(\omega)$ , and  $\langle\langle Y(t) \rangle\rangle$ . This fact appears as the signature of the exponential growth of the dendrimer [13, 33]. In particular, the storage modulus [ $G'(\omega)$ ] at intermediate frequencies can be well described through [ $G'(\omega)$ ]  $\sim (1 + \ln(\omega\tau_0))$ , which is clearly different from the  $(\omega\tau_0)^{1/2}$ -behavior typical of Rouse chains.

### 8.3 Generalized Dendrimers

Apart from the trifunctional dendrimers considered above, more general structures are possible. The functionality of the inner branching points, the functionality of the core (central monomer), and the number of spacers may vary [74, 180, 184, 196]. We consider first the basic dendrimer topology (a single spring between branching points), and introduce a generalized dendrimer (GD), characterized by the functionality of the core,  $f_c$ , by the functionality of the other inner branching points,  $f$ , and by the number of generations,  $g$ , see an example in Fig. 19 [74]. Such a GD represents a wide class of dendritic structures, which include among others the “classical” dendrimers ( $f_c = f$ ) and the dendritic wedges [78] ( $f_c = (f - 1)$ ). Furthermore, star polymers are GD with  $f = 2$  and  $f_c$  arbitrary, the latter being just the number of arms of the star.

We recall that for large GGS (and for dendrimers in particular) the numerical diagonalization methods are extremely time-consuming; today’s reasonable limit (in terms of computer time and accuracy) is  $N_{\text{tot}} \simeq 10^4$ , given that all of the eigenvalues are needed. Also, the direct analytical diagonalization of the connectivity matrix of the GD (in line with the methods discussed in the previous section) is rather cumbersome. Fortunately, it turns out that it is possible to get all of the GD eigenvalues and eigenfunctions in a more analytically-minded way, without going into a detailed analytical matrix diagonalization [74]. The idea, as in the case of topologically-regular mesh-like networks, see Sect. 5, is to use a judicious analytical form for the eigenmodes, which then serves as an ansatz to simplify the equations. The method which we display below was first developed for classical dendrimers [196] (for them  $f = f_c$ , so all the beads have the same functionality), and then applied to

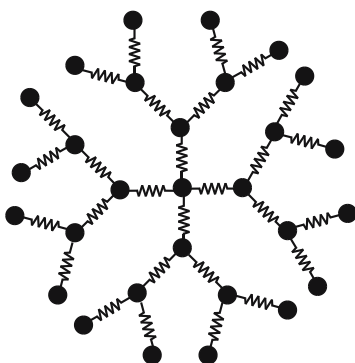


**Fig. 19** Example of a generalized dendrimer of third generation,  $g = 3$ . The functionality of the core,  $f_c$  and the functionality of the inner beads,  $f$ , differ and equal 4 and 3, respectively

dendritic wedges [78] (a wedge has one main branch less than the classical dendrimer).

In order to solve (as far as possible analytically) the eigenvalue problem, it is important to focus on the underlying topological symmetry of the GD. Taking this symmetry into account at a very early stage significantly simplifies the procedure. The classification of the normal modes, originally proposed by Cai and Chen for trifunctional dendrimers [179], can be naturally extended to GD. The eigenmodes of the GD belong, as before, to two general classes: class (i) involves normal modes in which the core is mobile, class (ii) consists of normal modes with an immobile core. That this assumption is correct is verified *a posteriori*, by counting all of the independent modes determined in this way. We continue by displaying the analytical approach and the main results.

A generalized dendrimer characterized by  $f_c$ ,  $f$ , and  $g$  consists of

$$N_d = f_c \frac{(f-1)^g - 1}{f-2} + 1 \quad (195)$$

beads for  $f \geq 3$  and of

$$N_d = (f_c g + 1) \quad (196)$$

beads for  $f = 2$ . When the core is mobile, the motion of the GD may involve all of its beads. The Langevin equations for the inner GD beads, Eq. 2, can be rewritten as [74]:

$$\zeta \frac{d\mathbf{R}_{j,m}(t)}{dt} + K \left[ f\mathbf{R}_{j,m}(t) - \mathbf{R}_{j-1,n}(t) - \sum_{l=1}^{f-1} \mathbf{R}_{j+1,l}(t) \right] = 0, \quad (197)$$

using the fact that each inner bead is connected to one bead from the previous and to  $(f-1)$  beads from the next generation. Here, for simplicity's sake, the stochastic force  $f(t)$  was excluded (say, by thermally averaging over the external fluctuations), since at this stage we are interested only in linear relations involving the normal modes, and thus the averaging can be performed at every stage in the calculations. In Eq. 197  $\mathbf{R}_{j,m}(t)$  is the position vector of the  $m$ th bead of the inner generation  $j$ , where  $0 < j < g$  and  $j = 0$  corresponds to the core.

In order to simplify the picture we assume the following structure for the solutions [74, 78]:

$$\mathbf{R}_{j,m}(t) = \sum_k C_k \Pi_k(j, m) \exp[-\lambda_k t / \tau_0], \quad (198)$$

where  $\tau_0 = \zeta/K$ , the  $C_k$  are  $j$ -independent constants, and  $\lambda_k$  and  $\Pi_k(j, m)$  are the eigenvalues and eigenfunctions, respectively. Equation 198 may be viewed as being a normal mode transformation, such as Eq. 9. To proceed, we use the following observation: the normal modes can be characterized by motions involving one root bead (branching point) and all its descendants of higher

generations. For such a subwedge that has the root as its ancestor, beads that belong to the same generation move in the same manner [74, 78, 196]. Thus, if the GD core moves, (in other words the core is the root), one has

$$\Pi_k(j, m) = \Pi_k(j) \quad (199)$$

for all of the beads of generation  $j$ , see also Fig. 3 in [179]. Now, using Eqs. 198 and 199, the Langevin equation, Eq. 197, gets simplified to

$$(-\lambda_k)\Pi_k(j) + [f\Pi_k(j) - \Pi_k(j-1) - (f-1)\Pi_k(j+1)] = 0. \quad (200)$$

One immediately obtains  $\Pi_k(j) = \text{const}$  as a solution of Eq. 200; its eigenvalue  $\lambda_1 = 0$  is related to the displacement of the dendrimer as a whole, under the influence of fluctuating forces. In the same fashion one can also simplify the boundary conditions – the equations of motion for the core,  $j = 0$ , and for the peripheral beads,  $j = g$ . In so doing, the eigenvalue problem for the normal modes of class ( $i$ ) is readily solved. We outline the final results and refer to [74, 78] for the details.

The eigenvalues  $\lambda_k$  and the eigenfunctions  $\Pi_k(j)$  corresponding to normal modes with a mobile core (class ( $i$ )) read [74]:

$$\lambda_k = f - 2\sqrt{f-1} \cos \psi_k \quad (201)$$

and

$$\begin{aligned} \Pi_k(j) = & \{ (f-1) \sin [(j+1)\psi_k] + (f_c - f)\sqrt{f-1} \sin (j\psi_k) \\ & + (f - f_c - 1) \sin [(j-1)\psi_k] \} (f-1)^{-j/2}, \end{aligned} \quad (202)$$

where the  $\psi_k$  are fixed by

$$\sin [(g+1)\psi_k] = \frac{f - f_c - 1}{\sqrt{f-1}} \sin (g\psi_k). \quad (203)$$

Interestingly, as long as the inequality  $(g+1)/g > |f - f_c - 1|/\sqrt{f-1}$  holds, Eq. 201 gives  $g$  distinct solutions.

In contrast, when  $(g+1)/g \leq |f - f_c - 1|/\sqrt{f-1}$ , only  $(g-1)$  modes (spatially periodic) follow from Eqs. 201, 202, and 203. In this case one additional normal mode (essentially spatially exponential) appears. For the new mode two cases must be distinguished: when  $(f - f_c - 1) > 0$  the new eigenvalue  $\Lambda$  and its eigenfunction  $\Pi(j)$  are given by [74]

$$\Lambda = f - 2\sqrt{f-1} \cosh \psi \quad (204)$$

and

$$\begin{aligned} \Pi(j) = & \{ (f-1) \sinh [(j+1)\psi] + (f_c - f)\sqrt{f-1} \sinh (j\psi) \\ & + (f - f_c - 1) \sinh [(j-1)\psi] \} (f-1)^{-j/2}, \end{aligned} \quad (205)$$

where  $\psi$  is the solution of

$$\sinh [(g+1)\psi] = \frac{f-f_c-1}{\sqrt{f-1}} \sinh (g\psi). \quad (206)$$

On the other hand, when  $(f-f_c-1) < 0$  the eigenvalue and eigenfunction of the exponential normal mode obey [74]

$$\Lambda = f + 2\sqrt{f-1} \cosh \psi \quad (207)$$

and

$$\begin{aligned} \Pi(j) = & (-1)^j \left\{ (f-1) \sinh [(j+1)\psi] - (f_c-f)\sqrt{f-1} \sinh (j\psi) \right. \\ & \left. + (f-f_c-1) \sinh [(j-1)\psi] \right\} (f-1)^{-j/2}, \end{aligned} \quad (208)$$

where  $\psi$  is determined from (refer to Eq. 206):

$$\sinh [(g+1)\psi] = - \frac{f-f_c-1}{\sqrt{f-1}} \sinh (g\psi). \quad (209)$$

We note that the case  $(f-f_c-1) = 0$  does not lead to the appearance of exponential normal modes, because one always has  $(g+1)/g > 0$  in this case.

Thus, in class (i) (normal modes involving the core) one finds  $(g+1)$  distinct, *nondegenerate* eigenvalues. In general, GD may have *both* spatially periodical and exponential normal modes of class (i). Note that classical dendrimers ( $f_c = f$ ) [196] and dendritic wedges ( $f_c = (f-1)$ ) [78] have only periodic normal modes in class (i), because for these two systems the inequality  $(g+1)/g > |f-f_c-1|/\sqrt{f-1}$  is automatically fulfilled.

It is important to emphasize that the minimal nonvanishing eigenvalue of class (i) is finite and does not depend on the generation number  $g$ , so it is insensitive to the GD size. Indeed, one can demonstrate that for spatially periodical normal modes the eigenvalues are bound from below by  $f-2\sqrt{f-1}$ , which is always positive, see Eq. 201. In turn, the eigenvalue  $\Lambda$  of the spatially exponential mode (when it exists) is bound from below by  $(f_c+1) - (f-1)/(f-f_c-1)$  for large  $g$ , so it is independent of  $g$  (note that for  $f_c = (f-1)$  no eigenvalue of exponential type exists). Thus, the values of the eigenvalues in class (i) are not very sensitive to  $g$ ; this is, however, not the case for the eigenvalues of class (ii).

The normal modes of class (ii) have an immobile core. In the case when only the core is immobile, the degeneracy of the corresponding eigenvalues is  $(f_c-1)$ -fold: one can consider those in which the main GD branches move to be eigenmodes. In order to keep the core immobile, only two neighboring main branches have to move against each other. Now focusing on one such branch, one can pick for it exactly  $(f_c-1)$  different partner branches [74, 78, 179, 196].

When the core is immobile, the problem turns (due to the symmetry of the system) into that of separate, mobile subwedges. The Langevin equations of

motion simplify in the same way as before. When only the core is immobile, the eigenvalues  $\lambda_k$  are again defined by Eq. 201, but the eigenfunctions  $\Pi_k(j)$  and  $\psi_k$  are given [74, 78] by

$$\Pi_k(j) = (f - 1)^{-j/2} \sin(j\psi_k) \quad (210)$$

and

$$\sin[(g + 1)\psi_k] = \sqrt{f - 1} \sin(g\psi_k), \quad (211)$$

where  $j = 1, \dots, g$ . The number of distinct solutions  $\psi_k$  again depends on an expression involving the parameters of the GD; Eq. 211 gives  $g$  distinct solutions if  $(g + 1) > \sqrt{f - 1} g$ . We note that this inequality can be fulfilled only for  $(f = 3; g = 1)$ ,  $(f = 3; g = 2)$ , and  $(f = 4; g = 1)$ . In all other cases, Eq. 211 gives only  $(g - 1)$  solutions. Then an exponential normal mode also appears, whose eigenvalue is of the form of Eq. 204, with  $\Pi(j)$  and  $\psi$  given by [74, 78]:

$$\Pi_k(j) = (f - 1)^{-j/2} \sinh(j\psi_k) \quad (212)$$

and

$$\sinh[(g + 1)\psi] = \sqrt{f - 1} \sinh(g\psi). \quad (213)$$

In this way one has  $g$  different eigenvalues in all cases. Now, taking into account the  $(f_c - 1)$ -fold degeneracy discussed before, one has a total of  $(f_c - 1)g$  class (ii) normal modes, in which next-neighbors to the core move.

In general, larger groups of non-core GD beads can stay immobile. One can use  $n$  (with  $0 < n < (g - 1)$ ) to denote the last generation in which all  $f_c(f - 1)^{n-1}$  beads are immobile. Evidently,  $(f - 1)$  mobile beads are attached to each of the immobile beads. A set of  $(f - 1)$  subwedges implies a  $(f - 2)$ -fold degeneracy, so that the total degeneracy is now  $f_c(f - 1)^{n-1}(f - 2)$ -fold, with  $n \in \{1, \dots, g - 2\}$ . In the general case the eigenvalues  $\lambda_k$  are still given by Eq. 201, with  $\Pi_k(j; n)$  and  $\psi_k$  obeying [74, 78]:

$$\Pi_k(j; n) = (f - 1)^{-j/2} \sin[(j - n)\psi_k] \quad (214)$$

and

$$\sin[(g + 1 - n)\psi_k] = \sqrt{f - 1} \sin[(g - n)\psi_k]. \quad (215)$$

Similar to the situation when only the core is immobile, Eq. 215 has  $(g - n)$  distinct solutions if  $(g - n + 1) > \sqrt{f - 1} (g - n)$ . If this condition is not fulfilled, one obtains only  $(g - n - 1)$  solutions in this way. Then one additional solution exists; it obeys Eq. 204, where now the corresponding eigenfunction  $\Pi(j; n)$  and the  $\psi$  are given by [74, 78]:

$$\Pi(j; n) = (f - 1)^{-j/2} \sin[(j - n)\psi] \quad (216)$$

and

$$\sinh[(g - n + 1)\psi] = \sqrt{f - 1} \sinh[(g - n)\psi]. \quad (217)$$

Furthermore, in the special situation in which only the peripheral beads move ( $n = (g - 1)$ ) one has the  $f_c(f - 1)^{(g-2)}(f - 2)$ -fold degenerate eigenvalue  $\lambda = 1$ .

Thus, in class (ii) one has  $(g - n)$  distinct eigenvalues for each  $n \in \{1, \dots, g - 1\}$ ; these are  $f_c(f - 2)(f - 1)^{n-1}$ -fold degenerate. The case  $n = 0$  provides  $g$  distinct eigenvalues, each  $(f_c - 1)$  times degenerate. Taking into account the  $(g + 1)$  eigenvalues of class (i) too, one has a total of  $N_d$  eigenvalues,  $N_d$  being given by Eqs. 195 and 196. In this way, one obtains *all* of the eigenvalues (relaxation times) of the GD, with their correct degeneracy.

The normal modes of two kinds found for GD correspond to two different physical pictures. Spatially periodic normal modes are internal modes inside the GD sub-branches; their eigenvalues are bound from below by a  $g$ -independent value,  $f - 2\sqrt{f - 1}$ , see Eq. 201. In turn, spatially exponential normal modes can be visualized through the motion of whole sub-branches against each other. The corresponding eigenvalues may be very small in value, providing a dominant contribution to the GD dynamics at long times. It was shown [74, 78, 196] that the minimal, non-vanishing eigenvalue of the whole GD,  $\lambda_{\min}^{\text{GD}}$ , does indeed belong to class (ii), and that for large  $g$  it is approximately:

$$\lambda_{\min}^{\text{GD}} \simeq \frac{(f - 2)^2}{(f - 1)^{(g+1)}}. \quad (218)$$

In other words it decreases exponentially with  $g$ . As expected, the minimal GD eigenvalue,  $\lambda_{\min}^{\text{GD}}$ , corresponds to a mode in which the largest (main) branches of the GD move.

Thus, the approach described above avoids having to perform direct operations on the connectivity matrix and makes it possible to get all of the GD eigenvalues and eigenfunctions. All of these analytical findings were also checked by extensive numerical matrix diagonalizations [74], which establish perfect agreement. Moreover, the general results obtained in this section reproduce the special results obtained previously for the classical dendrimers ( $f_c = f$ ) [179, 196] and for the dendritic wedges ( $f_c = f - 1$ ) [78] nicely. For instance, Eq. 218 for  $f = 3$  agrees with the approximate expression for the minimal eigenvalue of trifunctional dendrimers, Eq. 192. Also, the approach can be extended to copolymeric dendrimers built from beads with different mobilities [197].

In Fig. 20 we present the storage modulus  $[G'(\omega)]$  of GD of fourth generation with trifunctional inner branching beads, while the functionality of the core,  $f_c$ , varies from 1 to 10. Noteworthy is the fact that in the intermediate frequency domain the  $[G'(\omega)]$ -curves do not scale (they do not show a power-law behavior). In this region the  $G'(\omega)$ -curves reveal the underlying dendritic structure. Increasing the functionality of the core from  $f_c = 1$  to  $f_c = 10$  influences mainly the low-frequency domain, given that the contribution of the maximal relaxation time of the GD increases with  $f_c$  because of increasing

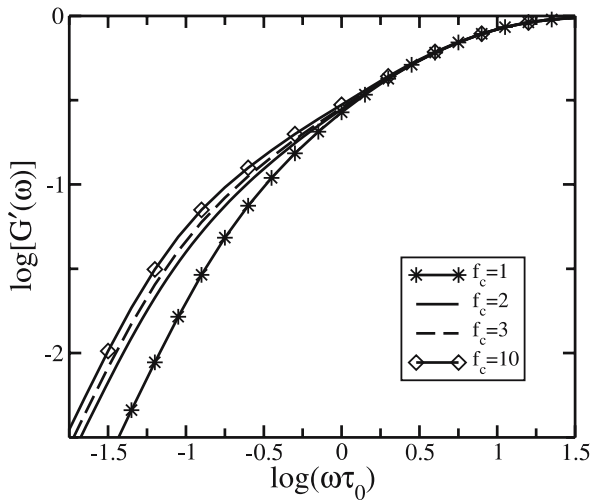


**Fig. 20** Reduced storage modulus  $[G'(\omega)]$  plotted on double logarithmic scales versus the reduced frequency  $\omega\tau_0$  for GD of fourth generation,  $g = 4$ , with trifunctional inner beads,  $f = 3$ . The functionality of the core,  $f_c$ , is varied from 1 to 10

mode degeneracy. As a result, the  $[G'(\omega)]$ -curves in Fig. 20 shift to the left when  $f_c$  increases [74].

As a final remark, we note that only the basic GD were discussed here. The approach presented here can be further generalized by replacing each interbead bond by Rouse chains with  $P$  bonds (spacers). The classification of the normal modes for such dendrimers with  $P > 1$  is similar to that for  $P = 1$  and was performed by Ganazolli et al [184]. It was demonstrated that in this case the eigenvalues can be grouped as follows. There are  $(1 + gP)$  nondegenerate eigenvalues corresponding to the class (i) normal modes in the terms of this section. The rest belong to class (ii); there are namely  $gP$  subgroups of  $(f_c - 1)$ -degenerate eigenvalues and  $(g - 1 - k)P$  subgroups of eigenvalues with degeneracy  $f_c(f - 1)^k(f - 2)$ , where  $k = 0, 1, 2, \dots, (g - 2)$  [184]. Note that the eigenvalues of such GD with  $P > 1$  were only obtained numerically [184]; the analytical treatment of these dendritic systems may be a subject for further study.

## 8.4

### Side-Chain Dendritic Polymers

As discussed in Sect. 8, the relaxation spectrum of a dendrimer differs considerably from that of a polymer chain. Due to the symmetry of the dendrimer many of its eigenvalues (relaxation times) are degenerate. This contrasts with the relaxation times of the Rouse chain which are all distinct (nondegenerate), see Sect. 4. Therefore, considering hybrid structures formed

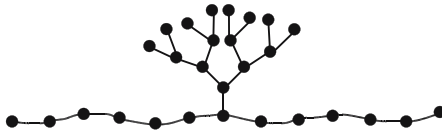


**Fig. 21** Polymer chain bearing a dendritic wedge in its middle

both by dendrimers and by chains is of particular interest. In this class one finds structures which consist of chains with pendant dendritic groups. These structures, called *side-chain dendritic polymers*, were recently synthesized [198–201].

A GGS model was used to treat side-chain dendritic polymers [78]. The model is given in Fig. 21; it consists of chains bearing dendritic wedges (CBDW) in their middles. A dendritic wedge (DW) differs from a conventional classical dendrimer in that its core has one main branch less:  $f_c = (f - 1)$ . For such DW the results of the previous section hold [74, 78]. In particular, the maximal relaxation time of a DW is the same as that of a classical dendrimer, because this time corresponds to the motion of two main branches against each other.

We do not expect the problem of determining the eigenvalues of CBDW to have a simple, analytical solution. In [78] the problem was solved numerically. The chains contain  $N_{\text{chain}}$  beads each; for symmetry's sake  $N_{\text{chain}}$  is taken to be an odd number, so that the DW divides the chain into two identical halves. Provided that the parameters of the wedge,  $f$  (functionality),  $g$  (generation number), and  $f_c = (f - 1)$ , are given, such a wedge consists of  $N_w$  beads, as given by Eq. 195.

An interesting question concerns the relationship between the chain length and the DW size. The longest relaxation times of a chain and of a wedge are given by  $\tau_{\text{max}}^{(\text{ch})} \simeq \tau_0 N_{\text{chain}}^2$  and  $\tau_{\text{max}}^{(\text{w})} \simeq \tau_0 (f - 1)^{g+1}$ , respectively, see Eqs. 57 and 218, where  $\tau_0 = \zeta/K$  is assumed to be the same both for the chain and for the wedge. In the case of short chains, when  $\tau_{\text{max}}^{(\text{w})} > \tau_{\text{max}}^{(\text{ch})}$ , the relaxation of the chain is strongly masked (screened) by the relaxation of the wedge, because of the high density (degeneracy) of the DW modes as compared to the modes of the chain. Thus, in the case of short chains one can expect an almost pure dendrimer-type relaxation.

Much more interesting is the situation when the chains is very long, so that  $\tau_{\text{max}}^{(\text{ch})} \gg \tau_{\text{max}}^{(\text{w})}$ ; this happens for  $N_{\text{ch}} \gg (f - 1)^{(g+1)/2}$ . In this case, for a fixed chain length, the CBDW storage and loss moduli decrease with increasing  $g$  in the intermediate frequency domain, see Fig. 22 for  $[G'(\omega)]$ . This happens as long as the inequality  $\tau_{\text{max}}^{(\text{ch})} \gg \tau_{\text{max}}^{(\text{w})}$  holds [78].

This theoretical result is in qualitative agreement with rheological data obtained for side-chain dendritic polymers that consist of a polyurethane main chain and of polyether wedges of second, third, and fourth generations [201].

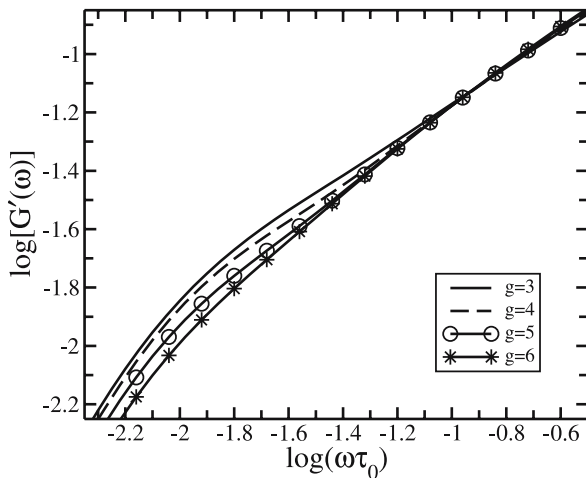


**Fig. 22** Reduced storage modulus  $[G'(\omega)]$  plotted on double logarithmic scales versus the reduced frequency  $\omega\tau_0$  for chains bearing trifunctional dendritic wedges of third, fourth, fifth, and sixth generation. All chains have the same length and consist of 51 beads ( $N_{\text{chain}} = 51$ ) [78]

It has a nice physical interpretation; as pointed out above, at high frequencies (at small length scales) the CBDW dynamics is determined by the DW and the influence of the chain is hidden. On the other hand, in the low-frequency domain the CBDW dynamics is governed mainly by the long chain, since the internal modes of the DW are not activated there. In fact, on such large length scales the wedge behaves as a single “massive” particle having an overall friction constant of  $N_w\zeta$ . With increasing  $g$  the particle gets more damped and hinders the mobility of the central bead of the chain to which it is attached more and more. This, in turn, inhibits the excitation of large-scale, *asymmetric* modes of the chain, leading to a speed-up of the terminal relaxation. Interestingly, this has no effect on the longest relaxation time of the chain, because the corresponding eigenmode is symmetric with respect to the central bead; in fact, this mode is related to the stretching of the Rouse chain at its ends, a motion in which the central bead stays fixed [40].

Furthermore, the fact that a dangling DW suppresses some low lying frequencies of the chain can be detected at  $\omega = 0$  by monitoring the zero shear viscosity  $[\eta'(0)]$ , see Eq. 22. In general,  $[\eta'(0)]$  is proportional to the sum of all finite relaxation times of the system in question. In the GGS framework, the  $[\eta'(0)]$  of an isolated DW is found to increase with  $g$ . We note that for dendrimers in dilute solutions, plotting the experimentally measured  $[\eta'(0)]$  versus  $g$  shows a maximum at some critical generation  $g_c$ . This feature is not found here; in [190] it was related to the role played by the hydrodynamic interactions. It turns out, however, that CBDW show the opposite trend, namely that  $[\eta'(0)]$  decreases with increasing  $g$  for CBDW, see Fig. 23. This stems

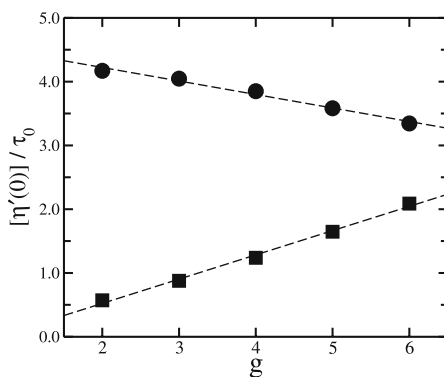


**Fig. 23** Reduced zero shear viscosity  $[\eta'(0)]/\tau_0$  plotted versus the number of generations,  $g$ , for trifunctional dendritic wedges. Shown are results for chains of 51 beads bearing dendritic wedges (*solid circles*) and for the corresponding individual dendritic wedges (*solid squares*)

from the fact that the main contribution to  $[\eta'(0)]$  is from the long relaxation times, some of which get suppressed when the size of the pendant DW gets larger. This effect was indeed confirmed by rheological experiments on side-chain dendritic polymers [201], in which  $g$  increased from 2 to 4. To conclude, we note that the GGS approach, although being rather simplified, reproduces qualitatively many important dynamical features.

## 9 Hyperbranched Polymers

As discussed in the previous section, the theoretical study of the dynamics of branched polymers and especially of dendrimers is extremely interesting. Viewed chemically, however, dendrimers are not simple to prepare, since their geometrical perfection requires a whole series of reaction steps, with necessary purification from unwanted by-products [172, 202–204]. For this reason one rather prefers to perform batch reactions, which lead to randomly structured (hyperbranched) macromolecules. Depending on the procedure, good preparation methods may result in products whose polydispersity is limited. The theoretical question which one is then confronted with is to know which of the macromolecular properties are most influenced by disorder and which change less when the reaction products are not as symmetric as perfect dendrimers. With this aim in mind, we will consider randomly-branched polymers, a class of substances that is also important from a theoretical point of view, given that hyperbranched structures are, topologically speaking, trees; in other words they do not have loops. The following sec-

tion is devoted to randomly-branched polymers, whereas after it we will discuss more regularly-shaped hyperbranched structures, namely comblike and regularly-hyperbranched polymers.

It is important to realize that the validity domain of the GGS description is better known for linear chains than for general branched polymers. The reason is similar to that discussed in Sect. 8.2 for the dendrimers: there is no clear (unique) way to define a  $\theta$ -temperature here, due to the higher local density of monomers around branching points [205]. For instance, for star polymers the  $\theta$ -temperature depends on the number and the molecular weights of the arms [193, 206, 207]. In dilute solutions the standard (pre-averaged) Zimm approximation fails for stars [208] and hyperbranched polymers [209] and, therefore, the hydrodynamic interactions have to be taken into account explicitly. Also of interest is the fact that, distinct from general fractals (see Sect. 6.3), the introduction of hydrodynamic interactions for fractal hyperbranched structures does not destroy the dynamic scaling properties [210]. For concentrated solutions and for melts of branched polymers entanglement effects seem to come into play at smaller molecular weights than for linear chains; such effects depend on the particular macromolecular architecture and on the size of the dangling chains. To account for entanglements, the tube theory was successfully applied to several branched structures, including stars [211, 212], tree-like (Cayley tree) polymers [213], pom-pom polymers [214, 215], combs and H-polymers [55, 195]. The limitations discussed in this paragraph have to be kept in mind when considering the GGS dynamics of hyperbranched polymers.

## 9.1

### Randomly-Branched Polymers

As stated above, topologically-hyperbranched macromolecules are trees; such structures are devoid of loops. One can then envisage the whole structure as starting from one central monomer, whose effective functionality in the network is  $f$ . In the simplest case the monomers attached to it may either have the same functionality (and thus be bound to other monomers) or be at the ends of dangling bonds. In this case (the functionality of each bead is either 1 or  $f$ ) the (percolating) network is a subset of the (infinite) Cayley tree; clearly the same holds for the dendrimers. More disorder can also be envisaged: this is the case when some monomers in the network have functionalities different from 1 or  $f$ . We will consider both cases of disorder in the following.

We start with the simpler case [216], in which the random branched structures are constructed analogously to the dendrimers; we take  $f = 3$  as an example. Then one begins with a three-functional starting unit but, distinct from the dendrimers, the branches are added not generation-wise but step-wise. We also keep track of orientation, taking it to point outwards from the origin. At each step a terminal vertex (TV) is chosen randomly and a pair of

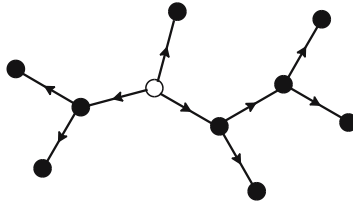


**Fig. 24** A randomly branched structure with  $N = 10$ . The open circle represents the point from which the GGS starts to grow

branches are attached to it (with outward orientation), by which two new TV are created, see Fig. 24. This procedure defines a particular class of branched polymers, for which the functionality of all internal vertices equals  $f = 3$ , and where  $N_t$ , the number of TV, is related to  $N$  by  $N_t = 1 + N/2$ . Evidently, the dendrimers belong to this class. When contrasting ordered with disordered structures, it is reasonable to take their  $N$  values to be very close, in order to highlight the effects of topological randomness on the dynamics. The above construction automatically attaches a direction to each bond, a feature which is useful when also taking angular constraints into account.

In [216] the dynamics of such randomly-branched objects were evaluated in the GGS framework, which was extended by also including angular and hydrodynamic interactions. In the calculations  $10^5$  realizations were used for objects as large as  $N = 190$  and for generations up to  $g = 6$ . We present  $[G''(\omega)]$  for such a random hyperbranched structure in Fig. 25. The data are from [216] and we consider two situations, namely one in which the angles between bonds are unrestrained (classical GGS-case) and one in which the angles have a preferential orientation, see [216] for details. Note that in Fig. 25 a shallow minimum for  $1 < \omega\tau_0 < 10$  appears, a fact also observed in [180]. Interestingly, in  $G'(\omega)$  and  $G''(\omega)$  the effect of the disorder is not very strong [216]. This, of course, may be due to the fact that the sixth generation ( $g = 6$ ) is still too small to show large structural variations. Much more pronounced in  $G'(\omega)$  and  $G''(\omega)$  are the influences of the hydrodynamic interactions and of the angular restrictions. The two effects go in different directions; while the hydrodynamic interactions act to reduce the dynamical range (and thus the width of the intermediate domain), the inclusion of angular restrictions increases the dynamical range (and hence the width of the intermediate domain). Interestingly, the effect goes in the same way for both regular structures and disordered hyperbranched molecules [216].

Moreover, the quantity that turns out to be most affected by disorder is  $G(t)$ . It shows large deviations from exponentiality and a clear-cut dependence on the geometrical and hydrodynamical aspects [216]. Evidently, it would be worthwhile to go to much larger values of  $N$ . Here, however, we reach a dilemma: while the eigenvalues of some regular structures can be obtained iteratively up to very high values of  $N$  [104–106], see also Sect. 6,

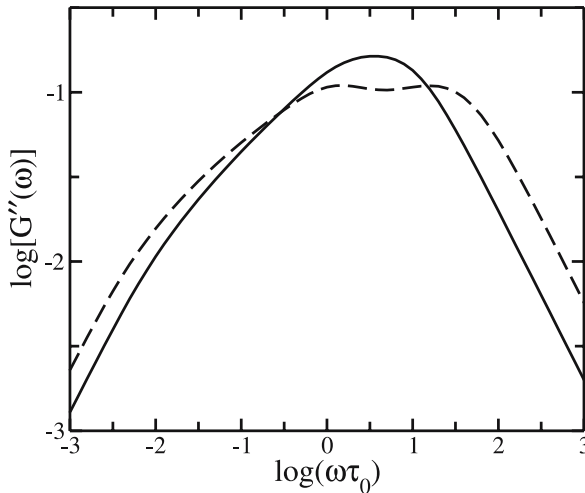


**Fig. 25** Reduced loss modulus  $[G''(\omega)]$  plotted on double logarithmic scales versus the reduced frequency  $\omega\tau_0$  for random branched polymers with  $g = 6$  and  $N = 190$ . Shown are the cases in which the angles between branching points are free (*solid line*) and in which a tetrahedral arrangement of angles is preferred (*dashed line*)

disordered structures do not offer such possibilities in general. In fact, with disordered structures the main problem does not stem from the technical difficulties associated with diagonalizing matrices for structures larger than, say  $N = 100$ , but from the need to average over many different realizations.

In this way one has consider other analytical methods apt to treating disorder. Here the advantage is that one deals with trees. Now, one may envisage the trees to have been created sequentially, according to a given probabilistic pattern. As we proceed to show, this feature allows us, based on the replica formalism, to develop a systematic way to compute the ensemble-averaged eigenvalue spectrum [217, 218]. In this way one automatically takes into account the averaging over distinct structural realizations. Here we follow the procedure of [219], which, by extending the theoretical study of gel dynamics given in [162], results in an integral equation formalism. Interestingly, as also found before [162], for specific probability distributions of the springs' strengths, the integral expressions take a particularly simple form.

In the model considered in [219], each realization of a randomly branched structure starts from a single monomer, to which one tries to attach a bond that ends in a new monomer with probability  $p$ . The attempt to add a bond is repeated  $f$  times, so that the number of bonds added to a starting monomer obeys a binomial distribution, and is, at most,  $f$ . The next step repeats the procedure of adding a bond ( $f - 1$ ) times at each of the monomers created in the previous step. Proceeding iteratively one obtains a randomly branched loopless structure [219]. The process of adding bonds ends if no bonds are

added in a given step. This event occurs with probability 1 below the percolation threshold  $p_c = 1/(f - 1)$  [220–222]; however, for  $p > p_c$ , there is a finite probability that the process never stops, and thus an infinite branched structure is formed.

For each of the structures obtained in this way, one has a Langevin equation, see Eq. 2, from whose eigenvalues the usual dynamic quantities follow. These involve for a certain structure  $S$  only the eigenvalues' density  $\varrho_S(\lambda)$  of the corresponding Laplace matrix  $A^S$ . Now, the ensemble-averaged density of eigenvalues is given by

$$\varrho(\lambda) = \langle \varrho_S(\lambda) \rangle \equiv \sum_S \omega_S \varrho_S(\lambda), \quad (219)$$

where the sum extends over all structures, each of the  $\varrho_S(\lambda)$  is normalized, and  $\omega_S$  denotes the probability that  $S$  is created in the iterative growth procedure. Each  $S$  created in this way is connected, so that  $A^S$  has only one zero eigenvalue, whose corresponding eigenvector is homogeneous. Therefore, it is convenient to split off the resulting delta peak of  $\varrho(\lambda)$  at  $\lambda = 0$  with weight  $\varrho_0$  by writing

$$\varrho(\lambda) = \varrho_0 \delta(\lambda) + \varrho_+(\lambda). \quad (220)$$

From the density of states  $\varrho(\lambda)$  one can obtain in a simple way the basic quantities, namely the mean bead displacement at time  $t$ , the relaxation modulus  $G(t)$  and the loss and storage moduli  $G'(\omega)$  and  $G''(\omega)$ . We dispense from displaying these expressions which depend on  $\varrho(\lambda)$  here, and point to [219] for the details.

The procedure used in [219] to determine  $\varrho(\lambda)$  is as follows. The construction of the class of randomly-branched macromolecules considered above is not changed if one places the monomers from which the structures are built on the nodes of an  $f$ -functional Cayley tree and fills in the bonds, with probability  $p$ , in the order of increasing chemical distance from the starting monomer 0 at the origin. On the other hand, one may draw the bonds in arbitrary order, given that their probabilities of showing up are independent. Therefore, the  $w_S$  defined in Eq. 219 is the same as the probability of finding that the origin belongs to an  $S$ -cluster in the bond-diluted Cayley tree. Due to the symmetry of the Cayley tree, this probability is also independent of the choice of any particular monomer as being the origin.

One then considers, in the diluted Cayley tree picture for a particular monomer  $j$ , the diagonal element  $R_{jj}(\lambda) = R(\lambda)$  of the resolvent  $R(\lambda) = \langle (A^C - \lambda 1)^{-1} \rangle$ , averaged over all bond distributions [219]:

$$R(\lambda) = \left\langle (A^C - \lambda 1)_{jj}^{-1} \right\rangle. \quad (221)$$

A particular realization  $C$  of the Cayley tree for a certain placement of bonds is formed by disjoint clusters of beads, a cluster being a set of beads connected

to each other by bonds. Because of this, the  $A^C$  corresponding to  $C$  can be written in block diagonal form, with block matrices given by the  $A^S$  of the corresponding clusters. One has therefore

$$(A^C - \lambda 1)_{jj}^{-1} = (A^S - \lambda 1)_{jj}^{-1}, \quad (222)$$

where  $S$  consists only of the monomers belonging to the cluster of  $j$ . Furthermore, the probabilities  $\omega_{k,S}$  that a certain monomer is at a certain position  $k$  of  $S$  do not depend on  $k$ ; one has thus  $\omega_{k,S} = \omega_S / |S|$ , where  $|S|$  denotes the number of monomers inside  $S$ . This leads to

$$R(\lambda) = \sum_S \sum_{k=1}^{|S|} \omega_{k,S} (A^S - \lambda 1)_{kk}^{-1} = \sum_S \omega_S \frac{1}{|S|} \sum_{k=1}^{|S|} (A^S - \lambda 1)_{kk}^{-1}. \quad (223)$$

Using the relation

$$\varrho(\lambda) = \lim_{\varepsilon \rightarrow 0} \frac{1}{\pi} \text{Im} R(\lambda + i\varepsilon), \quad (224)$$

one has for the normalized density of states of the  $S$  cluster,

$$\varrho_S(\lambda) = \lim_{\varepsilon \rightarrow 0} \frac{1}{\pi} \frac{1}{|S|} \text{Im} \sum_{k=1}^{|S|} (A^S - (\lambda + i\varepsilon)1)_{kk}^{-1}. \quad (225)$$

In fact, due to the symmetries mentioned, one can even choose for  $j$  in Eq. 221 the origin

$$R(\lambda) = \left\langle (A^C - \lambda 1)_{00}^{-1} \right\rangle. \quad (226)$$

Now, the average over the disorder can be performed [219] with the help of the replica method, see [223]. Allowing the strength of each bond to be weighted [162] according to a normalized coupling strength distribution  $D(\mu)$

$$F(r_j, r_k) \equiv q + p \int_0^\infty d\mu D(\mu) \exp \left[ -i \frac{\mu}{2} (r_j - r_k)^2 \right], \quad (227)$$

and performing the necessary recursive integrations, one is led [219] to the equations for a tree of generation  $g$ , namely to

$$R^{(g)}(\lambda) = -\frac{1}{\lambda} \int_0^\infty dx e^{-x} \left\{ \phi^{(g)}(x) \right\}^f \quad (228)$$

and to

$$\phi^{(g)}(x) = q + p \widehat{O} e^{-x} \left\{ \phi^{(g-1)}(x) \right\}^{f-1}. \quad (229)$$

Here  $\widehat{\mathcal{O}}$  is the linear operator

$$\widehat{\mathcal{O}} = \int_0^\infty d\mu D(\mu) \exp \left[ -\frac{\lambda}{\mu} x \partial_x^2 \right] = \sum_{k=0}^\infty \frac{\langle \mu^{-k} \rangle_\mu}{k!} (-\lambda)^k (x \partial_x^2)^k, \tag{230}$$

where  $\langle \dots \rangle_\mu$  denotes the average over the distribution  $D(\mu)$ . For an infinite Cayley tree the recursion relations take the form of a single integral equation of the function  $\phi(x) \equiv \lim_{g \rightarrow \infty} \phi^{(g)}(x)$ :

$$\phi(x) = q + p \widehat{\mathcal{O}} e^{-x} \{\phi(x)\}^{f-1}, \tag{231}$$

and furthermore

$$R(\lambda) = -\frac{1}{\lambda} \int_0^\infty dx e^{-x} \{\phi(x)\}^f. \tag{232}$$

As shown in [219] and paralleling [162], the analytical work simplifies considerably for the following distribution of bond strengths:

$$D(\mu) = \frac{1}{\mu^2} \exp(-1/\mu), \tag{233}$$

since for it the operator  $\widehat{\mathcal{O}}$ , Eq. 230, takes the form

$$\widehat{\mathcal{O}} = \int_0^\infty d\mu \frac{1}{\mu^2} \exp(-1/\mu) \exp \left[ -\frac{\lambda}{\mu} x \partial_x^2 \right] = [1 + \lambda x \partial_x^2]^{-1}. \tag{234}$$

For instance, applying  $1 + \lambda x \partial_x^2 = \widehat{\mathcal{O}}^{-1}$  to both sides of Eq. 229, one obtains the ordinary second-order differential equation

$$\phi(x) + \lambda x \partial_x^2 \phi(x) = q + p e^{-x} \{\phi(x)\}^{f-1}. \tag{235}$$

For large  $\lambda$  one obtains analytically [219] that  $\varrho(\lambda)$  obeys

$$\varrho(\lambda) \simeq fp \lambda^{-2}. \tag{236}$$

Equation 235 has to be solved subject to the boundary conditions

$$\phi(0) = 1 \text{ and } \phi(\infty) = q. \tag{237}$$

These equations allow us to determine  $\varrho(\lambda)$ , as shown in [219]. The correspondence between the theoretically-determined  $\varrho(\lambda)$  and the results of numerical diagonalizations turns out to be very good for small and medium-sized GGS. This leads us to expect that the analytic results may be also trusted for even larger GGS, constructed in the manner described above.

We turn now to quantities of special experimental importance, such as  $G'(\omega)$  and  $G''(\omega)$ , which were evaluated using the method already discussed [219], and which turned out to be rather smooth curves. This fact is caused by the vast number of different hyperbranched structures with bonds

of different strengths, which all contribute to  $G'(\omega)$  and  $G''(\omega)$ , and differs from the cases of single dendrimers or of hyperbranched structures with a fixed number of monomers [216]. In these cases one recognizes the signature of the underlying structures in the behavior of  $G'(\omega)$  and  $G''(\omega)$  at intermediate  $\omega$ ; thus doubly logarithmic plots of  $G'(\omega)$  and  $G''(\omega)$  in [33] and [13] showed logarithmic-type behavior for the dendrimers, which is related to their exponential growth with  $g$ .

## 9.2

### Comblike Polymers

Comblike structures [205] form a special class of regularly-branched polymers. A comblike network is constructed starting from a Rouse chain of  $N$  beads called the root chain (or zeroth generation). Other  $N$  chains of the same or of different lengths are connected at one of their ends to the root chain. In general, this is the usual form of a regular comb (of first generation). On the other hand, one can also let each chain of this first generation act as a root chain, which leads to the next (second) generation, see a particular example in Fig. 26. The continuation of this procedure was proposed in [224], which leads to a comblike network of generation  $g$ , which, letting each chain have  $N$  beads, consists of  $N_{\text{ch}} = 1 + N + N^2 + N^3 + \dots + N^g$  chains. Using the underlying symmetry of the system in question, the eigenvalue problem can be recursively reduced to that of a related problem for smaller matrices. The resulting characteristic equation  $|A - \lambda I| = 0$  was then analyzed in the limit of short and long relaxation times [224].

The authors [224] found that, in the short time limit, the relaxation times of the comblike structure are very close to the relaxation times of the corresponding number,  $N_{\text{ch}} = (N^{g+1} - 1)/(N - 1)$ , of free linear chains [224]. In the limit of long relaxation times, the complex dynamic modulus of the comblike

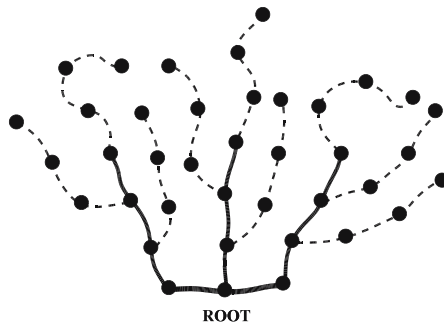


**Fig. 26** Comblike structure of second generation growing from a root Rouse chain (generation zero). All chains of the comb consist of three beads,  $N = 3$ . The chains belonging to the last (second) generation, are represented by dashed lines

network turns out to be well approximated by [224]

$$[G^*(\omega)] \simeq \sum_{k=1}^g N^k \frac{i\omega\tau_k}{1 + i\omega\tau_k}, \quad (238)$$

where the sum only goes over the long relaxation times  $\tau_k$  of each generation, which are given by [224]

$$\tau_k = \tau_0 \frac{(N^{g-k+1} - 1)N}{N - 1}, \quad (239)$$

with  $\tau_0 = \zeta/K$  being, as usual, the characteristic time. From Eq. 239 it follows that the longest relaxation time of the comb of generation  $g$  is of the order of  $\tau_0 N^g$ , see Eq. 239 for  $k = 1$ . Using Eqs. 238 and 239 the storage modulus  $[G'(\omega)]$  of the comblike network at low frequencies reduces to [224]:

$$[G'(\omega)] \simeq \frac{N^2}{(N - 1) \ln N} (\omega\tau_0) \times \left[ \arctan\left(\frac{N - 1}{N} \frac{1}{\omega\tau_0}\right) - \arctan\left(\frac{N - 1}{N^{g+1}} \frac{1}{\omega\tau_0}\right) \right]. \quad (240)$$

Thus, in the low-frequency region,  $1/\tau_1 \ll \omega \ll 1/\tau_0$  (where  $\tau_1 \sim \tau_0 N^g$ , see Eq. 239 for  $k = 1$ ), one has  $[G'(\omega)] \sim (\omega\tau_0)$ . This differs from the intermediate region, where one finds a Rouse chain behavior,  $[G'(\omega)] \sim (\omega\tau_0)^{1/2}$ , given that at higher frequencies the network behaves as an ensemble of free Rouse chains [224]. The above comblike structure, which can be thought of as being an example of a polymer network with dangling chains, has a dynamic behavior which qualitatively resembles that of a regular 2-D network built from Rouse chains, see Sect. 5.2.2.

The stretching of comblike networks of the first generation under external forces was studied in [225]. The authors considered a comb-ring (a comblike structure with the root being a closed Rouse chain (ring) of  $N$  beads). Based on the direct numerical diagonalization of the connectivity matrix  $A$  of the comb-ring,  $\langle \delta Y_m(t) \rangle = \langle Y_m(t) \rangle - F_0^{(\text{ext})} t / N_{\text{tot}} \zeta$  was calculated; this expression gives the displacement under an external force of the  $m$ th bead with respect to the center of mass of the system, see also Sect. 3.3. Here the index  $m$  numbers the beads in the chains attached to the backbone ring and ranges from  $m = 1$  (the bead belongs the backbone) to  $m = N$  (the bead is situated at the free end of one of the chains which form the comb-ring). It was found that the response of comb-rings to external forces depends much on the distance from the backbone to the particular bead on which the external force acts [225].

In the domain of very short times,  $\langle \delta Y_m(t) \rangle$  is mainly governed by the functionality  $f$  of a particular bead. The stretching  $\langle \delta Y_m(t) \rangle$  is minimal for beads which belong to the backbone ring ( $f = 3$ ) and is maximal for beads at the tips of the chains ( $f = 1$ ). The case of inner beads of chains ( $f = 2$ ) is intermediate. In the region of very long times, the stretching  $\langle \delta Y_m(t) \rangle$  reflects

the distance between the  $m$ th bead and the backbone. The limiting value of  $\langle \delta Y_m(t) \rangle$  at  $t \rightarrow \infty$  is found to be proportional to  $m$  (to the distance from the root ring). At intermediate times the quantity  $\langle \delta Y_m(t) \rangle$  displays scaling, in other words  $\langle \delta Y_m(t) \rangle \sim t^\alpha$  [225]. Remarkably, the exponent  $\alpha$  depends on  $m$  (on the position of the bead in the chain). For instance, in the case  $N = 50$  one has  $\alpha = 0.24$  for  $m = 1$  and  $\alpha = 0.53$  for  $m = 50$ , demonstrating again the strong sensitivity of  $\langle \delta Y_m(t) \rangle$  on the bead–backbone distance. After averaging  $\langle \delta Y_m(t) \rangle$  over all beads,  $\alpha$  turns out to be  $\alpha = 0.5$ , an exponent typical of the standard Rouse chain, see Eq. 69.

### 9.3

#### Regular Hyperbranched Polymers

In this subsection we will consider (distinct from the dendrimers of Sect. 8) another class of regular hyperbranched polymers. We recall that the quest for simplicity in the study of complex systems has led to fruitful ideas. In polymers such an idea is scaling, as forcefully pointed out by de Gennes [4]. Now, the price to be paid in going from linear chains to star polymers [33, 194], dendrimers [13, 33, 194, 205] and general hyperbranched structures [216] is that scaling (at least in its classical form) is not expected to hold anymore (at least not in a simple form, which implies power-law dependences on the frequency  $\omega$  or on the time  $t$ ). One of the reasons for this is that while several material classes (such as the Rouse chains) are fractal, more general structures do not necessarily behave as fractals.

Interestingly, there exists a family of hyperbranched structures which obey dilation symmetry. These regular hyperbranched polymers (RHP) can be constructed iteratively, by going from generation  $g$  to generation  $g + 1$  in a deterministic way (very reminiscent of the construction of the dendrimers, Sect. 8, and of the dual Sierpinski gaskets, Sect. 6). The original RHP with coordination number  $f = 4$  were introduced by Vicsek [226], and their dynamical properties were later investigated in [227–230]. From this work it became clear that the eigenfunctions of RHP, and especially their eigenvalues, obey rather simple rules; the authors of [227–230] computed the eigenvalues of RHP with  $f = 4$ , the Vicsek fractals, by determining the roots of iteratively-constructed polynomials numerically.

Theoretically, when searching for scaling [9, 95], it is important to study other RHP in which  $f$  varies, as done in [231, 232]. The topology of RHP is displayed in Fig. 27, which shows the  $f = 3$  structure schematically in 2-D. One starts from the object of generation  $g = 1$ , consisting here of  $f + 1 = 4$  beads arranged in a star pattern, the central bead having three neighbors. To this object one attaches  $f$  identical copies of itself at the next generation, through  $f$  bonds, in a star-wise fashion. Hence the next stage object ( $g = 2$ ) consists of 16 beads. The iteration is now obvious; Fig. 27 presents the finite  $f = 3$  RHP for  $g = 3$ . Note that the structure is quite ramified in this way; the regular pattern

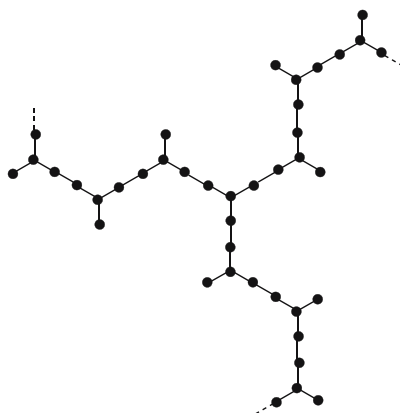


**Fig. 27** An example of a regular hyperbranched polymer, RHP

of Fig. 27 has a fractal dimension  $\bar{d}_r$  of

$$\bar{d}_r = \frac{\ln(f + 1)}{\ln 3}, \quad (241)$$

since increasing the distance from the center (the radius) by a factor of 3 increases the number of beads inside it by  $(f + 1)$ . Note that through Eq. 241, the extreme overcrowding found for dendrimers (where  $\bar{d}_r = \infty$ ) does not appear in RHP.

We first recall some aspects related to the chemical realization of RHP [232, 233]. These include the geometry in terms of composition, structure and steric requirements and also their synthesis. Now, RHP consist of structural entities in which the valence equals 1, 2 and  $f$ , entities denoted by  $M_1, M_2$  and  $M_f$ , respectively, which may be chosen from a set of different chemical species. One has then a large variety of  $M_f$  entities at one's disposal, such as the building blocks of polycarbosilanes [234, 235] or copolyesters [236–238]. For  $f = 3$ , condensed triarylamines are interesting candidates; they have been synthesized as bridged molecules [239, 240]. Moreover, even the case  $f = 6$  can be realized [232, 233] by using triarylamines bound to rather small benzene rings [241].

As shown in [231, 232], the eigenvalues of RHP can be obtained very easily, for arbitrary  $f$  and  $g$ , through an algebraic iterative procedure, which involves the Cardano-solution for cubic equations [242]. These findings open the way to studying the dynamics of arbitrarily large, finite RHP theoretically.

To describe the determination of the RHP eigenvalues we follow the procedure of [231, 232]. In order to solve  $(A - \lambda I) \Phi = 0$  one notes [231] that the architecture of a RHP displays  $f$ -coordinated centers (fCC), connecting bonds, and also dangling bonds; hence each of its beads has either  $f$ , 2 or 1 neighbors. Setting  $\phi_0$  for the component of the fCC in  $(A - \lambda I) \Phi = 0$ , typical

equations for its neighboring sites are [231]

$$(f - \lambda) \phi_0 = \sum_{j=1}^f \phi_j, \quad (242)$$

$$(2 - \lambda) \phi_f = \phi_0 + \phi_m, \quad (243)$$

and

$$(1 - \lambda) \phi_1 = \phi_0. \quad (244)$$

One can then transform [231], by simple algebraic means, Eqs. 242 to 244 to a set involving the coordinates of nearest-neighboring fCC, obtaining:

$$(f - P(\lambda)) \tilde{\phi}_0 = \sum_{j=1}^f \tilde{\phi}_j, \quad (245)$$

$$(2 - P(\lambda)) \tilde{\phi}_f = \tilde{\phi}_0 + \tilde{\phi}_m, \quad (246)$$

$$(1 - P(\lambda)) \tilde{\phi}_1 = \tilde{\phi}_0, \quad (247)$$

with

$$P(\lambda) = \lambda(\lambda - 3)(\lambda - f - 1). \quad (248)$$

The procedure is then iterated  $k$  times, during which  $P(\lambda)$  gets replaced by  $p_k(\lambda) = P(p_{k-1}(\lambda))$ .

For finite RHP Eq. 248 allows us to determine the eigenvalues at generation  $g + 1$  from those at generation  $g$  through the relation [231]

$$P\left(\lambda_i^{(g+1)}\right) = \lambda_i^{(g)}. \quad (249)$$

Evidently, in this way each previous eigenvalue gives rise to three new ones, a fact already noted [227–230, 243] for the case  $f = 4$ . Moreover, at every generation one has the non-degenerate mode  $\lambda_1 = 0$ ; furthermore there is one nondegenerate mode corresponding to the eigenvalue  $(f + 1)$  and  $\Delta_g$  new degenerate modes corresponding to the eigenvalue 1, where [231]

$$\Delta_g = (f - 2)(f + 1)^{g+1} + 1, \quad (250)$$

an expression which extends the findings of [227–230] to arbitrary  $f$ . One can then show [231] that one has obtained all the eigenvalues in this way.

Furthermore, Eqs. 245, 248 and 249 can be used to compute the  $\lambda_i^{(g)}$  iteratively [231], based on the roots of the polynomial

$$x^3 - (f + 4)x^2 + 3(f + 1)x - a = 0. \quad (251)$$

Introducing

$$p = \frac{1}{3} [f(f - 1) + 7] , \tag{252}$$

$$q = \frac{1}{27}(5 - f)(f + 4)(2f - 1) , \tag{253}$$

and

$$\varrho = |p/3|^{3/2} \tag{254}$$

the roots of this polynomial are given by the Cardano-solution, see [242]

$$x_\nu = (f + 4)/3 + 2\varrho^{1/3} \cos((\phi + 2\pi\nu)/3) , \quad \text{with } \nu \in \{1, 2, 3\} , \tag{255}$$

where

$$\phi = \arccos((a - q)/2\varrho) . \tag{256}$$

Using this procedure one can determine the eigenvalue spectrum of very large RHP to very high accuracy [231]. Moreover, the spectral dimension also follows from Eq. 251. One has

$$\tilde{d} = \frac{2 \ln(f + 1)}{\ln(3f + 3)} . \tag{257}$$

From the so-determined eigenvalue spectrum one can then calculate all of the dynamical quantities discussed in Sect. 3. We exemplify the situation using the storage modulus  $G'(\omega)$ , given by Eq. 20 and presented in

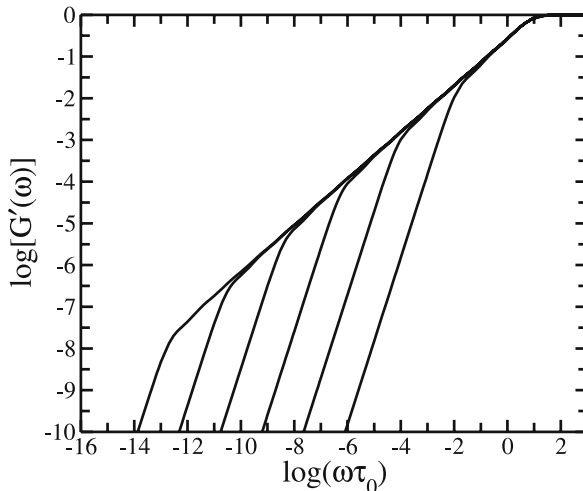


**Fig. 28** Reduced storage modulus  $[G'(\omega)]$  plotted on double logarithmic scales versus the reduced frequency  $\omega\tau_0$  for RHP with  $f = 3$ . Shown are results for the fractals with  $N = 4^3$ ,  $N = 4^5$ ,  $N = 4^7$ ,  $N = 4^9$ ,  $N = 4^{11}$ , and  $N = 4^{13}$  beads (from right to left)

Fig. 28. For this calculation finite fractals extending from  $N = 4^3$  to  $N = 4^{13}$  were used [231]. Clearly evident from Fig. 28 are the limiting, connectivity-independent behaviors at very small and very high  $\omega$ ; for  $\omega \ll 1$  one has  $G'(\omega) \sim \omega^2$  and for  $\omega \gg 1$  one finds  $G'(\omega) \sim \omega^0$ . Again the fractal connectivity aspect is given by the in-between region; here by going from  $N = 4^3$  to  $N = 4^{13}$  one finds [231] a change in the minimal slope from 0.621 to 0.557. Comparing the last value to  $\tilde{d}/2 \cong 0.55788$ , Eq. 257, demonstrates, as for the fractals discussed in Sect. 6, that for the dynamic properties of fractals the fundamental quantity is the spectral dimension.

## 10 Hybrid Polymer Structures

### 10.1 Regular Structures Constructed From Small-World Rouse Networks

We end this review with a discussion of complex polymer systems which have two levels of organization. First, we further develop the domain approach formulated in Sect. 7.5 to describe heterogeneous polymer networks. There the cross-link agglomerations (clusters) formed due to random cross-linking were treated independently of each other. However, for sufficiently dense polymer systems the clusters are themselves interconnected; this is reflected, for example, in the non-zero values of the equilibrium moduli of polymer networks and gels [3]. In fact, the networks appear to be disordered on small length scales, but they are rather homogeneous on larger scales.

A simple way to take into account these structural features is to cross-link highly disordered pieces of a network in some regular fashion. To model such a situation, topologically-regular structures built from small-world Rouse networks (SWRN) were considered, see Fig. 29 [31, 73]. The SWRN themselves were discussed in Sect. 7.2 and the general treatment of topologically-regular networks built from arbitrary cells was the subject of Sect. 5.3. Bringing these developments together allows us to “decorate” a regular network (say square or cubic) by replacing its bonds with SWRN subunits. As an example, we consider here square networks composed of such SWRN. In the construction of a SWRN realization one starts from a Rouse chain consisting of  $n$  beads. Then one connects each bead in a random way to some other bead by means of additional bonds (springs), with a probability  $q/n$ . Finally, the SWRN realization is used as a pattern for the subunits of a 2-D  $N \times N$  square network. In this way all of the SWRN subunits in the network are identical and one is fixed in each realization with respect to the pattern and size of the SWRN. This, on the other hand, allows us to use the procedures displayed in Sect. 5.3; one has a 2-D square network built from identical cells, each cell

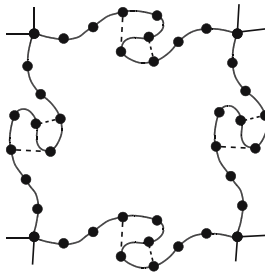


**Fig. 29** Two-dimensional regular lattice built from SWRN subunits

consisting of one lattice junction and two SWRN attached to it ( $s = (2n + 1)$  beads in total).

In Fig. 30 we show the storage modulus  $[G'(\omega)]$  of a network built from SWRN. The case  $q = 0$  corresponds to a regular network built from Rouse chains [25, 66, 68, 69], see also Sect. 5.2; for  $q = 0$   $[G'(\omega)]$  displays several characteristic frequency ranges. Just next to the domain of very high frequencies one has a frequency region dominated by the internal relaxation of Rouse chains,  $[G'(\omega)] \sim (\omega\tau_0)^{1/2}$ ; this domain is followed by the relaxation of the network, which for a square pattern is characterized by  $[G'(\omega)] \sim \omega\tau_0$ . Finally, at even lower frequencies, one has the domain of terminal relaxation, with the usual  $[G'(\omega)] \sim (\omega\tau_0)^2$  dependence.

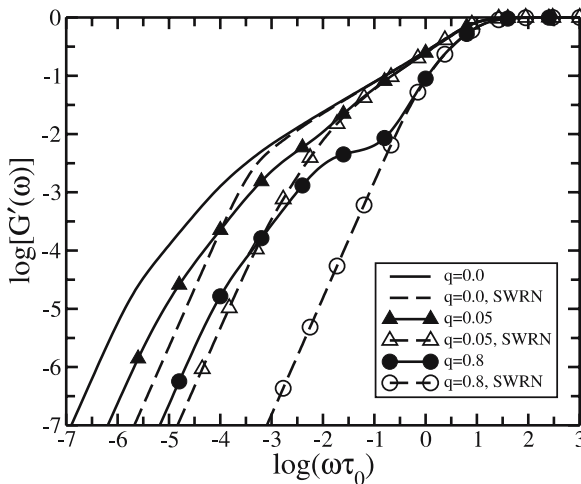


**Fig. 30** Reduced storage modulus  $[G'(\omega)]$  versus the reduced frequency  $\omega\tau_0$  plotted on double logarithmic scales. Shown are results for  $20 \times 20$  networks of SWRN-subunits ( $n = 200$ ) with  $q = 0$  (solid line),  $q = 0.05$  (solid line with triangles), and  $q = 0.8$  (solid line with circles). To point out the intra-subunit domains of relaxation, also displayed are the results for the corresponding, individual SWRN (dashed lines)

Remarkably, even a small number of additional bonds,  $q \neq 0$ , which transform the Rouse chains to SWRN, drastically change the relaxation behavior, see Fig. 30. With increasing  $q$  the domain of the intra-subunit (in other words, the intra-SWRN) relaxation gets smaller, revealing the increase with  $q$  of the rigidity of the SWRN subunits; parallel to this finding, for  $q \neq 0$  the scaling (power-law) behavior disappears. Interestingly, for large  $q$  one observes a plateau-type behavior in  $G'(\omega)$ , in the region intermediate between intra-subunit and pure network relaxation. Such an unusual behavior is due to the gap in the relaxation spectrum of the network: this gap extends between the maximal relaxation time of a SWRN subunit and the minimal relaxation time of the network of cross-links [31, 73].

Similar dynamic features are displayed by the average displacement of the beads under external forces  $\langle\langle Y(t) \rangle\rangle$ , see Fig. 31. Again, with increasing  $q$  (number of additional bonds) the domain of internal relaxation of the SWRN-subunits becomes narrower. For large  $q$  one even observes a plateau-type behavior in the time region lying between the internal SWRN modes and the modes of the underlying network of cross-links. More specifically, after an initial domain of very short times one can see a regime corresponding to the internal relaxation of the SWRN. After this domain ends, the individual SWRN do not yet “feel” the large network structure and they behave like SWRN with immobile ends. The existence of a region leading to a plateau-like behavior is related to the previously-discussed pseudogap in the eigenvalue spectrum of individual SWN [133], see also Sect. 7.2. Now, this pseudogap lies between the minimal non-vanishing SWRN eigenvalue

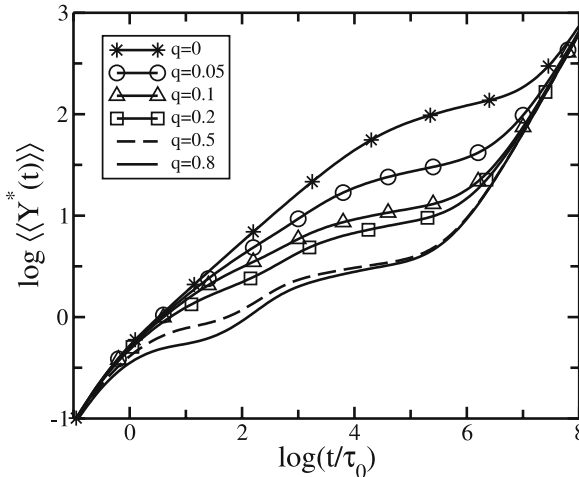


**Fig. 31** Reduced average displacement  $\langle\langle Y^*(t) \rangle\rangle = \langle\langle Y(t) \rangle\rangle \zeta/\tau_0 F_0^{(\text{ext})}$  versus the reduced time  $(t/\tau_0)$  plotted on double logarithmic scales for 2-D networks built from SWRN-subunits. Here  $q$  varies from 0 to 0.8. All curves are averaged over 100 SWN realizations

and the maximal eigenvalue of the underlying network of cross-links: in this regime the dynamics of the network are intermediate between those of SWRN with a free and with a frozen center of mass (given that through embedding the displacement of the center of mass gets hindered), so it tends to a flatter form [73]. Then one has an intermediate regime corresponding to the combined dynamics of the SWRN subunits and of the 2-D network. At longer times a cross-over domain appears, corresponding to the dynamics of the 2-D network, a domain which extends up to the region of the drift of the center of mass, see Fig. 31. In this way specific features of hybrid heterogeneous networks (which combine high local disorder and mesoscopic order) are mirrored by their relaxation forms, such as the shear dynamic modulus and the displacement of monomers under external forces [31, 73].

## 10.2

### Polymer Networks Bearing Dendritic Wedges

In Sect. 8.4 we discussed side-chain dendritic polymers. Recently, even more complex polymer structures have been synthesized, namely polyurethane networks which bear dendritic wedges (DW) of different generations [244]. In these networks the DW are grafted to the middle of each chain of the network; see the sketch in Fig. 32. The existence of branched dangling DW in polymer networks renders these systems very interesting for dynamic studies, since we can achieve direct control over the mobility of the chains in the network by varying the generation number (the size) of the dangling DW [244]. Evidently, increasing the size of the DW leads to a corresponding decrease in the mobility of the elastic network strands to which the DW are attached.

The simplest GGS model for such polymer networks is the so-called “fixed-chain-ends” model: a single chain bearing dendritic wedges (CBDW), whose ends are fixed in space (immobile) [78]. From a physical point of view, it cor-

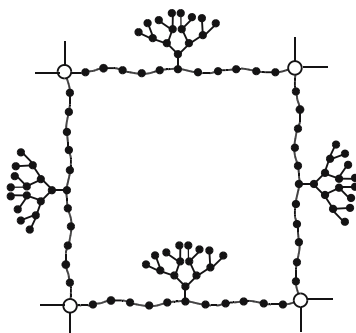


**Fig. 32** 2-D polymer network built from chains bearing dendritic wedges. Note that in the simplified “fixed-chain-ends” model the cross-linking points (depicted here as open beads) are assumed to be fixed in space, see text for details

responds to a situation in which the cross-links have extremely low mobility. In such a case the scales of motion of the network strands and of the cross-links are well separated [61, 142]. As we will see, even such a simple model captures some of the features of the dynamics of polymer networks bearing DW. As before in Sect. 8.4, we are mostly interested in the situation when the linear chain is long with respect to the length scale of the wedge (when its longest relaxation time exceeds that of the DW).

In Fig. 33 we display  $[G'(\omega)]$  for chains with 51 beads, while varying  $g$  (the size) of the DW. Comparing the storage modulus  $[G'(\omega)]$  for CBDW with free and with fixed ends reveals that at the beginning of the low-frequency domain (at moderately low frequencies) both systems behave in very similar fashions, which indicates that fixing the chain's ends in this  $\omega$ -range does not affect the dynamics. At lower frequencies, however, the  $[G'(\omega)]$  decay becomes slower for cross-linked CBDW than for free CBDW; this even leads for large  $g$  to a tendency to form a plateau close to the region where the terminal  $\omega^2$ -behavior starts, see Fig. 33. Interestingly, the width of the quasi-plateau domain increases with  $g$ , so that for larger  $g$  the terminal relaxation of the storage modulus shows up at lower frequencies [78]. This flattening of  $[G'(\omega)]$  appears in the low-frequency domain where no internal relaxation of the DW takes place; the behavior, hence, can be well reproduced by a simplified model

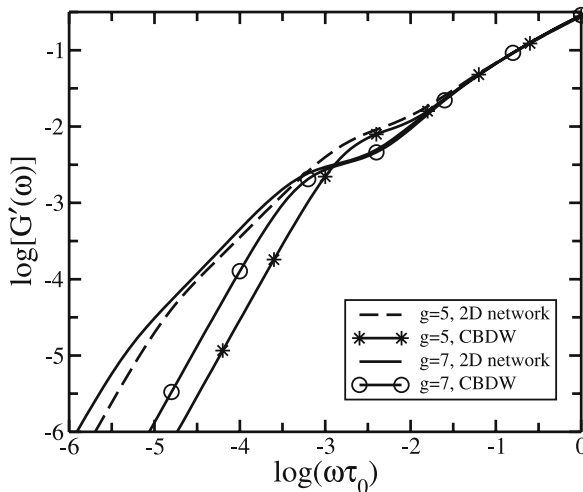


**Fig. 33** Reduced storage modulus  $[G'(\omega)]$  versus the reduced frequency  $\omega\tau_0$  plotted on double logarithmic scales. Shown are results for 2-D networks bearing trifunctional dendritic wedges of fifth (*dashed line*) and seventh (*solid line*) generations. Also displayed are the results obtained from a simplified “fixed-chain-ends” model for the same dendritic wedges, namely  $g = 5$  (*line with stars*) and  $g = 7$  (*line with circles*). The chains between the cross-links consist of 51 beads each

in which a DW (grafted to a chain with fixed ends) is replaced by a single “big” bead accumulating the friction of the whole wedge, see also Sect. 8.4.

The tendency of the  $[G'(\omega)]$ -curves to form a plateau, see Fig. 33, implies, in fact, a very slow relaxation process. Given that the motion of the central monomer of the chain with fixed ends is hindered by the “massive” dangling DW, the behavior of the system in the low-frequency domain (where the intra-wedge relaxation is unimportant) is given by the relaxation of the two (almost independent) halves of the original chain. Such a behavior has a maximal relaxation time equal to  $\tau_{\text{chain}}/4$ , where  $\tau_{\text{chain}}$  is given by Eq. 57. A slower relaxation process involves the center of mass of the whole CBDW with free ends (note that  $\lambda_1 \neq 0$  because of the fixed ends). Therefore, a DW acting as a single big bead with friction constant  $N_w\zeta$  also participates in this motion. This increases the overall friction involved and leads to a corresponding jump in the relaxation times [78]. Thus, one can attribute the flattening in  $[G'(\omega)]$  to the difference between the longest relaxation time of the whole CBDW,  $\tau_{\text{max}}^{(\text{CBDW})}$ , and of the corresponding time for a half chain,  $\tau_{\text{chain}}/4$ .

In real polymer networks the mobility of the cross-link points is intermediate between immobile and free, leading to cooperative modes which involve simultaneous, correlated motions of several CBDW. To model this situation one can use the approach based on regular networks built from complex cells, which was discussed in Sect. 5.3. More specifically, a topologically-square network formed from CBDW (see Fig. 32) can model a CBDW network [244]. In the framework of Sect. 5.3 the elementary cell consists of a cross-link point and two CBDW.

It turns out that the relaxation features observed for CBDW with immobile ends (or immobile cross-links) carry over to the regular networks built from CBDW, see Fig. 33. For large  $g$  one again sees the tendency of  $[G'(\omega)]$  to form a plateau at intermediate frequencies; this behavior is followed at low frequencies by a power-law relaxation due to the underlying network of cross-links. As pointed out above, such a plateau stems from the gap in the spectrum of CBDW with fixed ends. This picture is very different from that encountered in the study of regular networks of Rouse chains, where the relaxation spectrum is continuous and no plateau appears [25, 66, 68, 69], see Sect. 5.2. Thus, the plateau-type behavior of  $[G'(\omega)]$  found in polymer networks bearing DW is due to the large dangling DW, which slow down the relaxation at intermediate frequencies. As a final remark, we note that the choice of the regular network is not crucial here, since it affects only the low-frequency behavior. The most interesting and non-trivial domain is situated at higher frequencies and, therefore, is hardly influenced by the type of the network [78].

### 10.3 Dendrimer-Based Polymer Networks

We end our exposition of “hybrid” polymer systems with two levels of structural organization with dendrimer-based polymer networks. Due to the topological features of dendrimers (a tree-like structure growing from a central core), the number of peripheral monomers increases exponentially with the number of generations. Under certain conditions these monomers may be chemically active; this makes dendrimers very attractive for use as building blocks (dendrimer building blocks, DBB-blocks) in the construction of new types of hybrid polymer materials with well-structured, complex architectures. Recently DBB-based networks have attracted much attention [245–249]. Note that the connections between the DBB in a network can be permanent, leading to chemically cross-linked networks, as well as transient, giving rise to physical networks. We continue now in the GGS framework and discuss the case of permanently cross-linked DBB-based networks [74].

We follow now the description of [74]. The general approach of Sect. 5.3 of treating complex structures (cells) linked into topologically regular networks can be easily extended to the structures discussed here. A DBB based on a generalized dendrimer, characterized by  $f_c$ ,  $f$ , and  $g$ , is used as the repeat unit, see Fig. 34. The main variable here is the number of connections,  $M_{cr}$ , between neighboring DBB, which can be simply computed as being the total number of connections stemming from each DBB divided by the number of its neighboring DBB.

The minimal value of  $M_{cr}$  in networks equals unity, meaning that the network is loosely cross-linked; tighter cross-linked situations,  $M_{cr} > 1$ , are also possible. Now, the DBB peripheral beads are most prone to serve as connec-

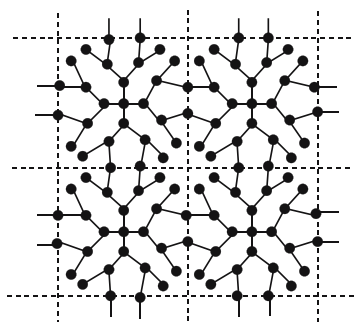


**Fig. 34** Portion of a 2-D dendrimer-based polymer network, built from DBB of the third generation,  $g = 3$ , with trifunctional inner branching points,  $f = 3$ , and a tetrafunctional core,  $f_c = 4$ . The number of connections between the neighboring dendritic blocks,  $M_{cr}$ , is equal to 2

tions, given that their functionality inside the dendrimer is less than  $f$ . It is easy to show that a generalized dendrimer has  $N_{\text{per}} = f_c(f - 1)^{(g-1)}$  peripheral beads. In the case of a simple hypercubic topological structure, each building block has  $2d_{\text{lat}}$  nearest neighbors, where  $d_{\text{lat}}$  is the dimensionality. Therefore, by cross-linking DBB in a symmetric way, one can use up to  $N_{\text{per}}/2d_{\text{lat}}$  beads to connect neighboring DBB.

Now, in order to apply the general approach formulated in Sect. 5.3, one needs to specify the matrices  $\mathbf{B}^{(\text{int})}$  and  $\mathbf{B}^{(\text{ext})}$ , see Eq. 106. Again following [74], we consider the case in which a link between two precursor dendrimers is established by the elimination of one bead, say, through a disproportionation reaction. As a side remark, we note that other cross-linking procedures are also possible, such as through the insertion of additional bonds. Due to the newly-created  $M_{\text{cr}}$  connections between each pair of neighboring dendritic cells, each cell now has  $M_{\text{cr}}d_{\text{lat}}$  beads less than the precursor dendrimer with  $N_{\text{d}}$  beads,  $N_{\text{d}}$  being given by Eq. 195. Such a dendritic cell therefore contains  $s = (N_{\text{d}} - M_{\text{cr}}d_{\text{lat}})$  beads, and the matrix  $\mathbf{B}^{(\text{int})}$  can be built on the basis of the connectivity matrix of the original, precursor dendrimer by the removal of  $M_{\text{cr}}d_{\text{lat}}$  beads. Furthermore, given that there are  $2d_{\text{lat}}$  nearest neighbors to each dendritic cell, there are  $2d_{\text{lat}}$  non-vanishing  $\mathbf{B}^{(\text{ext})}$  matrices; each of them containing  $M_{\text{cr}}$  non-zero elements equal to  $(-1)$ , see Sect. 5.3 for details.

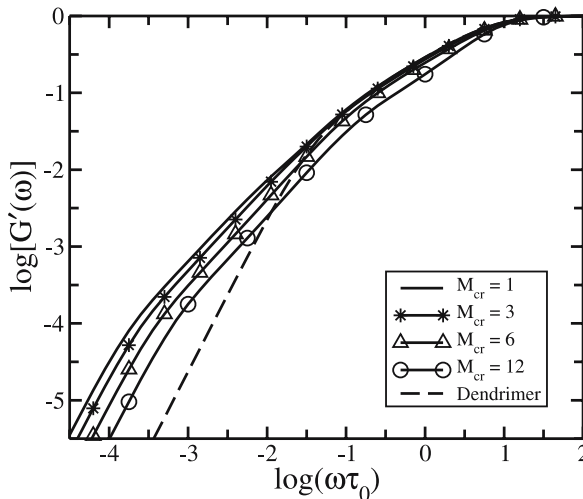


**Fig. 35** Reduced storage modulus  $[G'(\omega)]$  versus the reduced frequency  $\omega\tau_0$  plotted on double logarithmic scales for 2-D ( $20 \times 20$ ) networks based on dendritic blocks with  $f_c = 3, f = 3$ , and  $g = 5$ . The number of connections,  $M_{\text{cr}}$ , (see text) ranges from 1 (loosely cross-linked) to 12 (fully cross-linked dendrimers without dangling bonds). The  $[G'(\omega)]$ -curve of the corresponding individual dendrimer is also displayed

Applying the method of Sect. 5.3, one can evaluate the viscoelastic behavior of dendrimer-based networks and focus on how far the number of connections between neighboring dendritic blocks,  $M_{\text{cr}}$ , affects the dynamics. It was found [74] that increasing  $M_{\text{cr}}$  leads to a systematic narrowing of the region of high frequencies, in which the pure dendrimer-like behavior dominates [74]. For larger  $M_{\text{cr}}$  the  $[G'(\omega)]$ -curves depart earlier from the corresponding  $[G'(\omega)]$ -curve of an individual dendrimer, see the  $[G'(\omega)]$ -plots for particular network systems presented in Fig. 35. The explanation is straightforward: the long relaxation times of the individual dendrimers are controlled by large amplitude motions, which involve whole dendrimer (sub)branches, see Sect. 8.3 for details. The connections between the dendritic blocks hinder these motions. This effect is found to be generic – it does not depend significantly on the parameters  $f_c$ ,  $f$ , and  $g$  of the DBB, nor on the particular type (2-D or 3-D) of underlying regular topological structure into which the DBB are cross-linked [74]. Thus, the finding that connecting DBB into a network (by which the mobility of the peripheral DBB monomers is hindered) leads to a narrowing of their internal relaxation domain is a general fact, which can be used as a signature for cross-linking.

## 11

### Conclusions

In this article we focused on the use of generalized Gaussian structures (GGS) to study the dynamics of complex polymer systems. Of particular interest to us were systems which (because of their underlying symmetry) could be treated to a large extent analytically. These systems included topologically-regular polymer networks, polymer networks built from subunits, fractal polymer networks and gels, dendrimers, hyperbranched polymers, and side-chain dendritic polymers. As systems of special recent interest we also considered hybrid systems, which are characterized by two levels of organization; as examples, we treated polymer networks bearing dendritic wedges and dendrimer-based polymer networks. The GGS-considerations show that iterative and hierarchical structuring procedures are well reflected both energetically (in the eigenvalue spectra) and in the dynamical features (relaxation). Many of the dynamical observables discussed here allow us to determine the structural aspects of polymer materials with complex topologies. Thus, in many cases the GGS-treatment of particular structures may help us to understand their basic dynamic features, and should be considered as a worthwhile first stage before moving on to more realistic (and, therefore, more involved) theoretical models.

**Acknowledgements** The authors dedicate this work to Prof. Yuli Ya. Gotlib (IMC RAS, St. Petersburg, Russia) on the occasion of his 77th birthday. We had the support of the

Deutsche Forschungsgemeinschaft, of the Fonds der Chemischen Industrie, and of the Russian Foundation of Basic Research (Grant 05-03-32332). A.A.G. acknowledges the support of the Academy of Finland (Grant 202598) and of the Alexander von Humboldt Foundation. Special thanks go to A. Jurjiu and Ch. von Ferber, who provided the data for Figs. 12, 25, and 28. We greatly appreciate the joint work and the helpful discussions with Yu.Ya. Gotlib, T.M. Birshtein, A.A. Darinsky, R. Descas, Ch. von Ferber, G.M. Golovachev, S. Jespersen, A. Jurjiu, T. Koslowski, A.V. Lyulin, S.V. Lyulin, D.A. Markelov, G. Oshanin, C. Satmarel, and I. M. Sokolov. A.A.G. thanks A.P. Ivanova for permanent support.

## References

1. Rouse PE (1953) *J Chem Phys* 21:1272
2. Doi M, Edwards SF (1986) *The theory of polymer dynamics*. Clarendon, Oxford
3. Ferry JD (1980) *Viscoelastic properties of polymers*, 3rd edn. Wiley, New York
4. de Gennes PG (1979) *Scaling concepts in polymer physics*. Cornell University Press, Ithaca, NY
5. Zimm BH (1956) *J Chem Phys* 24:269
6. Sommer J-U, Blumen A (1995) *J Phys A—Math Gen* 28:6669
7. Schiessel H (1998) *Phys Rev E* 57:5775
8. Friedrich Ch, Schiessel H, Blumen A (1999). In: Siginer DA, DeKee D, Chhabra RP (eds) *Advances in the flow and rheology of non-Newtonian fluids*. Elsevier, Amsterdam, p 429
9. Schiessel H, Friedrich Ch, Blumen A (2000). In: Hilfer R (ed) *Applications of fractional calculus in physics*. World Scientific, Singapore, p 331
10. Eichinger BE, Martin JE (1978) *J Chem Phys* 69:4595
11. Graessley WW (1980) *Macromolecules* 13:372
12. Kloczkowski A, Mark JE, Frisch HL (1990) *Macromolecules* 23:3481
13. Biswas P, Kant R, Blumen A (2001) *J Chem Phys* 114:2430
14. Hansen DR, Shen M (1975) *Macromolecules* 8:343
15. Hall WE, De Wames RE (1975) *Macromolecules* 8:349
16. Stockmayer WH, Kennedy JW (1975) *Macromolecules* 8:351
17. Wang FW, DiMarzio EA (1975) *Macromolecules* 8:356
18. Wang FW (1975) *Macromolecules* 8:364
19. Man VF, Schrag JL, Lodge TP (1991) *Macromolecules* 24:3666
20. Denneman AIM, Jongschaap RJJ (1996) *J Rheol* 40:589
21. Satmarel C, Gurtovenko AA, Blumen A (2003) *Macromolecules* 36:486
22. Yamakawa H (1971) *Modern theory of polymer solutions*. Harper and Row, New York
23. Peterlin A (1967) *J Polym Sci Pol Phys* 5:179
24. Gotlib YY, Gurtovenko AA (1997) *Macromol Theor Simul* 6:523
25. Gurtovenko AA, Gotlib YY (2000) *Macromolecules* 33:6578
26. Tschoegl NW (1989) *The phenomenological theory of linear viscoelastic behavior*. Springer, Berlin Heidelberg New York
27. Williams G (1972) *Chem Rev* 72:55
28. Stockmayer WH, Baur ME (1964) *J Am Chem Soc* 86:3485
29. Stockmayer WH (1967) *Pure Appl Chem* 15:539
30. Gotlib YY, Gurtovenko AA (1996) *Macromol Theory Simul* 5:969
31. Gurtovenko AA, Blumen A (2002) *Macromolecules* 35:3288

32. Blumen A, Gurtovenko AA, Jespersen S (2002) *J Non-Cryst Solids* 305:71
33. Biswas P, Kant R, Blumen A (2000) *Macromol Theor Simul* 9:56
34. Perkins TT, Smith DE, Larson RG, Chu S (1995) *Science* 268:83
35. Wirtz D (1995) *Phys Rev Lett* 75:2436
36. Quake SR, Babcock H, Chu S (1997) *Nature* 388:151
37. Amblard F, Maggs AC, Yurke B, Pergellis AN, Leibler S (1996) *Phys Rev Lett* 77:4470
38. Kargin VA, Slonimskii GL (1948) *Dokl Akad Nauk SSSR* 62:239
39. Bueche F (1954) *J Chem Phys* 22:603
40. Gotlib YY, Darinsky AA, Svetlov YE (1986) *Physical kinetics of macromolecules. Khimiya, Leningrad*
41. Grosberg AY, Khokhlov AR (1994) *Statistical physics of macromolecules. AIP, New York*
42. Edwards SF, Freed KF (1974) *J Chem Phys* 61:1189
43. Freed KF, Edwards SF (1974) *J Chem Phys* 61:3626
44. de Gennes PG (1976) *Macromolecules* 9:594
45. Ahlrichs P, Everaers R, Dünweg B (2001) *Phys Rev E* 64:040501(R)
46. Richter D, Binder K, Ewen B, Stühn (1984) *J Phys Chem* 88:6618
47. Ewen B, Richter D (1997) *Adv Polym Sci* 134:1
48. Kremer K, Grest GS (1990) *J Chem Phys* 92:5057
49. Paul W, Smith GD, Yoon DY (1997) *Macromolecules* 30:7772
50. Mondello M, Grest GS (1997) *J Chem Phys* 106:9327
51. Harmandaris V, Mavrantzas VG, Theodorou DN (1998) *Macromolecules* 31:7934
52. Padding JT, Briels WJ (2001) *J Chem Phys* 114:8685
53. Lyulin AV, Balabaev NK, Michels MAJ (2002) *Macromolecules* 35:9595
54. Paul W, Smith GD, Yoon DY, Farago B, Rathgeber S, Zirkel A, Willner L, Richter D (1998) *Phys Rev Lett* 80:2346
55. McLeish TCB (2002) *Adv Phys* 51:1379
56. Rubinstein M, Colby RH (1988) *J Chem Phys* 89:5291
57. Paul W, Binder K, Heermann DW, Kremer K (1991) *J Chem Phys* 95:7726
58. Pütz M, Kremer K, Grest GS (2000) *Europhys Lett* 49:735
59. Harmandaris VA, Mavrantzas VG, Theodorou DN, Köger M, Ramirez J, Öttinger HC, Vlassopoulos D (2003) *Macromolecules* 36:1376
60. Gotlib YY, Volkenshtein MV (1953) *Dokl Akad Nauk SSSR* 89:821
61. Mooney M (1959) *J Polym Sci* 34:599
62. Gotlib YY (1981) *Pure Appl Chem* 53:1531
63. Gotlib Y, Golovachev G (1994) *J Non-Cryst Solids* 172:850
64. Denneman AIM, Jongschaap RJJ, Mellema J (1998) *J Eng Math* 34:75
65. Denneman AIM, Jongschaap RJJ, Mellema J (1999) *J Rheol* 43:327
66. Gurtovenko AA, Gotlib YY (1998) *Macromolecules* 31:5756
67. Ronka G, Allegra G (1975) *J Chem Phys* 63:4104
68. Gotlib YY, Gurtovenko AA (2000) *Macromol Theor Simul* 9:407
69. Gurtovenko AA, Gotlib YY (2000) *Macromol Theor Simul* 9:416
70. Chompff AJ, Duiser JA (1966) *J Chem Phys* 45:1505
71. Gotlib YY, Salikhov KM (1963) *Akust Zh (Acoustic J)* 9:301
72. Ham JS (1957) *J Chem Phys* 26:625
73. Gurtovenko AA, Blumen A (2001) *J Chem Phys* 115:4924
74. Gurtovenko AA, Markelov DA, Gotlib YY, Blumen A (2003) *J Chem Phys* 119:7579
75. Kittel C (1986) *Introduction to solid state physics, 6th edn. Wiley, New York*
76. Ashcroft NW, Mermin ND (1981) *Solid state physics. Sanders College, Philadelphia, PA*

77. Ziman JM (1972) Principles of the theory of solids, 2nd edn. Cambridge University Press, Cambridge
78. Gurtovenko AA, Gotlib YY, Blumen A (2002) *Macromolecules* 35:7481
79. Scher H, Lax M (1973) *Phys Rev B* 7:4491
80. Scher H, Lax M (1973) *Phys Rev B* 7:4502
81. Scher H, Montroll EW (1975) *Phys Rev B* 12:2455
82. Shlesinger MF (1984) *J Stat Phys* 36:639
83. Zumofen G, Blumen A, Klafter J, Shlesinger MF (1989) *J Stat Phys* 54:1519
84. Schiessel H, Oshanin G, Blumen A (1995) *J Chem Phys* 103:5070
85. Blumen A (2001) *Philos Mag B* 81:1021
86. Klafter J, Blumen A, Shlesinger MF (1987) *Phys Rev A* 35:3081
87. Montroll EW, Weiss GH (1965) *J Math Phys* 6:167
88. Blumen A, Klafter J, White BS, Zumofen G (1984) *Phys Rev Lett* 53:1301
89. Schnörer H, Haarer D, Blumen A (1988) *Phys Rev B* 38:8097
90. Blumen A, Zumofen G, Klafter (1989) *Phys Rev A* 40:3964
91. Blumen A, Schnörer H (1990) *Angew Chem* 102:158
92. Blumen A, Schnörer H (1990) *Angew Chem Int Edit* 29:113
93. Hilfer R (ed) (2000) *Applications of fractional calculus in physics*. World Scientific, Singapore
94. Metzler R, Klafter J (2000) *Phys Rep* 339:1
95. Sokolov IM, Klafter J, Blumen A (2002) *Physics Today* 55:48
96. Blizard RB (1951) *J Appl Phys* 22:730
97. Schiessel H, Blumen A (1993) *J Phys A–Math Gen* 26:5057
98. Heymans N, Bauwens J-C (1994) *Rheol Acta* 33:210
99. Schiessel H, Metzler R, Blumen A, Nonnenmacher TF (1995) *J Phys A–Math Gen* 28:6567
100. Schiessel H, Blumen A (1995) *Macromolecules* 28:4013
101. Chambon F, Winter HH (1987) *J Rheol* 31:683
102. Winter HH, Morganelli P, Chambon F (1988) *Macromolecules* 21:532
103. Scanlan JC, Winter HH (1991) *Macromolecules* 24:47
104. Blumen A, Jurjii A (2002) *J Chem Phys* 116:2636
105. Cosenza MG, Kapral R (1992) *Phys Rev A* 46:1850
106. Jurjii A, Friedrich Ch, Blumen A (2002) *Chem Phys* 284:221
107. Cates ME (1984) *Phys Rev Lett* 53:926
108. Cates ME (1985) *J Phys (Paris)* 46:1059
109. Sommer J-U, Vilgis TA, Heinrich G (1994) *J Chem Phys* 100:9181
110. Marconi UMB, Petri A (1997) *J Phys A–Math Gen* 30:1069
111. Vilgis TA, Stapper M (1998) *Eur Phys J B* 2:69
112. Zilman AG, Granek R (1998) *Phys Rev E* 58:R2725
113. Licinio P (2001) *Physica A* 294:51
114. Mandelbrot BB (1982) *The fractal geometry of nature*. W.H. Freeman and Co., San Francisco, CA
115. Dhar D (1977) *J Math Phys* 18:577
116. Jurjii A, Koslowski Th, Blumen A (2003) *J Chem Phys* 118:2398
117. Blumen A, Jurjii A, Koslowski Th (2003) *Macromol Symp* 191:141
118. Brotzman RW, Eichinger BE (1981) *Macromolecules* 14:1445
119. Neuburger NA, Eichinger BE (1988) *Macromolecules* 21:3060
120. Zhao Y, Eichinger BE (1992) *Macromolecules* 25:6988
121. Gottlieb M, Gaylord RJ (1984) *Macromolecules* 17:2024
122. McKenna GB, Flynn KM, Chen YH (1989) *Macromolecules* 22:4507

123. Crissman JM, McKenna GB (1992) *Polym Mater Sci Eng* 67:487
124. McKenna GB, Crissman JM (1993) *Polym Mater Sci Eng* 68:280
125. Bastide J, Leibler L, Prost J (1990) *Macromolecules* 23:1821
126. Mendes E, Lindner P, Buzier M, Boué F, Bastide J (1991) *Phys Rev Lett* 66:1595
127. Martin JE, Eichinger BE (1978) *J Chem Phys* 69:4588
128. Martin JE, Eichinger BE (1980) *Macromolecules* 13:626
129. Watts DJ, Strogatz SH (1998) *Nature (London)* 393:440
130. Watts DJ (1999) *Small worlds: The dynamics of networks between order and randomness*. Princeton University Press, Princeton, NJ
131. Newman MEJ, Watts DJ (1999) *Phys Rev E* 60:7332
132. Barthélémy M, Amaral LAN (1999) *Phys Rev Lett* 82:3180
133. Monasson R (1999) *Eur Phys J B* 12:555
134. Newman MEJ, Moore C, Watts DJ (2000) *Phys Rev Lett* 84:3201
135. Jespersen S, Sokolov IM, Blumen A (2000) *Phys Rev E* 62:4405
136. Jespersen S, Sokolov IM, Blumen A (2000) *J Chem Phys* 113:7652
137. Vilgis TA, Heinrich G (1994) *Phys Rev E* 49:2167
138. Vilgis TA, Heinrich G (1994) *Macromol Theor Simul* 3:271
139. Deam RT, Edwards SF (1976) *Philos T Roy Soc A* 280:317
140. Vilgis TA (1992) *Macromolecules* 25:399
141. Vilgis TA, Boué F (1988) *J Polym Sci Pol Phys* 26:2291
142. Sommer J-U (1991) *J Chem Phys* 95:1316
143. Glatting G, Winkler RG, Reineker P (1995) *Macromolecules* 28:5906
144. Schultz M, Sommer J-U (1992) *J Chem Phys* 96:7102
145. Thirion P, Chasset R (1968) *Rev Gen Caout Plast* 45:859
146. McKenna GB, Gaylord RJ (1988) *Polymer* 29:2027
147. Weiss N, van Vliet T, Silberberg A (1981) *J Polym Sci Pol Phys* 19:1505
148. Wun KL, Prins W (1974) *J Polym Sci Pol Phys* 12:533
149. Hecht AM, Duplessix R, Geissler E (1985) *Macromolecules* 18:2167
150. Lindemann B, Schröder UP, Oppermann W (1997) *Macromolecules* 30:4073
151. Gurtovenko AA, Gotlib YY (2001) *J Chem Phys* 115:6785
152. Friedrich C, Heymann L (1988) *J Rheol* 32:235
153. te Nijenhuis K, Winter HH (1989) *Macromolecules* 22:411
154. Izuka A, Winter HH, Hashimoto T (1992) *Macromolecules* 25:2422
155. Alfrey T, Doty P (1945) *J Appl Phys* 16:700
156. Cohen MH, Grest GS (1981) *Phys Rev B* 24:4091
157. Degiorgio V, Bellini T, Piazza R, Mantegazza F, Goldstein RE (1990) *Phys Rev Lett* 64:1043
158. Blumen A, Klafter J, Zumofen G (1986) In: Zschokke I (ed) *Optical spectroscopy of glasses*. Reidel, Dordrecht, p 199
159. Bunde A, Havlin Y, Klafter J, Gräff G, Shehter A (1997) *Phys Rev Lett* 78:3338
160. Gurtovenko AA, Gotlib YY, Kilian H-G (2000) *Macromol Theor Simul* 9:388
161. Broderix K, Löwe H, Müller, Zippelius A (2001) *Physica A* 302:279
162. Broderix K, Aspelmeier T, Hartmann AK, Zippelius A (2001) *Phys Rev E* 64:021404
163. Chompff AJ (1970) *J Chem Phys* 53:1577
164. Doi M (1974) *Polym J* 6:108
165. Chompff AJ (1970) *J Chem Phys* 53:1566
166. Ronca G (1980) *J Chem Phys* 72:48
167. Graessley WW (1975) *Macromolecules* 8:186
168. Graessley WW (1975) *Macromolecules* 8:865
169. Kloczkowski A (2002) *Polymer* 43:1503

170. Kloczkowski A, Mark JE, Erman B (1989) *Macromolecules* 22:1423
171. Abramowitz M, Stegun IE (1964) *Handbook of mathematical functions*. National Bureau of Standards, Washington DC
172. Tomalia DA, Naylor AM, Goddard WA (1990) *Angew Chem Int Edit* 29:138
173. Hawker CJ, Fréchet JMJ (1990) *J Am Chem Soc* 112:7638
174. Fréchet JMJ (1994) *Science* 263:1710
175. NewKome GR (1996) *Advances in dendritic macromolecules*. JAI, London
176. de Gennes PG, Hervet H (1983) *J Phys (Paris)* 44:L351
177. Biswas P, Cherayil BJ (1994) *J Chem Phys* 100:3201
178. Boris D, Rubinstein M (1996) *Macromolecules* 29:7251
179. Cai C, Chen ZY (1997) *Macromolecules* 30:5104
180. La Ferla R (1997) *J Chem Phys* 106:688
181. Chen ZY, Cai C (1999) *Macromolecules* 32:5423
182. Ganazzoli F, La Ferla R (2000) *J Chem Phys* 113:9288
183. Ganazzoli F, La Ferla R, Terragni G (2000) *Macromolecules* 33:6611
184. Ganazzoli F, La Ferla R, Raffaini G (2001) *Macromolecules* 34:4222
185. Lescanec RL, Muthukumar M (1990) *Macromolecules* 23:2280
186. Mansfield ML, Klushin LI (1992) *J Phys Chem* 96:3994
187. Mansfield ML, Klushin LI (1993) *Macromolecules* 26:4262
188. Murat M, Grest GS (1996) *Macromolecules* 29:1278
189. Chen ZY, Cui SM (1996) *Macromolecules* 29:7943
190. Lyulin AV, Davies GR, Adolf DB (2000) *Macromolecules* 33:3294
191. Lyulin SV, Evers LJ, van der Schoot P, Darinskii AA, Lyulin AA, Michels MAJ (2004) *Macromolecules* 37:3049
192. Sheng YJ, Jiang S, Tsao HK (2002) *Macromolecules* 35:7865
193. Ganazzoli F (2002) *Macromol Symp* 190:55
194. Kant R, Biswas P, Blumen A (2000) *Macromol Theor Simul* 9:608
195. McLeish TCB, Milner ST (1999) *Adv Polym Sci* 143:195
196. Gotlib YY, Markelov DA (2002) *Polymer Sci A* (translated from *Vysokomol Soedin, Russia*) 44:1341
197. Satmarel C, Gurtovenko AA, Blumen A (2004) *Macromol Theor Simul* 13:487
198. Yin R, Zhu Y, Tomalia DA, Ibuki H (1998) *J Am Chem Soc* 120:2678
199. Percec V, Ahn CH, Ungar G, Yearly DJP, Möller M, Sheiko SS (1998) *Nature* 391:161
200. Jahromi S, Coussens B, Meijerink N, Braam AWM (1998) *J Am Chem Soc* 120:9753
201. Jahromi S, Palmén JHM, Steeman PAM (2000) *Macromolecules* 33:577
202. Roovers J (ed)(1999) *Branched Polymers I*. *Adv Polym Sci* 142:1
203. Roovers J (ed)(1999) *Branched Polymers II*. *Adv Polym Sci* 143:1
204. Newkome GR, Morefield CN, Vögtle F (1996) *Dendritic macromolecules: concepts, syntheses, perspectives*. VCH, Weinheim
205. Freire JJ (1999) *Adv Polym Sci* 143:35
206. Ganazzoli F, Allegra G (1990) *Macromolecules* 23:262
207. Dondos A, Papanagopoulos D (1997) *Polymer* 38:6255
208. Shida K, Ohno K, Kawazoe Y, Nakamura Y (2004) *Polymer* 45:1729
209. Lyulin AV, Adolf DB, Davies GR (2001) *Macromolecules* 34:3783
210. Blumen A, Jurjiu A, Koslowski Th (2004) *Macromol Symp* 210:301
211. Milner ST, McLeish TCB (1997) *Macromolecules* 30:2159
212. Milner ST, McLeish TCB (1998) *Macromolecules* 31:7479
213. Blackwell RJ, Harlen OG, McLeish TCB (2001) *Macromolecules* 34:2579
214. Bishko G, McLeish TCB, Harlen OG, Larson RG (1997) *Phys Rev Lett* 79:2352
215. McLeish TCB, Larson RG (1998) *J Rheol* 42:81

216. von Ferber Ch, Blumen A (2002) *J Chem Phys* 116:8616
217. Kim Y, Harris AB (1985) *Phys Rev B* 31:7393
218. Rodgers GJ, Bray AJ (1988) *Phys Rev B* 37:3557
219. Jasch F, von Ferber Ch, Blumen A (2003) *Phys Rev E* 68:051106
220. Grimmet G (1989) *Percolation*. Springer, Berlin Heidelberg New York
221. Fisher ME, Essam JW (1961) *J Math Phys* 2:609
222. Ben-Avraham D, Havlin S (2000) *Diffusion and reactions in fractals and disordered systems*. Cambridge University Press, Cambridge, UK
223. Mezard M, Parisi G, Virasoro MA (1986) *Spin glass theory and beyond*. World Scientific, Singapore
224. Schulz M, Reineker P, Möller M (1995) *J Chem Phys* 103:10701
225. Burioni R, Cassi D, Blumen A (2002) *Chem Phys* 282:409
226. Vicsek T (1989) *Fractal growth phenomena*. World Scientific, Singapore
227. Jayanthi CS, Wu SY, Cocks J (1992) *Phys Rev Lett* 69:1955
228. Jayanthi CS, Wu SY (1993) *Phys Rev B* 48:10188
229. Jayanthi CS, Wu SY (1993) *Phys Rev B* 48:10199
230. Jayanthi CS, Wu SY (1994) *Phys Rev B* 50:897
231. Blumen A, Jurjiu A, Koslowski T, von Ferber Ch (2003) *Phys Rev E* 67:061103
232. Blumen A, von Ferber Ch, Jurjiu A, Koslowski T (2004) *Macromolecules* 37:638
233. Koslowski T, Jurjiu A, Blumen A (2004) *J Phys Chem B* 108:3283
234. Lach C, Müller P, Frey H, Mülhaupt R (1997) *Macromol Rapid Commun* 18:253
235. Frey H, Lach C, Schlenk C, Pusel T (2000) *Polym Prepr* 41:568
236. Möck A, Burgath A, Hanselmann R, Frey H (2001) *Macromolecules* 34:7692
237. Burgath A, Möck A, Hanselmann R, Frey H (1999) *Polym Mater Sci Eng* 80:126
238. Möck A, Burgath A, Hanselmann R, Frey H (1999) *Polym Mater Sci Eng* 80:173
239. Lambert C, Nöll G (1999) *J Am Chem Soc* 121:8434
240. Lambert C, Gaschler W, Schmäzlzin E, Meerholz K, Bräuchle C (1999) *J Chem Soc Perk T* 2:577
241. Lambert C, Nöll G (2002) *Chem Eur J* 8:3467
242. Bronstein IN, Semendjajev KA (1985) *Taschenbuch der Mathematik (Handbook of mathematics)*. Nauka and Teubner, Moscow and Leipzig, Ch 2.4.2
243. Schwalm WA, Schwalm MK, Giona M (1997) *Phys Rev E* 55:6741
244. Jahromi S, Litvinov V, Coussens B (2001) *Macromolecules* 34:1013
245. Kriesel JW, Tilley TD (1999) *Chem Mater* 11:1190
246. Jang WD, Jiang DL, Aida T (2000) *J Am Chem Soc* 122:3232
247. Gröhn F, Kim G, Bauer BJ, Amis EJ (2001) *Macromolecules* 34:2179
248. Gitsov I, Zhu C (2002) *Macromolecules* 35:8418
249. Dvornic PR, Li J, de Leuze-Jallouli AM, Reeves SD, Owen MJ (2002) *Macromolecules* 35:9323

Editor: L. Leibler